



Probabilistic Stability Analysis of Open Stopes in Sublevel Stopping Method by Numerical Modeling

By

Shahriyar Heidarzadeh

A thesis submitted to l'Université du Québec à Chicoutimi in partial fulfillment of the requirements for the degree of Doctor of Philosophy in Earth and atmospheric sciences

Department of Applied Sciences, Université du Québec à Chicoutimi

Saguenay, Quebec, Canada

© Shahriyar Heidarzadeh 2018

Abstract

Over the past years, maintaining the stability of underground excavations has grabbed attention with the growing tendency of exploitation of deep underground mineral resources. Since sublevel stoping is recognized as the most widely applied method in Canadian underground mines, assessing the open stope stability develops concern for rock mechanics engineers over preserving mining production capacity and providing safety for workers and equipment. Stress-induced failure is among the most common causes of instability for underground open stopes. The probability of failure (POF) depends on a number of factors including rock mass properties, *in situ* stress state and stope geometry.

One of the most reliable approaches for evaluating the influence of the above mentioned factors on open stope stability, is the use of probabilistic methods in conjunction with numerical analysis. Various powerful probabilistic methods (e.g. Monte Carlo Simulation, Random Monte Carlo Simulation and Response Surface Methodology) in conjunction with the finite difference code *FLAC3D* have been applied throughout our research.

In fact, the present research provides a comprehensive methodology to perform a numerical evaluation of the effect of open stope geometrical parameters (i.e., stope strike length, stope width, and etc.) on the potential of rock mass brittle damage, as well as the probability of stope failure (POF) by considering two modes of relaxation-related gravity driven (tensile) failure, and rock mass brittle failure. Monte Carlo Simulation (MCS) and Response Surface Methodology (RSM) are employed to determine the significant individual effects and their interactions of the geometric parameters. This study applies geometrical parameters derived from a survey of numerous open stopes from the Canadian Shield. Evaluation of the effect of stope geometry on the rock mass brittle damage indicates that independent from mining depth, the highest range of brittle damage

is observed for the stopes with moderate range of hanging wall hydraulic radius (HR) and high range of hanging wall dip. While the lowest values of brittle damage is observed for the stopes having low-moderate values of hanging wall HR and low-moderate values of hanging wall dip. Also, the individual and interactive effect of stope geometrical parameters on the rock mass brittle damage is found to be significant. Assessing of the effect of stope geometry on the probability of tensile failure (POF) has pointed out that three parameters, which are the stope hanging wall HR, stope span width and stope hanging wall dip, have a strong influence on the stope stability state. Also it was found that the POF is significantly controlled by interaction effects between span width / hanging wall HR and hanging wall dip / hanging wall HR. Moreover, according to the results of the mathematical optimization, the maximum stability (in terms of POF) occurs for shallow dipping narrow stopes having large hanging wall HR. Whereas, the minimum stability would happen in moderately to steeply dipping wide stopes with small hanging wall HR values.

Also, a probabilistic stability analysis was performed on seven primary open stopes located in mining blocks V and VI at the Niobec underground mine (Saint-Honoré, Québec). Probabilistic methods with the finite difference code *FLAC3D*, are employed to evaluate the stability state of each studied stope, taking into consideration the inherent variability associated with the geomechanical parameters of the rock mass. The stability state is defined via the tensile and compressive probabilities of failure (POF) and the probability of brittle damage initiation (PDI). Monte Carlo simulation generates the probabilistic rock mass input parameters while Random Monte Carlo simulations applied a random spatial distribution of the geomechanical parameters within the rock mass. The results indicate that for the evaluated open stopes, tensile and compressive failures share similar POFs. However, according to the PDI values around all the

open stopes, no brittle failure is expected to occur under the existing conditions of rock mass quality and in-situ stress regime in mining blocks V and VI at the Niobec Mine.

RÉSUMÉ

Pendant les dernières années, le maintien de la stabilité des excavations souterraines a attiré l'attention avec la tendance croissante à l'exploitation des ressources minérales souterraines profondes. Étant donné que la méthode des chantiers ouverts est reconnue comme la méthode la plus largement utilisée dans les mines souterraines canadiennes, l'évaluation de la stabilité de ces chantiers suscite des inquiétudes chez les ingénieurs en mécanique des roches quant à la préservation de la capacité de production minière et à la sécurité des travailleurs et de l'équipement. La rupture induite par la concentration des contraintes est l'une des causes les plus courantes d'instabilité pour les chantiers souterrains ouverts. La probabilité de rupture (POF) dépend d'un certain nombre de facteurs, dont les propriétés du massif rocheux, l'état de contrainte *in situ* et la géométrie du chantier.

L'utilisation de méthodes probabilistes en conjonction avec l'analyse numérique est l'une des approches les plus fiables pour évaluer l'influence des facteurs susmentionnés sur la stabilité des chantiers. Diverses méthodes probabilistes ayant fait leurs preuves (par exemple, la simulation de Monte Carlo, la simulation de Monte Carlo aléatoire et la méthodologie de surface de réponse), associées au code de différences finies *FLAC3D*, ont été appliquées tout au long de la présente recherche.

En fait, la présente recherche fournit une méthodologie complète pour effectuer une évaluation numérique de l'effet des paramètres géométriques des chantiers ouverts (c'est-à-dire la longueur du chantier, la largeur du chantier, etc.) sur le potentiel des dommages et la probabilité de rupture du chantier (POF) en considérant deux modes de rupture, soit celle due à la gravité (traction) liée à la relaxation et la rupture fragile de la masse rocheuse. La simulation de Monte

Carlo (MCS) et la méthodologie de surface de réponse (RSM) sont utilisées pour déterminer les effets individuels et d'interaction significatifs des paramètres géométriques. Cette étude applique des paramètres géométriques dérivés d'un inventaire de nombreux chantiers ouverts dans le Bouclier canadien. L'évaluation de l'effet de la géométrie du chantier sur des dommages fragiles du massif rocheux indique qu'indépendamment de la profondeur des chantiers, les chantiers présentant un rayon hydraulique modéré et une pente élevée montre un plus grand dommage fragile. Par contre, les chantiers avec les valeurs de rayon hydraulique du toit bas à modéré, et un pendage de toit également bas à modéré montrent un dommage fragile minimal.

En outre, l'effet individuel et interactif des paramètres géométriques du chantier sur les dommages fragiles du massif rocheux s'avère significatif. L'évaluation de l'effet de la géométrie du chantier sur la probabilité de rupture en traction a montré que trois paramètres, qui sont le rayon hydraulique du toit, la largeur du chantier et le pendage de la paroi, ont une forte influence sur la stabilité du chantier. Il a également été constaté que le POF est contrôlé de manière significative par des effets d'interaction entre la largeur du chantier / le rayon hydraulique du toit, et le pendage du toit / le rayon hydraulique du toit. De plus, selon les résultats de l'optimisation mathématique, la stabilité maximale (en termes de POF) se produit pour les chantiers étroits peu profonds, à faible pendage et ayant de fortes valeurs de rayon hydraulique du toit. Alors que la stabilité minimale se produirait pour des chantiers larges et de pendage modéré à élevé, avec un toit ayant faibles valeurs de rayon hydraulique.

De plus, une analyse de stabilité probabiliste a été effectuée sur sept chantiers principaux parmi les ouvrages souterrains situés aux niveaux V et VI de la mine souterraine Niobec (Saint-Honoré, Québec). Les méthodes probabilistes utilisant le code de différences finies *FLAC3D* sont utilisées pour évaluer l'état de stabilité de chaque chantier étudié, en tenant compte

de la variabilité inhérente associée aux paramètres géomécaniques de la masse rocheuse. L'état de stabilité est défini par les probabilités de rupture en traction et en compression (POF), et la probabilité d'initiation de dégradation fragile (PDI). La simulation de Monte Carlo génère les paramètres probabilistes du massif rocheux tandis que les simulations aléatoires de Monte Carlo ont appliqué une distribution spatiale aléatoire des paramètres géomécaniques dans le massif rocheux. Les résultats indiquent que pour les chantiers ouverts évalués, les ruptures de traction et de compression partagent des POF similaires. Cependant, selon les valeurs de PDI autour de tous les chantiers ouverts, aucune défaillance fragile ne devrait se produire dans les conditions existantes de la qualité du massif rocheux et du régime de contraintes in situ aux niveaux V et VI de la mine Niobec.

Table of Contents

Abstract	ii
Résumé	v
Table of Contents	viii
List of Tables	xi
List of Figures	xii
Dedication	xv
Acknowledgment	xvi
Contribution of Authors	xvii
Chapter 1 - Introduction	1
1.1. Statement of problem.....	1
1.2. Research objectives.....	3
1.3. Research methodology.....	5
1.4. Originality and contribution.....	7
1.5. Thesis outline	9
Chapter 2 - Literature review	11
2.1. Sublevel stoping excavation method	11
2.2. Instability of underground excavations.....	12
2.2.1. Effect of stope geometrical parameter variations	17
2.2.2. Effect of uncertainties in the rock mass geomechanical parameters	20
2.2.2.1. Geological Strength Index (GSI).....	22
2.2.2.2. The generalized Hoek-Brown failure criterion	24
2.3. Stability analysis of an underground open stope	26
2.3.1. Probabilistic Approaches	30
2.3.1.1. Monte Carlo Simulation (MCS).....	34
2.3.1.2. Random Monte Carlo Simulation (RMCS).....	35
2.3.1.3. Response Surface Methodology (RSM).....	35
2.4. References.....	37

Chapter 3 - Assessing the effect of open stope geometry on the rock mass brittle damage in Canadian underground mines using response surface methodology 42

3.1. Abstract	42
3.2. Introduction.....	43
3.3. Methodology	47
3.3.1. Determination of rock mass parameters	48
3.3.2. State of <i>in situ</i> stress	49
3.3.3. Determination of model geometry.....	51
3.3.4. Selecting a failure criteria.....	53
3.3.5. Experimental Design	54
3.3.6. Numerical Modeling.....	57
3.4. Results and discussion	59
3.4.1. Effects of geometrical parameters on BSR in cluster I	65
3.4.2. Effects of geometrical parameters on BSR in cluster II	68
3.4.3. Effects of geometrical parameters on BSR in cluster III.....	71
3.4.4. Slope geometry optimization corresponding brittle rock mass failure.....	74
3.5. Conclusion	76
3.6. References.....	77

Chapter 4 - Evaluation of the effect of geometrical parameters on the stope probability of failure in the open stoping method using numerical modeling..... 81

4.1. Abstract	81
4.2. Introduction.....	82
4.3. Methodology	85
4.3.1. Determination of rock mass parameters	86
4.3.2. State of <i>in situ</i> stress	88
4.3.3. Determination of model geometry.....	89
4.3.4. Selecting a failure criteria.....	92
4.3.5. Determination of the probability of failure.....	93
4.3.6. Numerical modeling	94
4.4. Results and discussion	95

4.4.1.	Effect of open stope hanging wall HR on the probability of failure	100
4.4.2.	Effect of open stope span width on the probability of failure	103
4.4.3.	Effect of open stope hanging wall dip on the probability of failure.....	104
4.4.4.	Interaction effect of open stope geometric and inclination parameters on the probability of failure.....	107
4.5.	Conclusions.....	111
4.6.	References.....	113

Chapter 5 - Use of probabilistic numerical modeling to evaluate the effect of geomechanical parameter variability on the probability of open stope failure: a case study of the Niobec Mine, Quebec (Canada)..... 116

5.1.	Abstract	116
5.2.	Introduction.....	119
5.3.	Niobec Mine.....	122
5.4.	Methodology	124
5.4.1.	Determining rock mass properties	125
5.4.2.	Determining model geometry	129
5.4.3.	State of in-situ stress.....	130
5.4.4.	Selecting a failure criteria.....	133
5.4.5.	Determining the probability of failure.....	134
5.4.6.	Numerical modeling	135
5.5.	Results and discussion	136
5.5.1.	Evaluation of the probability of compressive and tensile failure	138
5.5.2.	Evaluation of the probability of brittle damage initiation	146
5.5.3.	Deterministic analysis.....	151
5.6.	Conclusion.....	153
5.7.	References	158

Chapter 6 - Conclusions 160

6.1.	Assessing the effect of open stope geometry on the rock mass brittle damage.....	161
6.2.	Evaluation of the effect of geometrical parameters on the stope probability of failure ..	162

6.3. Probabilistic evaluation of the effect of rock mass geomechanical variability on open stope probability of failure.....	163
6.4. Perspectives for further research.....	164

Appendices	166
-------------------------	------------

List of Tables

Table 3-1: The values of <i>in situ</i> stress components at three mining depths.....	50
Table 3-2: Stope geometry classes used in numerical modeling. HW: hanging wall.....	52
Table 3-3: Actual and coded values of the input parameters for each geometry class. HW: hanging wall.....	55
Table 3-4: Box–Behnken design matrix for Cluster I and response values at three depths.....	55
Table 3- 5: Box–Behnken design matrix for Cluster II and response values at three depths.	56
Table 3-6: Box–Behnken design matrix for Cluster III and response values at three depths.	57
Table 3-7: ANOVA results of the regression model for Cluster I at three depths.....	61
Table 3-8: ANOVA results of the regression model for Cluster II at three depths.....	62
Table 3-9: ANOVA results of the regression model for Cluster III at three depths.	63
Table 3-10: The values of determination coefficient (R^2), adjusted, and predicted determination coefficients.	64
Table 3-11: Numerical optimization of four independent variables and the responses based on the desirability value for three clusters at three mining depths.....	75
Table 4-1: Intact rock properties.....	86
Table 4-2: Rock mass geomechanical parameters.....	87
Table 4-3: The values of <i>in situ</i> stress components.....	88
Table 4-4: Stope geometrical categories the corresponding number of Monte-Carlo simulation for each category.....	91
Table 4-5: The 36-full factorial experimental runs and the corresponding values of POF obtained from numerical modellings.....	98
Table 4-6: ANOVA results of the regression model applied to POF data.....	99
Table 4-7: The values of determination coefficient (R^2), adjusted and predicted determination coefficients.	99
Table 5-1: Statistical moments for the intact rock parameters.....	127
Table 5-2: Statistical moments of the geomechanical parameters of the rock mass.....	128

Table 5-3: The range of values for the in-situ stress components.....	132
Table 5-4: The mean values of minimum Hoek-Brown compressive and tensile safety factors (SF) and their associated probabilities of failure for each open stope.	144
Table 5-5: The mean values of maximum brittle shear ratio (BSR) and the associated probability of brittle damage initiation for each open stope.....	150

Table of Figures

Figure 2-1- Schematic view – sublevel stoping method (Hustrulid 2001)	12
Figure 2-2- Types of failure and instability problems in massive, moderately and highly fractured rock masses under low, intermediate and high in situ stresses (Adapted from Kelvis 2013).	13
Figure 2-3- (a) Spalling and slabbing around an excavation; (b) Potential of structurally-controlled gravity-driven failure (Adapted from Villaescusa 2014).....	14
Figure 2-4- (a) Creation of the compression-induced tension cracking parallel to σ_1 ; (b) Field-scale spalling to excavation walls; (Adapted from Diederichs 2004).	15
Figure 2-5- Schematic of strength envelope, presenting different rock mass failure mechanisms: no damage, shear failure, spalling, and unraveling. σ_c stands for the unconfined compressive strength (UCS) of intact rock (Adapted from Diederichs 2004)	16
Figure 2-6- Schematic of an open stope geometry and its associated geometrical parameters (Adapted from Wang 2004).....	18
Figure 2-7- Geological Strength Index table for jointed rocks (Hoek 2007)	23
Figure 3-1 - Model boundary conditions and the state of in situ stresses.	58
Figure 3-2- Contour of maximum shear stress (Pa).	59
Figure 3-3- Contour of the brittle stress ratio (BSR).	59
Figure 3-4 - Response surface plots for geometry Cluster I. (a) interaction between width/length at mining depth 1125 m; (b) interaction between HW dip/width at mining depth 1125 m; (c) interaction between width/length at mining depth 1375 m; (d) interaction between HW dip/width at mining depth 1375 m; (e) interaction between width/length at mining depth 1625 m; (f) interaction between HW dip/width at mining depth 1625 m.....	66
Figure 3-5 - Sensitivity analysis of the effect of stope strike length variation on (a) maximum and (b) minimum induced stress.	67
Figure 3-6 - Sensitivity analysis of the effect of stope hanging wall dip variation on (a) maximum and (b) minimum induced stress.	68

Figure 3-7 - Response surface plots for geometry Cluster II. (a) interaction between height/length at mining depth 1125 m; (b) interaction between height/width at mining depth 1125 m; (c) interaction between HW dip/height at mining depth 1125 m; (d) interaction between length/width at mining depth 1375 m; (e) interaction between height/length at mining depth 1375 m; (f) interaction between HW dip/height at mining depth 1375 m; (g) interaction between length/width at mining depth 1625 m; (h) interaction between HW dip/height at mining depth 1625 m.	70
Figure 3-8- Effect of stope width variation on (a) maximum and (b) minimum induced stress.....	71
Figure 3-9 - Response surface plots for geometry Cluster III. (a) interaction between width/length at mining depth 1125 m; (b) interaction between HW dip/width at mining depth 1125 m; (c) interaction between width/length at mining depth 1375 m; (d) interaction between HW dip/width at mining depth 1375 m; (e) interaction between width/length at mining depth 1625 m; (f) interaction between HW dip/height at mining depth 1625 m.....	72
Figure 4-2 - An open stope geometrical parameters (Adopted from Wang [2])......	89
Figure 4-3 - Distribution plots of (a) stope strike length, (b) stope height, (c) stope hanging wall HR, (d) stope hanging wall dip and (e) stope span width; for 150 open stope cases adopted from Wang [(Wang 2004)]......	90
Figure 4-4 - Model boundary conditions and the state of in situ stress.	95
Figure 4-5 - Contour of the brittle shear ratio (BSR).....	96
Figure 4-6 - Contour of (a) minimum principal induced stress – σ_3 (MPa), (b) minimum principal induced stress – $\sigma_3 \geq 0$	96
Figure 4-7 - POF plots for hanging wall HR variations for three average span width groups. (a) hanging wall dip range 20-45°; (b) hanging wall dip range 45-60°; (c) hanging wall dip range 60-75°; (d) hanging wall dip range 75-90°.....	101
Figure 4-8- POF plots for span width variations for four hanging wall dip classes. (a) hanging wall HR range 2.5-5 m; (b) hanging wall HR range 5-7 m; and (c) hanging wall HR range 7-10 m.	104
Figure 4-9 - POF plots for hanging wall dip variation for three span width groups. (a) hanging wall HR range 2.5-5 m; (b) hanging wall HR range 5-7 m; (c) hanging wall HR range 7-10 m.	106
Figure 4-10 - General factorial analysis plots showing interaction effects between stope span width and stope hanging wall HR in (a) hanging wall dip range 20-45°; (b) hanging wall dip range 45-60°; (c) hanging wall dip range 60-75°; (d) hanging wall dip range 75-90°	108
Figure 4-11 - General factorial analysis plots showing interaction effects between stope hanging wall dip and stope hanging wall HR for (a) span width of 4 m; (b) span width of 8 m; (c) span width of 12 m. ..	110
Figure 5-1 - Location of the Niobec Mine near Saguenay, Quebec (Canada) (Vallieres et al. 2013).	123

Figure 5-2 - The methodology used to evaluate the effect of geomechanical variability of the rock mass on open-stope stability.	124
Figure 5-3 - The truncated normal probability distribution functions (PDFs) for (a) the uniaxial compressive strength (UCS) of the intact rock, (b) the geological strength index (GSI) of the rock mass, (c) the Hoek-Brown material constant m_i , and (d) Young's modulus E_i of the intact rock (data compiled by Lavoie 2018).	126
Figure 5-4 - The seven primary open stopes and the excavation sequence of mining blocks V and VI at the Niobec Mine.....	130
Figure 5-5 - (a) Power trend curves applied to the calculated horizontal to vertical stress ratio K at various depths and (b) variations of the maximum and minimum horizontal in-situ stress components as the function of depth (after Lavoie 2018).	131
Figure 5-6 - The linear variation gradient of (a) the maximum horizontal in-situ stress component as a function of depth and (b) the vertical in-situ stress component as a function of depth.	132
Figure 5-7 - (a) & (b) The sectional views of generated numerical model containing the seven primary open stopes and (c) the plan view of the constructed numerical model containing the seven primary stopes. .	136
Figure 5-8 - Example of the random spatial distribution of (a) the Hoek-Brown “s” failure constant parameter and (b) the uniaxial compressive strength (UCS) of intact rock for a random seed.	138
Figure 5-9 - Normal probability density functions (PDFs) of the minimum Hoek-Brown compressive safety factor around the area of interest for each primary open stope.	141
Figure 5-10 - Normal probability density functions (PDFs) of the minimum Hoek-Brown tensile safety factor around the area of interest for each primary open stope.	143
Figure 5-11 - A plan view of maximum principal induced stress contours around open stopes and (b) a plan view of minimum principal induced stress contours around open stopes.....	145
Figure 5-12 - The (a) profile view and (b) plan view of brittle shear ratio (BSR) contours around open stopes.	146
Figure 5-13 - Normal probability density functions (PDFs) of the maximum brittle shear ratio (BSR) value around the area of interest for each primary open stope.	149
Figure 5-14 - A plan view of maximum shear stress contours around the open stopes.	151
Figure 5-15- Outcomes from deterministic and probabilistic numerical analyses for (a) the minimum Hoek-Brown compressive safety factor and (b) the minimum Hoek-Brown tensile safety factor.	152

DEDICATION

This work is dedicated to my lovely family for their kindness, devotion and endless support.

ACKNOWLEDGMENTS

I would like to express my sincerest appreciation to my supervisor **Prof. Ali. SAEIDI**, for his valuable supervision, his kindness, his permanent encouragement, and his important technical and financial support throughout this research.

I would like to express my gratitude to **Prof. Alain. ROULEAU** as my co-supervisor for his precious advices and his valuable suggestions throughout this research.

This research is financially supported by a research grant from the Natural Sciences and Engineering Research Council of Canada (NSERC) and a research grant provided by the Niobec Mine. I would like to thank them for their financial support.

I hereby appreciate all my professors, colleagues and friends at the department of Applied Sciences at the University of Quebec at Chicoutimi for their help and considerations along my journey.

Last but not least, I want to express my deepest appreciation to my mother **Shiva**, to my father **Hassan**, to my dear brother **Kamyar** and to my true friend **Parinaz** for their full support and endless love over all these years.

CONTRIBUTIONS OF AUTHORS

- Heidarzadeh S, Saeidi A, Rouleau A. Assessing the effect of open stope geometry on rock mass brittle damage using a response surface methodology. *International Journal of Rock Mechanics and Mining Sciences*. 2018; 106:60–73.
- Heidarzadeh S, Saeidi A, Rouleau A. Evaluation of the effect of geometrical parameters on stope probability of failure in the open stoping method using numerical modeling. *International Journal of Mining Science and Technology*; 2018.
- Heidarzadeh S, Saeidi A, Rouleau A. Use of probabilistic numerical modeling to evaluate the effect of geomechanical parameter variability on the probability of open stope failure: a case study of the Niobec Mine, Quebec (Canada). *Journal of Rock Mechanics and Geotechnical Engineering* (Submitted)

Conference papers:

- Heidarzadeh S, Saeidi A, Rouleau A. Numerical assessment of the effect of geometrical parameters on the stope probability of failure. *Quebec Mines 2017* (Poster).
- Heidarzadeh S, Saeidi A, Rouleau A. Probabilistic evaluation of the effect of open stope geometrical parameters on the rock mass brittle damage. *The 70th Canadian Geotechnical Conference, GeoOttawa 2017*.

All the above mentioned articles are co-authored by **Prof. Ali SAEIDI**, as the supervisor and **Prof. Alain ROULEAU** as the co-supervisor of the thesis.

Chapter 1 - Introduction

1.1. Statement of problem

During the recent decades, due to the shortage of easily minable near-surface mineral deposits, the tendency to extract deep underground resources has been growing extensively in the mining industry (Govett 1976; Potvin 2000). Therefore, maintaining the stability of underground excavations has become a critical issue for underground engineers since it not only affects the mining production capacity but also lowers the risk of fatalities and major financial loss (Einstein 1996; Idris 2011; Abdellah et al. 2014b).

Among numerous underground excavation methods, sublevel stoping is considered as the most widely practiced technique in Canadian underground mines (Hudson 1993; Wang 2004; Zhang and Mitri 2008; Abdellah et al. 2014b). Sublevel stoping creates large underground openings called “Stopes” whose level of stability is influenced by several factors including rock mass geomechanical parameters, natural and mining-induced stresses, and stope geometrical parameters (Diederichs and Kaiser 1996; Chen et al., 1997; Henning and Mitri 2007; Idris et al. 2013; Villaescusa 2014). Underground instability and the probable failure conditions, for open stopes located in deep hard rock, occur as a result of high magnitude mining-induced stresses. Low confinement stress-induced failure consists of the two dominant modes, namely; (1) stress-induced spalling and slabbing (brittle failure); and (2) structurally-controlled gravity-driven failures (i.e. tensile) (Castro et al., 2012). Effects of these factors on different modes of stope instability, can be assessed by using different analytical, empirical and numerical approaches. Among these approaches, numerical methods offer more advantages and less drawbacks compared to the other

two methods (Idris 2014), therefore they are widely used to analyze the stability of underground open stopes.

Although, numerical evaluation of the effects of stope geometrical parameter variations on open stope stability has been investigated by several important studies (Chen et al. 1983, Germain and Hadjigeorgiou 1997, Clark 1998, Henning and Mitri 2007); the aforementioned studies and their corresponding assumptions present a number of drawbacks. First of all, the existing literature provides many studies that investigate the effect of excavation geometry on low confinement tensile (gravity-driven) modes of failure. However, in real conditions the occurrence of different modes of stress-driven failure are possible therefore it would be more reasonable to consider multiple possible failure scenarios when evaluating the state of stope stability. Even for a particular instability mode, no comprehensive evaluation has been made to investigate the combined effects of open stope size, shape and inclination on their state of stability. In other words, the previous studies mainly focused on the effects of individual geometric parameters with limited variation ranges (mostly case specific studies) while not considering the simultaneous variation of other geometrical parameters. Therefore, in the case of studying the effect of stope geometry, the present thesis attempts to provide a methodology to assess individual effects and their interactions of stope geometrical parameter variations (considering typical stope dimensions in Canadian underground mines) on multiple underground failure modes. The provided methodology uses different probabilistic methods (e.g. Response Surface Methodology and Monte Carlo Simulation) in conjunction with the finite difference code *FLAC3D* (Itasca 2015), to simulate a large number of stopes, grouped in different geometric categories. Furthermore, mathematical optimization techniques are employed to predict the most stable conditions for underground open stopes in terms of geometry setups.

On the other hand, the effect of the geomechanical parameters of the rock mass on stope stability is recognized to be significant and not negligible. Due to the heterogeneous nature of a rock mass, its physio-mechanical properties are intrinsically variable (Idris 2011). The uncertainties associated with the inherent variability of the geomechanical parameters of a rock mass cannot be captured and accounted for by conventional deterministic approaches. Hence, appropriate probabilistic methods should be used to incorporate the effect of uncertainties associated with the rock mass inherent variability in strength and stiffness characteristics. Therefore, in the present thesis, different probabilistic methods (e.g. Monte Carlo Simulation and Random Monte Carlo Simulation) are utilized combined with the finite difference code *FLAC3D* (Itasca 2015) to evaluate the stability state of multiple neighboring stopes, taking into consideration the inherent variability associated with the geomechanical parameters of the rock mass. The probabilistic stability analysis has been applied on seven primary open stopes located in mining blocks V and VI at the Niobec underground mine (Saint-Honoré, Québec), considering different underground instability modes. Moreover, to clarify the role of the aforementioned uncertainties on the different modes of instability, we use a deterministic numerical model simulation to compare rock mass behavior under both a deterministic and a probabilistic stability analysis.

The general and specific objectives of the thesis are presented in the following section.

1.2. Research objectives

The general objective of this thesis is to apply a stochastic evaluation of the role of open stope geometric parameters as well as the variability of rock mass geomechanical parameters, on

different modes of open stope failure in the sublevel open stoping excavation method, using numerical analysis.

The specific objectives of this study are summarized as follows:

- Development of a comprehensive methodology for probabilistic evaluation of the effect of open stope geometry on the rock mass brittle damage by using the brittle shear ratio (BSR) as stability indicator.
- Employing an appropriate data clustering technique to assign realistic range of values to each open stope geometrical parameter in accordance to the common stope geometries of Canadian underground mines
- Applying the response surface methodology (RSM) to identify the significant individual and combined effects of open stope geometrical parameters on the rock mass brittle damage.
- Using the RSM optimization tools to obtain the most stable and the most unstable stopes in terms of brittle damage, by determining the optimum values of stope geometrical parameters.
- Development of a methodology to assess the individual and combined effects of stope geometrical parameters on the open stope's "probability of failure" (POF) by considering both relaxation-related gravity driven failure, and rock mass brittle failure modes.
- Applying a general multi-level factorial analysis to determine the significant individual and interactive effects of open stope geometrical parameters accompanied by

mathematical optimization techniques to predict the most stable stope states (in terms of the POF) by determining the optimal ranges for each geometrical parameter.

- Quantification of the inherent variabilities associated with the rock mass geomechanical parameters, by determining their means, standard deviations and probability density functions.
- Using the Random Monte-Carlo simulation (RMCS) tool in the finite difference code *FLAC3D* in order to incorporate spatial random distributions of rock mass geomechanical parameters in numerical simulations.
- Evaluation of open stope stability in terms of tensile and compressive probabilities of failure (POF) and the probability of brittle damage initiation (PDI), respectively by using the Hoek-Brown tensile and compressive safety factor and the brittle shear ratio (BSR) as stability indicators.
- Probabilistic evaluation of the state of stability for the primary open stopes located in mining blocks V and VI at Niobec underground mine, by considering the inherent variability associated to rock mass geomechanical parameters for the first time.

The adopted methodology to reach the mentioned general and specific objectives of the thesis are presented in the following section.

1.3. Research methodology

The methodology used to meet the objectives of the thesis is summarized through the following procedures. At first, a literature review is conducted on different modes of underground

instability, significant factors influencing the stability of underground open stops (e.g. stope geometry and rock mass geomechanical parameters), common methods of stability analysis and the probabilistic approaches which are used to handle the variability associated to geometric and geomechanical parameters. The effect of open stope geometry on rock mass brittle damage is then assessed using Response Surface Methodology (RSM) in conjunction with numerical analysis. The assessment is accomplished through the determination of rock mass geomechanical properties, state of *in situ* stress and realistic ranges of stope geometric parameters (based on the typical stope dimensions in Canadian underground mines) as input parameters for numerical modeling. Due to the wide range of values for each geometrical parameter in the database, we used cluster analysis by *K*-means clustering technique to partition the data into groups to determine more appropriate parameter variations. The evaluation continued by determination of the significant individual and interaction geometrical parameters on rock mass brittle damage, as well as predicting the most stable stope geometries by using RSM and mathematical optimization techniques.

As the next step, similar procedure is adopted to evaluate the individual and combined effects of stope geometrical parameters on probabilities of tensile and brittle failure considering different instability criteria. A Monte-Carlo simulation technique combined with the finite difference code *FLAC3D* (Itasca 2015) are utilized to simulate 3600 numerical models consisting of stopes divided into different categories of geometry setups. General multi-level factorial analysis determined significant individual and interaction effects of geometrical parameters on probability of failures for each geometric category. Mathematical optimization techniques are ultimately used to predict the most stable stope states (in terms of the POF) by determining the optimal ranges for each geometrical input parameter.

Lastly, probabilistic evaluation of the effect of rock mass geomechanical parameter variability on different modes of underground stability is accomplished on multiple primary stopes at mining levels V and VI at the Niobec Mine, Quebec, using numerical modeling. The variability associated to rock mass geomechanical parameters are incorporated into numerical modeling by using Monte Carlo simulation and Random Monte Carlo simulation methods; while the stability around each open stope is evaluated by calculating the tensile and compressive probabilities of failure, based on the Hoek-Brown tensile and compressive safety factor, and the probability of brittle damage initiation (PDI), via the brittle shear ratio (BSR). Ultimately, by comparing probabilistic numerical model results with those run using a deterministic numerical approach the effect of variability of rock mass geomechanical parameters on stope stability is highlighted.

1.4. Originality and contribution

The novelty of this work in terms of the effect of open stope geometry on its state of stability is to propose a comprehensive methodology to investigate on the significant individual and combined effects of open stope geometrical parameters on various modes of underground failure by using different probabilistic methods in conjunction with numerical analysis. Although literature is rich of studies investigating the effect of excavation geometry on low confinement tensile (gravity-driven) modes of failure, a literature review by the authors indicated that the influence of open stope geometrical parameters on rock mass brittle damage (ultimately causing spalling and slabbing failure) has not fully been studied yet. Moreover, the previous studies mainly focused on the effects of individual parameters while not considering the simultaneous variation of other geometrical parameters. Therefore, the aforementioned studies and their corresponding assumptions present a number of drawbacks. Firstly, most of the previous studies were case

specific, and the variation ranges for selected geometric parameters were limited. Therefore, obtaining a comprehensive interpretation of the effect of selected geometric parameters on the slope stability seemed to be difficult. Secondly, in previous studies, single or multiple parameter(s) were evaluated individually, and therefore the interferences caused by variation of other slope geometric parameters have been underestimated. Finally, in previous studies either relaxation-related tensile failure or rock mass brittle mode of failure was selected to evaluate the state of stability; however, in real conditions the occurrence of different modes of stress-driven failure are possible depending on the applied *in situ* stress regime and rock mass geomechanical characteristics. Thus, it would be more reasonable to consider all possible failure scenarios when evaluating the state of slope stability. Therefore in this study, the probability of open slope failure was also considered as the targeted stability indicator.

Besides, in terms of investigating the effect of rock mass geomechanical variability, the novelty of this study is to employ appropriate probabilistic methods in conjunction with numerical analysis to take into account the inherent uncertainties associated to the rock mass geomechanical parameters in stability analysis. The applied methodology is also applied for stability evaluation of several open slopes in multiple mining blocks at the Niobec underground mine for the first time, as a test for it. Since in reality different modes of stress-induced failure have the possibility of occurrence depending on the applied *in situ* stress regime and rock mass geomechanical characteristics, a comprehensive stability analysis would necessitate adopting multiple failure criteria to address all possible failure mechanism.

1.5. Thesis outline

This thesis resulted in three scientific journal articles which are presented in separate chapters (Chapters 3,4 and 5). Each article chapter in the thesis includes an Introduction and a Conclusion. In addition, a general statement of the problem accompanied with a brief but selected literature review, as well as some of the thesis objectives and outlines as stated in this chapter.

Chapter 1 explains the statement of problems, and describes the research objectives and the adopted methodology to reach the defined objectives, as well as the novelty of the research.

In Chapter 2, a summary literature review is presented on different modes of underground instability, key parameters affecting the stability of underground open stopes and common stability analysis techniques.

Chapter 3 provides a comprehensive evaluation of the effect of stope geometric parameters on the “Brittle Shear Ratio” (BSR) of the rock mass surrounding a stope for three different mining depths. A response surface methodology with a Box–Behnken Design in conjunction with the finite difference code *FLAC3D* (Itasca 2015) is utilized to evaluate the individual and interaction effects of aforementioned input parameters.

Chapter 4 presents a methodology to assess the individual and combined effects of stope geometric parameters on the “probability of failure” (POF) by considering realistic open stope dimensions existing in Canadian underground mines. The POF is calculated considering both relaxation-related gravity driven (tensile) failure, and rock mass brittle failure mode. A Monte-Carlo simulation technique combined with the finite difference code *FLAC3D* (Itasca 2015) are utilized to simulate a large number of stopes, grouped in categories of stope geometry. The individual and interactive effects of the aforementioned geometrical parameters are evaluated by

using a general multi-level factorial analysis. Mathematical optimization techniques are ultimately used to predict the most stable slope states (in terms of the POF) by determining the optimal ranges for each geometrical input parameter.

In chapter 5 seven primary open stopes located in mining blocks V and VI at Niobec underground mine (Saint-Honoré, Québec) are subjected to probabilistic stability analysis using numerical modeling to investigate the effect of inherent variability associated to the rock mass geomechanical parameters. Niobec underground mine has been selected as the case study, due to its unique features in terms of open stope geometry setups, hard rock quality and reported minor collapses and failures. Therefore, probabilistic methods are employed in conjunction with the finite difference code *FLAC3D* (Itasca 2015), to evaluate the state of stability for each aforementioned stopes, by considering the inherent variability associated to rock mass geomechanical parameters. The stability state is defined as tensile and compressive probabilities of failure (POF) and the probability of brittle damage initiation (PDI), respectively by using the Hoek-Brown tensile and compressive safety factor and the brittle shear ratio (BSR) as stability indicators. Monte-Carlo simulation is used to generate the probabilistic rock mass input parameters while Random Monte-Carlo simulation would be utilized to perform one hundred numerical modeling realizations with spatial random distributions of rock mass geomechanical parameters.

Finally in Chapter 6, conclusions, recommendations and perspectives of the future researches are presented.

Chapter 2 - Literature review

2.1. Sublevel stoping excavation method

Among numerous underground excavation methods, sublevel stoping is considered as the most widely practiced technique in Canadian underground mines (Hudson 1993; Wang 2004; Zhang and Mitri 2008; Abdellah et al. 2014b). Depending on the characteristics of the orebody and the surrounding rock mass, stoping methods are classified into three general categories: Unsupported methods, Supported methods and Caving methods (Tatiya 2005). Sublevel stoping method is an Unsupported stoping technique, which is appropriate for fairly strong orebodies having steep inclination and competent wall rock mass (Hustrulid 2001). This method creates large underground openings called “Stopes”, which are formed by vertically dividing the orebody into levels (Fig. 2-1). In this method, two nearby stopes are being separated by a rib pillar left in between. The upper level is being protected by keeping a crown pillar at the top of the stope, while the lower level is used to haul out the crushed ore. Also, the stope itself would be divided vertically into a number of levels called sublevels, referring to the name “Sublevel stoping”. In sublevel stoping technique, the shape of stopes and ore boundaries should be regular. For larger ore bodies, the area between the hanging wall and the footwall is partitioned as primary and secondary stopes. Since the blast hole drills could be used to accomplish drilling, this method is also known as “blast hole stoping” (Hustrulid 2001).

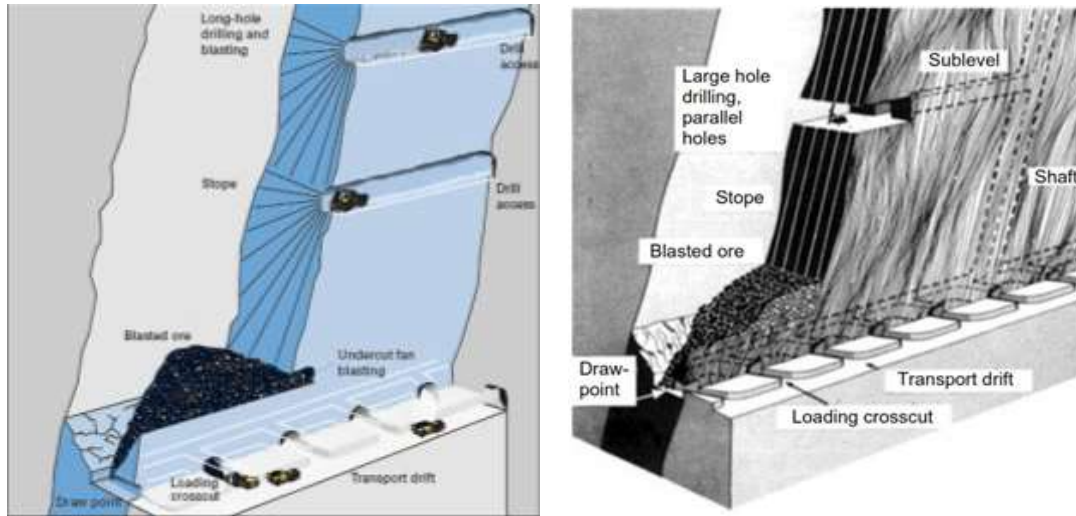


Figure 2-1- Schematic view – sublevel stoping method (Hustrulid 2001)

Recognizing the sources of underground instability is the building block of stability analysis since adopting reliable and efficient solutions for probability of failure estimations and controlling damage requires a comprehensive knowledge of instability reasons. In the following section, different modes of underground instability are presented.

2.2. Instability of underground excavations

Hoek and Brown (1980) identified four principal sources of underground instability (illustrated in Fig. 2-2) which are described by Kelvis (2013) as follows:

- i. *“High rock stress failure associated with hard rock. This kind of failure can occur e.g., when mining at great depth or for large excavations at shallow depth. Stress conditions for tunnelling in steep mountain regions or in weak rock conditions can also result in stress-induced instability problems”;*

- ii. “Structurally controlled failure tends to occur in faulted and jointed hard rocks, in particular when several joint sets are steeply inclined”;
- iii. “Weathered and/or swelling rock failure often associated with relatively poor rock. This kind of failure may also occur in isolated seams within an otherwise sound hard rock”; and
- iv. “Groundwater pressure or flow induced failure, which can occur in almost any rock mass. If this failure is combined with any of the other types of instability listed above, it could reach serious proportions”.

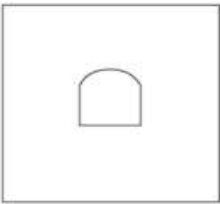
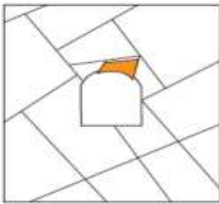
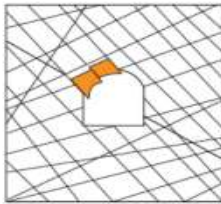
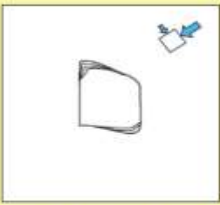
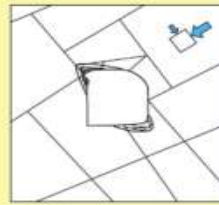
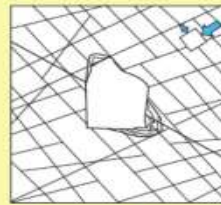
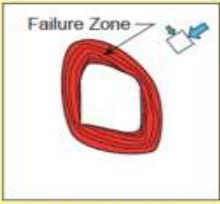
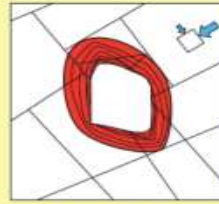
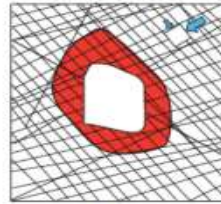
	Massive ($GSI > 75$)	Moderately Fractured ($50 > GSI < 75$)	Highly Fractured ($GSI < 50$)	
Low In-Situ Stress ($\sigma_1 / \sigma_c < 0.15$)	 Linear elastic response.	 Falling or sliding of blocks and wedges.	 Unravelling of blocks from the excavation surface.	$D_f < 0.4 (\pm 0.1)$
Intermediate In-Situ Stress ($0.15 < \sigma_1 / \sigma_c < 0.4$)	 Brittle failure adjacent to excavation boundary.	 Localized brittle failure of intact rock and movement of blocks.	 Localized brittle failure of intact rock and unravelling along discontinuities.	$0.4 (\pm 0.1) > D_f < 1.1 (\pm 0.1)$
High In-Situ Stress ($\sigma_1 / \sigma_c > 0.4$)	 Failure Zone Brittle failure around the excavation.	 Brittle failure of intact rock around the excavation and movement of blocks.	 Squeezing and swelling rocks. Elastic/plastic continuum.	$D_f > 1.1 (\pm 0.1)$

Figure 2-2- Types of failure and instability problems in massive, moderately and highly fractured rock masses under low, intermediate and high in situ stresses (Adapted from Kelvis 2013).

In the case of underground openings located in deep, hard moderately to highly fractured rock mines or for a brittle rock mass context, the high magnitude of mining-induced stresses could cause rock mass damage initiation and sometimes failure in the areas close to the excavation walls (Diederichs 1999a; Castro et al., 2012; Shnorhokian et al. 2015). Failure as a generic term, could be identified in many forms, i.e. plastic yielding, macroscopic boundary cracks, spalling or complete collapse of the excavation (Idris 2014). Hence, recognizing the damage process and subsequent failure modes plays an important role in assessment of underground stope instability. In general, under low confinement conditions, stress-induced instability occurs by two dominant processes, namely; (1) stress-induced spalling and slabbing failure (Fig. 2-3a), and; (2) structurally-controlled, gravity-driven failure (Fig. 2-3b) (Castro et al., 2012).

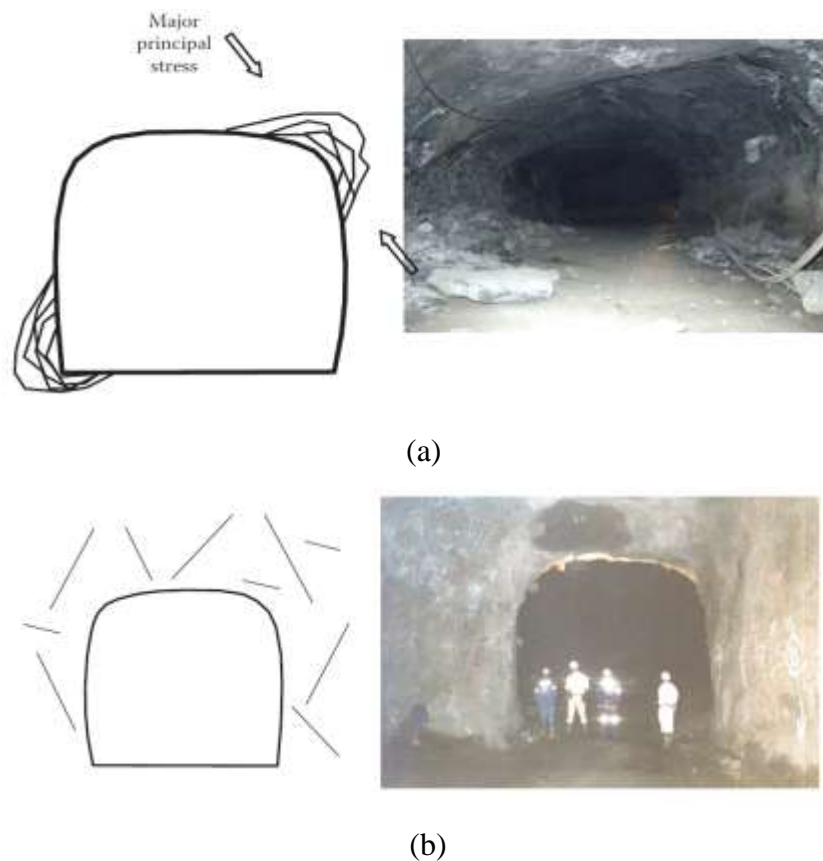


Figure 2-3- (a) Spalling and slabbing around an excavation; (b) Potential of structurally-controlled gravity-driven failure (Adapted from Villaescusa 2014)

The damage process commences with the creation of extension micro fractures within the intact rock bridges in the rock mass as a result of high compressive stress regime. These compression-induced tension cracks normally tend to form parallel to the major principal induced stress σ_1 or more accurately, normal to minor principal induced stress σ_3 (Fig. 2-4a). Accumulation and propagation of these cracks finally leads to the development of macro-fractures and release surfaces (Fig. 2-4b) (Diederichs 2004).

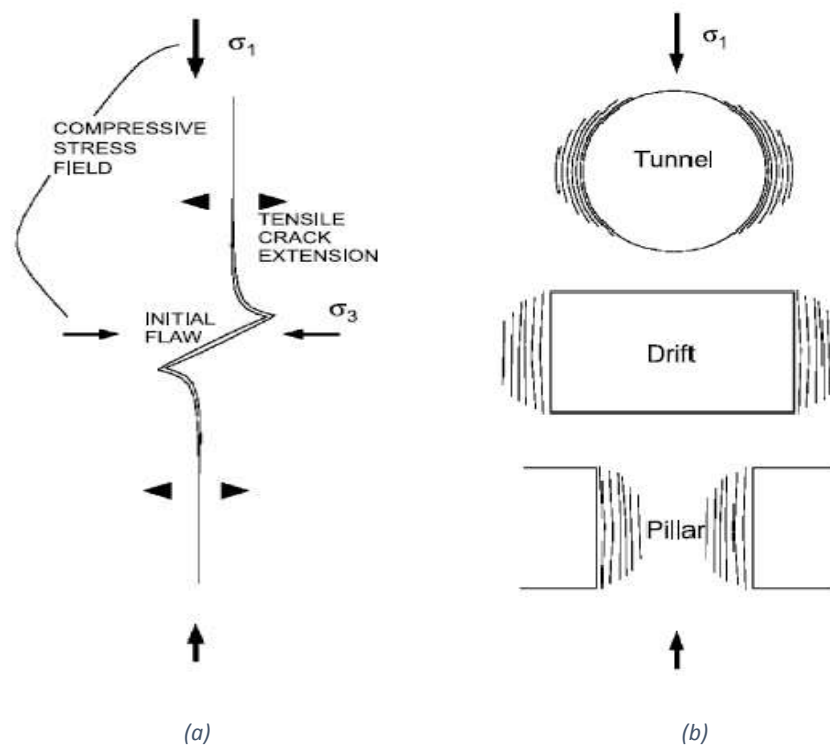


Figure 2-4- (a) Creation of the compression-induced tension cracking parallel to σ_1 ; (b) Field-scale spalling to excavation walls; (Adapted from Diederichs 2004).

For brittle rock masses, the result of the mechanics of tensile fracture accumulation and propagation and the consequent failure modes can be represented by the strength envelope (Fig. 2-5).

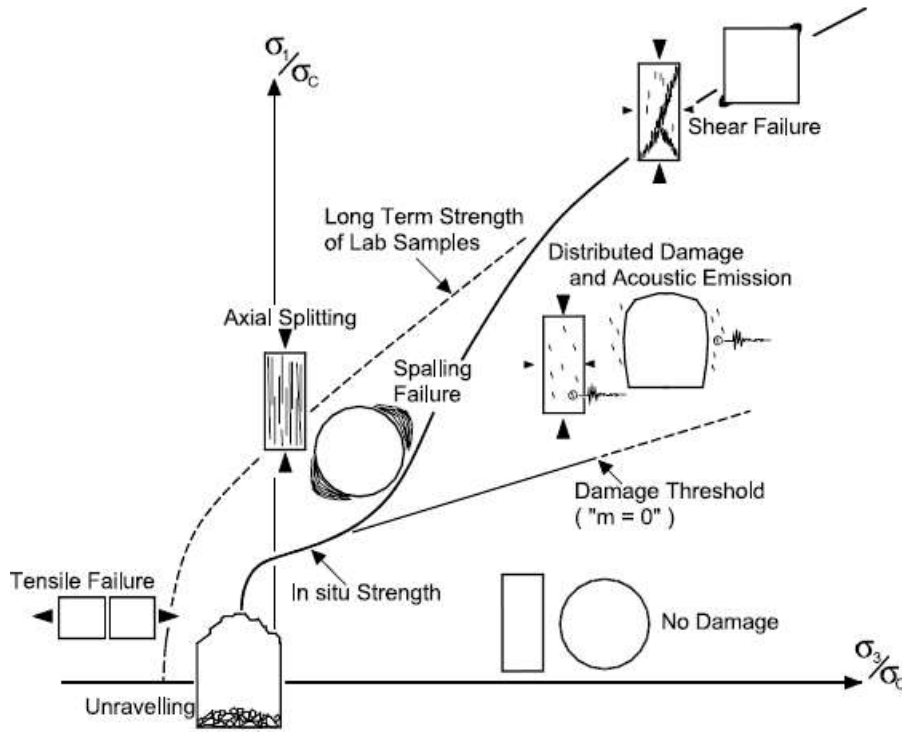


Figure 2-5- Schematic of strength envelope, presenting different rock mass failure mechanisms: no damage, shear failure, spalling, and unraveling. σ_c stands for the unconfined compressive strength (UCS) of intact rock (Adapted from Diederichs 2004)

As explained by Diederichs (2004), the rock is undisturbed below the “damage initiation threshold”. In the case of gravity-driven, structurally-controlled tensile failure, tangential and radial stresses decrease drastically, creating an unconfined area, or a relaxation zone, around the opening. Consequently, relaxation in the walls reduces the minor principal induced stress to zero or less and creates tensile stress (Diederichs 1999a; Kaiser et al. 2000; Diederichs 2004; Castro et al., 2012). It should be noted that, according to Kaiser et al. (2000), relaxation in excavation walls is attributed to the reduction of tangential stresses (the major and/or intermediate principal stress) parallel to the walls, not to the radial stress component which leads to low confinement (Henning 2007). In the case of spalling failure, when a stress path moves to the left side of the low confinement zone, (into the zone marked “spalling failure” in Fig. 2-5), and goes beyond the damage initiation threshold, the magnitude of the minor principal induced stress (σ_3) near the

excavation walls undergoes a significant reduction, whereas the tangential stress increases to its maximum, leading to spalling normal to the minor principal induced stress (Diederichs 2004). Normally, the spalling-slabbing failure continues to a certain depth within the wall boundaries creating notch shaped geometries.

Instability of an open slope is influenced by several factors such as rock mass geomechanical parameters, natural and mining-induced stress state, and slope geometrical parameters (Diederichs and Kaiser 1996; Chen et al., 1997; Henning and Mitri 2007; Idris et al. 2013; Villaescusa 2014). The literature is rich of studies which utilized different methods to explain and evaluate the effects of aforementioned factors on different instability modes. In the following sections, a brief review on previous important studies are presented.

2.2.1. Effect of slope geometrical parameter variations

Slope geometry plays a key role in defining the level of stability when it comes to stability analysis issues. However, effect of slope geometry has been found critical by many authors (Aglawe 1999; Zhang and Mitri 2008; Villaescusa 2014); detailed effect of these parameters on slope stability has not been fully understood yet. Geometry of an open slope is defined through its geometrical parameters such as slope strike length, slope span width, slope hanging wall dip and slope hanging wall size and shape (which is characterized by hanging wall hydraulic radius (HR)) (Fig. 2-6). The hydraulic radius (HR) is a parameter which is calculated for each exposed surface of a slope while taking into account the combined effect of surface size and shape (Wang 2004; Watson 2004). The hydraulic radius is also referred by the shape factor. The HR is calculated by dividing the area of a slope surface by the perimeter of that surface (Eqn 2-1).

$$HR = \frac{\text{Area of the surface}}{\text{Perimeter of the surface}} \quad (2-1)$$

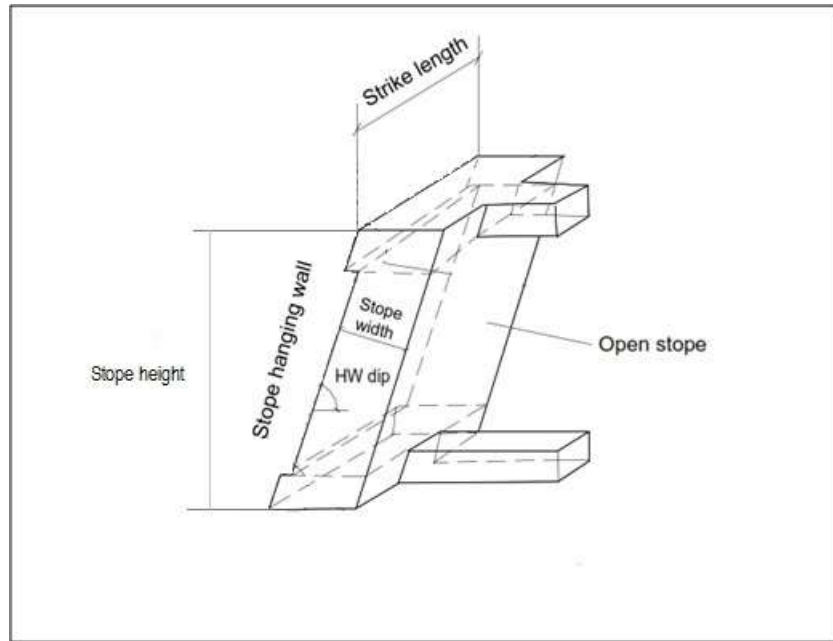


Figure 2-6- Schematic of an open stope geometry and its associated geometrical parameters (Adapted from Wang 2004)

Effect of open stope geometry (shape, size and inclination) on the state of stability, can be evaluated by using different analytical, empirical and numerical approaches.

Almost all empirical stability analysis systems have addressed the effects of excavation geometry on its stability (Germain and Hadjigeorgiou 1997). In tunnel design for instance, the influence of excavation's height and width on its state of stability was studied by Terzaghi (1946) for the first time (cited by Germain and Hadjigeorgiou 1997). Similarly, the notion of unsupported span and its stand-up time has been explained by Lauffer (1958) (cited by Germain and Hadjigeorgiou 1997). Moreover, conventional rock mass classification systems (e.g. RMR, Q) which are commonly used as underground stability evaluation tools, correlate rock mass quality

to excavation geometry (cited by Germain and Hadjigeorgiou 1997). Also, the effect of open stope geometry in terms of hanging wall hydraulic radius (HR) or radius factor (RF) has been incorporated in stability graph methods (Mathews 1981; Potvin 1988; Milne 1996; Wang 2004).

On the other hand, numerical analysis has been employed by many authors, mostly to assess the effect of stope geometrical parameters on low confinement tensile (gravity-driven) mode of failure. As a pioneering research, Chen et al. (1983) assessed the effect of open stope height by applying finite element method and found it as a critical design parameter. Pakalnis et al. (1995) reported that mining of narrow stopes increases the rate of instability. Milne (1997) linked the hanging wall geometry of an open stope with measured deformation as an instability indicator and successfully substituted the hanging wall HR with RF term in order to analyze more complex geometries. Germain and Hadjigeorgiou (1997) defined an index for stope geometry by dividing the volume of a stope and its real surface area (RVS) as a measure of stope geometrical complexity to assess the applicability of the stability graph method. Clark (1998) introduced a new parameter called ELOS (Equivalent Linear Overbreak or Slough) to evaluate the amount of dilution of a stope hanging wall and reported that increasing the HR of the stope hanging wall contributes in increasing the extent of hanging wall overbreak. Perron (1999) have shown that stope height and geometry complexity adversely affect the stability of the hanging wall and suggested that stopes having 60m height at the Langlois Mine be re-designed in order to reduce dilution (cited by Henning and Mitri 2007). Aglawe (1999), concluded that the geometry of the excavations is considered as the most significant factor influencing the occurrence of strainburst in highly stressed ground. Wang (2004) developed a method to correlate stope geometry and induced stress state through design graphs to evaluate stress relaxation related dilution. Afterwards, Wang et al. (2007) examined the effect of stope geometrical parameters on the extent of the zone of relaxation

by the aim of numerical modeling. Henning and Mitri (2007) assessed the effect of orebody dip on the unplanned dilution and reported that shallower hanging wall dip caused more dilution due to increasing the depth of overbreak. Hughes (2011) examined the effect of stope strike length on ore dilution in narrow vein longitudinal mining by using finite element method and realized that longer stope strike lengths generate larger volumes of dilution, while shorter strike lengths are less prone to dilution. In recent studies, El Mouhabbis (2013) investigated the effects of stope geometry on ore dilution and concluded that stope construction geometry has significant effect on overbreak in a way that increasing stope strike length increases overbreak, shallower ore dip causes hanging wall overbreak enhancement and finally narrow stopes exhibit higher dilutions.

In a review of previous studies, Villaescusa (2014) stated a general assumption that open stopes with high vertical and short horizontal dimensions, and/or long horizontal and short vertical dimensions have a higher degree of wall stability compared to square-shaped geometries, which are considered to generate the most unstable open stopes.

As mentioned above, literature is rich of studies investigating the effect of excavation geometry on low confinement tensile (gravity-driven) modes of failure. Nevertheless, a literature review by the authors indicates that the influence of open stope geometrical parameters on rock mass brittle damage (ultimately causing spalling and slabbing failure) has not fully been studied yet.

2.2.2. Effect of uncertainties in the rock mass geomechanical parameters

The term rock mass refers to the assembly of intact rock material which is being separated by different types of three dimensional discontinuities (Edelbro 2004, Idris 2014). In terms of geomechanical behavior, a discontinuity as a major mechanical breakage within the rock that has

zero or negligible tensile strength, low shear strength and high fluid conductivity in comparison to the intact rock material (Edelbro 2004). The intact rock itself has mechanical properties such as uniaxial compressive strength (UCS), tensile strength, Young's modulus, etc. Thus, the rock mass geomechanical properties are defined based on the properties of both the intact rock materials and the discontinuities (Idris 2014).

The aleatory uncertainty (inherent variability) associated with rock mass physio-mechanical properties is a result of natural spatial randomness in the rock mass caused by the geological processes (Nadim, 2007, Idris 2014). The existing aleatory uncertainty on one hand, cannot be eliminated or reduced (Bedi and Harrison 2012) and on the other hand cannot be neglected since it is reported (Idris 2014) to influence the rock mass behavior in terms of strength and stiffness.

There are several approaches to estimate the strength and deformability parameters of jointed rock mass which includes (Edelbro et al. 2007):

- (i) Empirical failure criterion combined with rock mass classification systems;
- (ii) Large-scale testing; and
- (iii) Back-analysis of existing failures;

Among the above mentioned approaches, using empirical failure criteria in conjunction with rock mass classification methods has received more attention due to their many advantages including flexibility and simplicity (Edelbro et al. 2007).

Among the numerous developed rock mass classification methods such as RQD (Deere, 1967), the rock mass rating (RMR) (Bieniawski, 1976, 1989), the tunnelling quality (Q) (Barton

et al. 1974), the geological strength index (GSI) (Hoek et al., 1995) and the rock mass index (RMI) (Palmström, 1995). The GSI method is considered as the only rock mass classification system which has a direct link to engineering parameters such as Hoek-Brown strength and deformability parameters (Cai et al. 2004). Since GSI method has been frequently used in this study to estimate the rock mass geomechanical parameters. A brief summary of the method is presented in the following subsections.

2.2.2.1. Geological Strength Index (GSI)

GSI rock mass classification system was introduced for the first time by Hoek et al. (1995) in order to enable their generalized rock failure criterion to calculate the Hoek-Brown strength parameters s , a and m_b . The value of GSI for different types of rock mass is obtained by using the GSI table (Fig. 2-7) which provides a qualitative description of the rock mass in terms of structural quality (blockiness) and surface conditions (Hoek 2007). An important feature of the GSI system is its easy application in the field since it uses the two key parameters of the geological process named “*the blockiness of the mass*” and “*the conditions of discontinuities*”. Moreover, since both the RMR and the Q classifications use the RQD classification to rate the rock mass, and since the RQD value in most of the weak rock masses is either very small or considered meaningless, it became essential to develop an alternative classification system which not only eliminates RQD as an input parameter but also put greater emphasis on basic geological observations of rock mass. Therefore, the new system not only reflects the material properties, structure and geological history, but also is developed particularly to estimate the rock mass geomechanical properties (Hoek 2007).

<p>GEOLOGICAL STRENGTH INDEX FOR JOINTED ROCKS (Hoek and Marinos, 2000)</p> <p>From the lithology, structure and surface conditions of the discontinuities, estimate the average value of GSI. Do not try to be too precise. Quoting a range from 33 to 37 is more realistic than stating that GSI = 35. Note that the table does not apply to structurally controlled failures. Where weak planar structural planes are present in an unfavourable orientation with respect to the excavation face, these will dominate the rock mass behaviour. The shear strength of surfaces in rocks that are prone to deterioration as a result of changes in moisture content will be reduced if water is present. When working with rocks in the fair to very poor categories, a shift to the right may be made for wet conditions. Water pressure is dealt with by effective stress analysis.</p>		SURFACE CONDITIONS				
STRUCTURE		VERY GOOD	GOOD	FAIR	POOR	VERY POOR
		Very rough, fresh unweathered surfaces	Rough, slightly weathered, iron stained surfaces	Smooth, moderately weathered and altered surfaces	Slickensided, highly weathered surfaces with compact coatings or fillings or angular fragments	Slickensided, highly weathered surfaces with soft clay coatings or fillings
		DECREASING SURFACE QUALITY →				
	INTACT OR MASSIVE - intact rock specimens or massive in situ rock with few widely spaced discontinuities	90	80		N/A	N/A
	BLOCKY - well interlocked undisturbed rock mass consisting of cubical blocks formed by three intersecting discontinuity sets		70			
	VERY BLOCKY - interlocked, partially disturbed mass with multi-faceted angular blocks formed by 4 or more joint sets		60			
	BLOCKY/DISTURBED/SEAMY - folded with angular blocks formed by many intersecting discontinuity sets. Persistence of bedding planes or schistosity		50			
	DISINTEGRATED - poorly interlocked, heavily broken rock mass with mixture of angular and rounded rock pieces		40		30	
	LAMINATED/SHEARED - Lack of blockiness due to close spacing of weak schistosity or shear planes	N/A	N/A		20	10
		← DECREASING INTERLOCKING OF ROCK PIECES				

Figure 2-7- Geological Strength Index table for jointed rocks (Hoek 2007)

In fact, by having the GSI value of the rock mass accompanied by the values of the uniaxial compressive strength of intact rock (UCS) and the petrographic constant m_i , geomechanical parameters of rock mass (such as the Hoek-Brown strength parameters (m_b , s and a) and the deformation modulus (E_m)) can be determined using the equations provided by the generalized Hoek-Brown failure criterion (Hoek 2007).

2.2.2.2. The generalized Hoek-Brown failure criterion

The general form of Hoek – Brown failure criterion is given by (Eqn 2-2):

$$\sigma_1 = \sigma_3 + \sigma_{ci} \left(m_b \frac{\sigma_3}{\sigma_{ci}} + s \right)^a \quad (2-2)$$

Where σ_1 and σ_3 are the major and minor effective principal stresses at failure, respectively, m_b is the Hoek-Brown constant which reflects the characteristics of the rock mass, and σ_{ci} is the uniaxial compressive strength (UCS) of the intact rock sample. Rock mass constants (m_b , s and a) would be calculated by the following equations (Eqns 2-3 to 2-5) (Idris 2014):

$$m_b = m_i e^{\left(\frac{GSI-100}{28-14D} \right)} \quad (2-3)$$

$$s = e^{\left(\frac{GSI-100}{9-3D} \right)} \quad (2-4)$$

$$a = \frac{1}{2} + \frac{1}{6} \left(e^{\frac{-GSI}{15}} - e^{\frac{-20}{3}} \right) \quad (2-5)$$

Where D is a parameter related to the degree of disturbance of the rock mass caused by blasting and stress relaxation. It varies from 0 for undisturbed *in situ* rock masses to 1 for very

disturbed rock masses. By setting $\sigma_3 = 0$ in equation 2-2, the uniaxial compressive strength of the rock mass will be calculated as follow (Eqn 2-6) (Idris 2014):

$$\sigma_{cm} = \sigma_{ci} s^a \quad (2-6)$$

By setting $\sigma_1 = \sigma_3 = \sigma_t$ in the equation 2-2 the tensile strength could be obtained (Eqn 2-7):

$$\sigma_t = \frac{s\sigma_{ci}}{m_b} \quad (2-7)$$

To calculate the deformation modulus of the rock mass E_m (Eqn 2-8) (Idris 2014):

$$E_m = E_i \left(0.02 + \frac{1 - \frac{D}{2}}{1 + e^{\frac{60 + 15D - GSI}{11}}} \right) \quad (2-8)$$

The required parameters for the Mohr-Coulomb failure criterion such as the friction angle, the cohesion and the tensile strength for each rock mass can also be obtained, using the Eqns (2-9 and 2-10):

$$\varphi = \sin^{-1} \left[\frac{6am_b(s + m_b\sigma_{3n})^{a-1}}{2(1+a)(2+a) + 6am_b(s + m_b\sigma_{3n})^{a-1}} \right] \quad (2-9)$$

$$c = \frac{\sigma_{ci} \left[(1+2a)s + (1-a)m_b\sigma_{3n} \right] (s + m_b\sigma_{3n})^{a-1}}{(1+a)(2+a) \sqrt{\frac{1 + 6am_b(s + mb\sigma_{3n})^{a-1}}{(1+a)(2+a)}}} \quad (2-10)$$

Where φ is friction angle, c is the cohesion and σ_{3n} is the normalized minor principal stress

and is equal to $\sigma_{3n} = \frac{\sigma_{3max}}{\sigma_{ci}}$.

In the case of an underground excavation which is bounded by a zone of failed rock that does not extend to the surface σ_{3max} can be determined by using the following equation (Eqn 2-11) (Idris 2014):

$$\frac{\sigma_{3max}}{\sigma_{cm}} = 0.47 \left(\frac{\sigma_{cm}}{\gamma H} \right)^{-0.94} \quad (2-11)$$

In the equation above, σ_{cm} refers to the rock mass strength, γ is the unit weight of the rock mass and H is the depth of the excavation from the surface. If the horizontal stresses, has a higher value than the vertical stress, the maximum horizontal stress value should be used instead of γH . In the Canadian shield, the horizontal stresses are higher than the vertical stress and therefore, the maximum horizontal stress is used instead of γH (Idris 2011b).

Due to the presence of the variability associated with the aforementioned rock mass classification/characterization parameters, Hoek (2007) suggested to use random values (range of values) as input for the Hoek-Brown-GSI method. Probabilistic methods provide solutions to incorporate the uncertainty associated to the rock mass geomechanical parameters into stability analysis of underground open stopes (Idris 2014). The application of probabilistic methods in conjunction with numerical stability analysis is described in the following sections.

2.3. Stability analysis of an underground open stope

There are three groups of approaches commonly used to analyze the stability of underground excavations (Brady and Brown 2004):

- i. Analytical methods;
- ii. Empirical Methods; and
- iii. Numerical Methods.

For simple excavation geometries such as circular openings and two dimensional wedges, the analytical methods are considered appropriate (Idris 2014). Applying an analytical method is dependent on the analysis of a structural instability and rock-support interaction. In the structural instability analysis, the shape and size of unstable wedges surrounding the structure, structure geometrical characteristics (such as size shape and orientation) and discontinuity directions in the region have to be taken into consideration. Since three-dimensional geometrical calculation of the structure is time consuming and frustrating (Gharavi 2008), the analytical methods such as those provided by Kirsch (1898), Ladanyi (1974) and Bray and Lorig (1988) (cited by Idris 2014) could not be efficient enough for complex mining problems.

The empirical methods can be divided into two main categories: The first category utilizes rock mass classification systems to rate the quality of the rock mass. Amongst the rock mass classifications, RMR and Q methods are the most commonly used systems in stability analysis of underground excavations (Gharavi 2008; Idris 2014). The second category is empirical underground excavation design which analyses the stability of an excavation by combining the geometry of excavation and the rock mass quality (Idris 2014). The most common method from this category is the Stability Graph Method introduced by Mathews et al. (1981) and modified by Potvin (1988) (cited by Idris 2014). The Q classification system is used in the stability graph method; the effect of stress state, joint orientations with regard to excavation and the geometry of the excavation are taken into consideration (Wang 2004; Idris 2014). This method is widely used

especially in Canadian mines although its application is limited by some types of boundaries. There are some limitations restricting the functionality of the stability graph which have been studied in numerous articles. These limitations are described by Idris et al. (2014) as follows “*poor representation of the sliding failure modes in footwalls by the gravity factor, the stress factor not taking into account instabilities by tension, oversimplification of complex geometry (as hydraulic radius can only be calculated from regular shape), effects of faults not considered and subjectivity in defining the stability zones*”. In addition, since the implementation of the stability graph method is site specific, no general application for this method is assumed (Idris 2014).

Most of the limitations of analytical and empirical methods are circumvented by the numerical methods and hence these methods are widely used in the past several decades for the design and stability analysis of underground excavations due to advances in computing power (Bobet 2010). Numerical modelling methods are utilized to simulate the induced stress distribution around an opening. Using the simulated stress situation, the stability of an excavation can be estimated by applying failure criteria based on the material strength properties (Wang 2004).

According to Jing and Hudson (2002) numerical methods applied for rock mechanics problems are:

(i) Continuum methods

- a. Finite Difference Method (*FDM*);
- b. Finite Element Method (*FEM*); and
- c. Boundary Element Method (*BEM*)

(ii) Discrete methods

- a. Discrete Element Method; and
 - b. Discrete Fracture Network Method
- (iii) Hybrid continuum/discrete methods.

In a broader classification, numerical methods are categorized into continuum and discontinuum methods. Continuum methods are able to incorporate the discontinuities in the medium, explicit or implicitly, whereas in discontinuum methods, discontinuities are incorporated only explicitly (Bobet 2010). Selection of continuum or discontinuum methods, for a particular problem, is accomplished by considering the size, or scale, of the discontinuities with respect to the size, or scale, of the problem. The Finite Difference Method (FDM), as the oldest numerical method used in geomechanics problems, utilizes differential equations represented by finite differences. This method is very well-designed to incorporate non-linear behavior of geomaterials (e.g. soil and rock mass) (Bobet 2010).

The above mentioned approaches usually use single or mean values of the input parameters to analyze the stability of the underground excavations and hence, they are considered as deterministic methods. Mostly, to avoid facing the inconveniences resulted by variations and uncertainties of rock properties, deterministic approaches which use single or mean values of rock mass properties are implemented. The results obtained by using traditional deterministic approaches are often considered as not reliable enough because uncertainties and variability in the rock mass properties have not been taken into account (Idris et al., 2013).

In order to prevent these drawbacks and obtain reliable results, probabilistic approaches have been increasingly used by many researchers. A probabilistic approach can be applied to all of the methods by assuming their input parameters as random variables. By using these

approaches, engineers are able not only to obtain the expected value but also their possible variation and subsequently a more comprehensive description of the rock mass behavior (Idris 2014). A comprehensive description of different common probabilistic methods used in geomechanics problems are presented in the following section.

2.3.1. Probabilistic Approaches

In order to handle the uncertainty associated with the variability of a parameter, it is assumed as a random variable within a range of values, of which certain values may occur more frequently than others (Whitman and Shuster 1984). For instance, in terms of variability in rock mass properties, for the parameters such as the uniaxial compressive strength of rock mass, rock mass deformation modulus or the Poisson's ratio, assign a single exact value is impossible while any value in a certain range can be assumed (Hoek and Brown 2007). In order to quantify this uncertainty, the probability distribution of the random variable should be determined through the determination of its statistical moments such as mean and variance. Subsequently, the probability density function (PDF) describes the relative likelihood that a random variable will adopt a specific value. The concept of probability theory would be applied through probabilistic methods (Idris 2014).

Probabilistic methods can be grouped into (i) analytical approximation methods and (ii) sampling based methods. Analytical approximation methods, such as the first-order second moment method, require readily available explicit functions which makes them unsuitable to apply for underground excavation problems. On the other hand, sampling based methods which are divided into discrete sampling and random sampling (simulation based) method are considered

suitable to be used for underground stability analysis especially in conjunction with numerical modeling (Park et al. 2012). The Point Estimate Methods (PEMs), the Response Surface Method (RSM) and the Artificial Neural Network (ANN) are among the most frequently used discrete sampling methods in rock mechanics problems, while Monte Carlo Simulation (MCS), Random Monte Carlo Simulation (RMCS) and Strength Classification Methods are considered as the most common simulation-based methods. Simulation based methods are able to consider the heterogeneous nature of the rock mass into the numerical modeling by randomly distributing the rock mass properties within the model domain (Idris 2014).

The application of different probabilistic methods in a wide range of geotechnical engineering problems such as block analysis, slope stability and others have been studied by numerous authors, as cited by Abdellah et al.(2014a) and Idris (2014): (Rosenblueth, 1975, 1981; Chang et al., 1995; Estherhuizen 1996; Diederichs and Kaiser 1996; Estherhuizen and Streuders 1998; Grenon and Hadjigorgiou 2003; Christian and Baecher, 1999, 2002, 2003; Peschl and Schweiger 2002; Schweiger and Thurner, 2007a; Hammah et al., 2008; Dunn et al. 2008; Musunuri et al., 2009 and Bagheri 2011).

In the case of underground stability problems, the application of probabilistic methods have been investigated in several studies, mostly related to stress induced problems. Diederichs and Kaiser (1996), developed a methodology to take into account the variability and uncertainty in calibration and input data of the modified stability graph method for stability assessment of open stopes. Chen et al. (1997), applied the first-order second-moment approximation method to determine the probability of failure for two underground excavation stability cases including a horizontal rock roof and an underground prism. The study indicated the important role of parameter values distributions of which high dispersion of input parameter values (more scattered

pattern), resulted in different probability of failures while the factor of safety remains unchanged. Langston et al. (2001), assessed the probability of hanging wall failure in sublevel open stopes at the Stillwater Mine in Montana and provided a skeletal graph relating probability of failure to rock mass parameters and stope geometry. Griffiths et al. (2002) applied probabilistic methods (Random field theory and Monte Carlo simulation) with numerical analysis to evaluate the influence of spatially varying compressive strength on stability of underground pillars. They concluded that the deterministic average value of rock strength is not a good indicator of the overall strength of the pillar.

Valley et al. (2010) implemented the PEM/FEM probabilistic approach to investigate the effect of variability in modelling the behavior of underground excavations. The study indicated that although PEM/FEM approach offers an attractive opportunity to handle inherent geomechanical uncertainty, it shows limitations and provide inaccurate results by increasing the number of random input variables. Cai et al. (2011) utilized a quantitative risk assessment to quantify the uncertainties in tunnel and cavern design parameters by numerical modelling. The proposed approach used the GSI system to characterize the rock mass and recommend the final required rock support. Lü and Low (2011) performed a probabilistic analysis using RSM and SORM (Second-order reliability method) to evaluate the stability of underground rock excavations considering multiple failure modes. Guarascio and Oreste (2012) proposed a probabilistic approach to evaluate the degree of safety of a pillar in the room and pillar mining method, which considers the typical uncertainty associated with the geomechanical parameters of the rock mass. Abdellah et al. (2013) used the RMCS in conjunction with finite difference FLAC to assess the effect of geomechanical parameter variability of the rock mass on the state of mine haulage drifts stability.

Goh et al. (2012) employed the shear strength reduction technique to determine the factor of safety with regard to stress-induced instability for deep underground caverns. By applying the neural networks analysis, they provided an empirical equation which correlates factor of safety to cavern dimensions and rock mass quality (Q). They also concluded that the probability of failure (reliability index) is majorly affected by the coefficient of variation of Q . Langford and Diederichs (2013) assessed the performance of a composite tunnel lining by using a new reliability-based design approach which utilized a modified Point Estimate Method (PEM), First Order Reliability Method (FORM), Monte Carlo sampling method and finite element analysis. The general rock mass and the composite lining system characteristics were considered as input parameters. By using the numerical modelling, the behavior of the lining over the range of possible rock mass and *in situ* stress values was investigated and the reliability index and probability of failure for a given liner section were determined. Pytel (2013) used RSM in conjunction with numerical modeling to assess the impact of rock mass geomechanical parameter variability on stability state of underground excavations. Abdellah et al. (2014b) proposed a methodology to assess the probability of instability of a mine development intersection at Vale's Garson Mine in Sudbury, Ontario, by employing the modified Point-Estimate Method (PEM) in conjunction with Finite difference modeling software *FLAC3D*. Idris (2014), evaluated different probabilistic methods such as Point Estimate Methods (PEM), Artificial Neural Network (ANN), Response Surface Method (RSM) and others to determine the role of uncertainties in rock mass properties on underground stope stability.

Zhao et al. (2016) used Monte Carlo simulation to incorporate the variability of the cohesion and friction angle of rock mass for stochastic evaluation of overall rock block failure in a copper mine site in Australia. The Monte Carlo Simulation method, Random Monte Carlo

Simulation method and Response Surface Method which are employed in this study, are briefly described in the following section.

2.3.1.1. Monte Carlo Simulation (MCS)

The Monte Carlo Simulation method (MCS) is considered as a computational algorithm, utilized by a wide range of engineering and scientific disciplines which employs repeated random sampling technique to obtain continuous numerical values from a distribution of an uncertain input variable. In fact, the MCS generates the probability distribution function (PDF) of an output variable, by generating random or pseudo-random values from the PDF of the input variables through a large number of realizations (Hoek 2007; Langford and Diederichs 2013; Idris 2014).

In underground stability problems, the MCS is recognized as a powerful probabilistic tool since it is able to define the heterogeneous nature of a rock mass into numerical models by randomly assigning various material properties in the model according to their PDFs (Idris 2014). It should be noted that, in Monte Carlo Simulation, the distribution of all the input variables should be known or properly assumed (Hoek 2007). Subsequently, by generating the distribution of the resulting output variables (e.g. strain, displacements), their statistical moments can be determined to calculate the probability of failure and reliability index (Langford and Diederichs 2013). Although, the accuracy of the MCS method increases by increasing the number of simulations, using relatively few number of simulations (e.g. 100 simulations) is reported to provide enough accuracy to approximate the statistical moments of response variables (Idris 2014).

MCS offers advantages such as the ability of generating a large number of various probability distributions with no need of much approximations while it suffers from drawbacks

such as being computationally expensive, operationally time consuming and requires large computer storage (Abdellah 2014b).

2.3.1.2. Random Monte Carlo Simulation (RMCS)

The RMCS is a probabilistic technique which considers the spatial variability of a variable at the local scale while the MCS incorporates the global variability associated to an input variable. In terms of rock mass characterization, the RMCS is capable of assigning spatially random values of geomechanical parameters within a given region of the rock mass in the model (Abdellah 2014a). RMCS generates a new initial seed values for each new spatial random assignment of input variable. It is reported by Abdellah et al., (2012) that the required number of simulations with RMCS is considerably smaller than with MCS. In this method, a random value of each input variable is selected from their PDF and is spatially assigned to the numerical grid model as a random seed. The process repeats for a certain number of random seeds (runs) to obtain the probability distribution of output variables and calculating the probability of failure based on the predefined failure criterion.

2.3.1.3. Response Surface Methodology (RSM)

Among numerous probabilistic approaches used in rock mechanic problems, response surface methodology (RSM) as a discrete sampling probabilistic method is capable of assessing individual and interaction effect of input parameters on single or multiple response variables. RSM consists of a set of mathematical and statistical tools employed to generate an implicit mathematical expression between a dependent output response and a collection of input variables

(Idris 2014). In other word, RSM as a collection of mathematical and statistical techniques, develops a functional relationship between an output variable and a number of independent input variables. The functional relationship between the output and input variables is generally defined by two common models of first-order and second-order equations.

RSM applies a sequential procedure starting through the design of experiments (DOE). DOE is a series of tests (runs), in which changes are made in the independent input variables in order to recognize the causes for changes in the dependent output variable (Ahmadi et al. 2014). DOE selects the points where the response variable should be assessed. Box-Behnken design (BBD), central composite design (CCD) and full factorial design are amongst the most useful DOE algorithms. The aim of using RSM is to design, improve and optimize different processes (Anderson and Whitcomb 2005). By using this approach, not only the effects of individual input variables, their relative significance and the interactive effect of two or more variables can be evaluated, but also the optimum conditions for desired responses can be determined.

The RSM approach generally applies the following two steps: the first step is to generate the model mathematical expression to determine which input parameters and their interactions have significant influence on the response; and the second step is to optimize the significant individual parameters to obtain the desired value of response (Ahmadi et al. 2014). The RSM is able to determine appropriate regression models and the significant input parameters (Ahmadi et al. 2014). RSM has been applied in conjunction with numerical modeling to evaluate the stability of underground rock excavations (Mollon and Dias 2009; Lü and Low 2011; Pytel and Świtoń 2013).

2.4. References

- Abdellah W, (2013). Geotechnical risk assessment of mine haulage drifts during the life of a mine plan. PhD thesis, McGill University, Montreal, Canada.
- Abdellah W, Mitri HS, Thibodeau D, Moreau-verlaan L, (2014)a. Stability of mine development intersections — a probabilistic analysis approach.;195:184–95.
- Abdellah W, Raju GD, Mitri HS, Thibodeau D. (2014)b. Stability of underground mine development intersections during the life of a mine plan. *Int J Rock Mech Min Sci.* 72:173–181.
- Aglawe JP. (1999). Unstable, violent failure around underground openings in highly stressed ground. PhD thesis, Queen’s University at Kingston.
- Ahmadi A, Heidarzadeh S, Reza A, Darezereshki E, Asadi H. (2014). Optimization of heavy metal removal from aqueous solutions by maghemite ($\gamma\text{-Fe}_2\text{O}_3$) nanoparticles using response surface methodology. *J Geochemical Explor.* 147:151-158.
- Anderson MJ, Whitcomb PJ. (2005). *RSM Simplified Optimizing Processes Using Response Surface Methods for Design of Experiments.* Productivity Press.
- Barton, N.R., Lien, R., Lunde, J., (1974). Engineering classification of rock masses for the design of tunnel support. *Rock Mech.* 6, 189-239.
- Baecher, G. B. & Christian J.T, (2003). *Reliability and Statistics in Geotechnical Engineering,* John Wiley & Sons Ltd, England.
- Bagheri, M. (2011). Block stability analysis using deterministic and probabilistic methods. Ph.D. Thesis, Royal Institute of Technology, Stockholm.
- Bedi, A., & Harrison, J. (2012). Dealing with epistemic uncertainty in fractured rock masses. Paper presented at the ISRM International Symposium-EUROCK 2012,
- Bieniawski, Z. T. (1976). Rock mass classification in engineering. Paper presented at the symposium on exploration for rock engineering, Johannesburg.
- Bieniawski, Z. T. (1989). *Engineering rock mass classifications: A complete manual for engineers and geologists in mining, civil, and petroleum engineering.* John Wiley & Sons.
- Bobet, A., (2010). Numerical methods in geomechanics. *The Arabian Journal for Science and Engineering,* 35(1B), pp.27–48.
- Brady, B. H. G., & Brown, E. T. (2004). *Rock mechanics for underground mining.* Springer.
- Bray BHG, Lorig L (1988) Analysis of rock reinforcement using finite difference methods. *Comp Geotech* 5: 123–49.
- Cai, M., Kaiser, P., Uno, H., Tasaka, Y., & Minami, M. (2004). Estimation of rock mass deformation modulus and strength of jointed hard rock masses using the GSI system. *International Journal of Rock Mechanics and Mining Sciences,* 41(1), 3-19.

- Cai, M., (2011). Rock mass characterization and rock property variability considerations for tunnel and cavern design. *Journal of Rock Mechanics and Rock Engineering*. 44 (4) pp. 379-399.
- Castro LAM, Bewick RP, Carter TG. (2012). An overview of numerical modelling applied to deep mining. In: Azevedo R, editor. *Innovative numerical modelling in geomechanics*. London: CRC Press — Taylor & Francis Group; p. 393–414.
- Chen D, Chen J, Zavodni ZM. (1983). Stability analysis of sublevel open stopes at great depth. The 24th U.S. Symposium on Rock Mechanics (USRMS).
- Chen G, Jia Z, Ke J. (1997). Probabilistic analysis of underground excavation stability. *Int. J. Rock Mech. & Min. Sci.* 34:3-4, paper No. 051.
- Christian, J. T., & Baecher, G. B. (2002). The point-estimate method with large numbers of variables. *International Journal for Numerical and Analytical Methods in Geomechanics*, 26(15), 1515-1529.
- Clark L. (1998). Minimizing dilution in open stope mining with a focus on stope design and narrow vein longhole blasting. MSc thesis, University British Columbia, Vancouver, Canada.
- Clow, G.G., (2011). Technical report on expansion options at the Niobec mine, IAMGOLD corporation Québec, Canada.
- Deere, D.U., (1968). Geological consideration, *Rock Mechanics in Engineering Practice*, Division of Civil Engineering, School of Engineering, University of Wales, Swansea. Wiley, New York, pp. 1-20.
- Diederichs MS, Kaiser PK. (1996). Rock instability and risk analyses in open stope mine design. *Can Geotech J.*; 33(3):431–439.
- Diederichs MS. (1999). Instability of hard rock masses: the role of tensile damage and relaxation. PhD Thesis. Waterloo, Ontario: University of Waterloo; Canada.
- Diederichs MS, Kaiser PK, Eberhardt E. (2004). Damage initiation and propagation in hard rock during tunneling and the influence of near-face stress rotation. *International Journal of Rock Mechanics and Mining Sciences* 41(5):785-812.48.
- Edelbro, C., (2004). Evaluation of rock mass strength criteria, PhD thesis, Department of Civil and Environmental Engineering, Division of Rock Mechanics, Luleå University of Technology.
- Einstein HH (1996) Risk and Risk Analysis in Rock Engineering. *Risk Anal Tunn* 11:141–155 . doi: 10.1016/0886-7798(96)00014-4
- Germain P, Hadjigeorgiou J (1997) Influence of stope geometry and blasting patterns on recorded overbreak. *Int J rock Mech Min Sci Geomech Abstr* 34:628.
- Gharavi, M., (2008). A comparison of underground opening support design methods in jointed rock mass. *International Journal of Rock Mechanics and Mining Sciences*, 21(3).
- Griffiths, D.V., Fenton, G.A., Lemons, C.B., (2002). Probabilistic analysis of underground pillar stability. *Int. J. Numer. Anal. Methods Geomech.*, 26, 775-791.

- Goh, A.T.C. and Zhang, W. (2012) Reliability assessment of stability of underground rock caverns. *Int. J. Rock Mech. Min. Sci.* 55, pp. 157- 163.
- Govett GJS, Govett MH. (1976). *World mineral supplies assessment and perspective*. Volume 3. New York. Elsevier.
- Guarascio M., Oreste P., (2012). Evaluation of the stability of underground rock pillars through a probabilistic approach. *American Journal of Applied Sciences*, 9 (8), 1273-1282.
- Henning JG (2007) *Evaluation of Long-Hole Mine Design Influences on Unplanned Ore Dilution*. PhD thesis, McGill University, Montreal, Canada.
- Henning JG, Mitri HS (2007) Numerical modelling of ore dilution in blasthole stoping. *Int J Rock Mech Min Sci.*; 44:692–703.
- Hoek E (2007) *Practical rock engineering*. <http://www.rocscience.com/hoek/PracticalRockEngineering.asp>, World Wide Web edition.
- Hoek, E., Kaiser, P. K., & Bawden, W. F. (1995). *Support of underground excavations in hard rock*. Balkema, A. A, Rotterdam.
- Hudson JA (1993) *Comprehensive Rock Engineering: Principles, Practice & Projects*. Vol 5. Pergamon Press.
- Hughes R (2011) *Factors influencing overbreak in narrow vein longitudinal retreat mining*. MSc thesis. McGill University, Montreal, Canada.
- Hustrulid, W., Bullock, R., (2001). *Underground Mining Methods*, Society for Mining, Metallurgy, and Exploration, Inc. (SME), Colorado, USA 80127.
- Idris MA, Saiang D, Nordlund E (2011) Probabilistic analysis of open stope stability using numerical modelling. *Int. J. Min. Miner. Eng.* 3(3):194–219.
- Idris MA (2014) *Probabilistic stability analysis of underground mine excavations*. PhD thesis, Lulea University of Technology, Lulea, Sweden.
- Idris MA, Basarir H, Nordlund E, Wettainen T (2013) The Probabilistic Estimation of Rock Masses Properties in MalMBERGET Mine, Sweden. *Electron J Geotech Eng* 18:269–287
- Itasca Consulting Group, Inc. (2015). *FLAC3D – Fast Lagrangian Analysis of Continua in 3 Dimensions*, Ver. 5.0, User's Guide. Minneapolis: Itasca.
- Jing, L. & Hudson, J. a., (2002). Numerical methods in rock mechanics. *International Journal of Rock Mechanics and Mining Sciences*, 39, pp.409–427.
- Kaiser PK, Diederichs MS, Martin CD (2000) *Underground works in hard rock tunnelling and mining*. In: *GeoEng2000, Proceedings of the International Conference on Geotechnical and Geological Engineering*, Melbourne, Australia.
- Kelvis, del C.P.H., (2013). *Deformation and failure of rock*, Stiftelsen Bergteknisk Forskning rock engineering research foundation, Norway.

- Kirsch, G. (1898) 'Die theorie der elastizitat und die bedvfnisse der festigkeitslehre', Veit. Ver.Deut. Ing., Vol. 42, pp.797–807.
- Ladanyi, B. (1974) 'Use of the long-term strength concept in the determination of ground pressure on tunnel linings', Paper presented at the 3rd Congress of International Society of Rock Mechanics, September, Denver, USA.
- Langford, J.C., Diederichs, M.S., (2013). Reliability based approach to tunnel lining design using a modified point estimate method. *International Journal of Rock Mechanics and Mining Sciences*. 60, pp. 263-276.
- Langston RB, Kirsten HAD, (2001). Probabilistic assessment of sub-level hangingwall stability at the Stillwater Mine, Nye, Montana. American Rock Mechanics Association. The 38th U.S. Symposium on Rock Mechanics (USRMS), 7-10 July, Washington, D.C.
- Lü Q, Low BK. (2011). Probabilistic analysis of underground rock excavations using response surface method and SORM. *Comput Geotech* 38:1008–21.
- Mathews KE (1981) Prediction of stable excavations for mining at depth below 1000 metres in hard rock. Ottawa
- Milne D. (1996). Underground design and deformation based on surface geometry. PhD Thesis, Mining Department, University of British Columbia, Vancouver, Canada.
- Mollon G, Dias D, Soubra AH. (2009). Probabilistic analysis of circular tunnels in homogeneous soil using response surface methodology. *J Geotech Geoen- viron Eng* 135:1314–25.
- Nadim, F. (2007). Tools and strategies for dealing with uncertainty in geotechnics. In: *Probabilistic methods in geotechnical engineering* (Griffiths, D.V., Fenton, G.A. (Eds.)), Springer Wien, New York, pp. 71–96.
- Pakalnis RC, Poulin R, Hadjigeorgiou J. (1995). Quantifying the cost of dilution in underground mines. *Mining Eng Dec*: 1136–41.
- Palmström, A. (1995). RMi - A rock mass characterization system for rock engineering purposes. Ph.D. Thesis, University of Oslo, Norway.
- Park, D., Kim, H., Ryu, D., Song, W., & Sunwoo, C. (2012). Application of a point estimate method to the probabilistic limit-state design of underground structures. *International Journal of Rock Mechanics and Mining Sciences*, 51, 97-104.
- Perron, J (1999) Simple solutions and employee's involvement reduced the operating cost and improved the productivity at Langlois mine. Proceeding 14th CIM Mine Operator's Conference. Bathurst, New Brunswick, Canada.
- Potvin Y. (1988). Empirical open stope design in Canada. PhD thesis, University of British Columbia, Vancouver, Canada.
- Potvin Y, Hudyma M. (2000). Open stope mining in Canada. In: *Proc MassMin 2000*, Brisbane, Australia, p. 661–74.

- Pytel W, Świtoń J (2013) Assessment of the Impact of Geomechanical Parameters Variability on Underground Excavations Stability Using Response Surface Method. *Stud Geotech Mech* 35: . doi: 10.2478/sgem-2013-0014
- Shnorhokian S, Mitri HS, Moreau-verlaan L (2015). Stability assessment of stope sequence scenarios in a diminishing ore pillar. *Int J Rock Mech Min Sci* 74:103–118 . doi: 10.1016/j.ijrmms.2014.12.005
- Tatiya, R.R., (2005). *Surface and underground excavations: methods, techniques and equipment*, Taylor & Francis Group, LLC, London, UK.
- Thivierge S, Roy DW, Chown EH, Gauthier A (1983) Évolution du complexe alcalin de St-Honoré (Québec) après sa mise en place. *Miner Depos* 2:267–283
- Urli V (2015) Ore-Skin Design to Control Sloughage in Underground Open Stope Mining by Ore-Skin Design to Control Sloughage in Underground Open
- Valley B, Kaiser P.K, Duff, D., (2010). Consideration of uncertainty in modelling the behaviour of underground excavations. In: *Proceeding of 5th International seminar on Deep and High Stress Mining*, Santiago, pp. 423-435.
- Vallieres D, Corp I, Pelletier P, et al (2013) NI 43-101 Technical Report , Update on Niobec Expansion, December 2013 Report
- Villaescusa E. *Geotechnical design for sublevel open stoping*. CRC Press. London, UK. 2014.
- Wang J (2004) Influence of stress, undercutting, blasting, and time on open stope stability and dilution. PhD thesis, University of Saskatchewan, Saskatoon, Canada.
- Wang J, Milne D, Wegner L, Reeves M (2007) Numerical evaluation of the effects of stress and excavation surface geometry on the zone of relaxation around open stope hanging walls. *Int J Rock Mech Min Sci* 44:289–298.
- Watson, B.P., (2004). A rock mass rating system for evaluating stope stability on the Bushveld Platinum mines. *The Journal of The South African Institute of Mining and Metallurgy*, 7(5), pp.229–238.
- Whitman, R. V & Schuster, B.R.L., (1984). Evaluating calculated risk in geotechnical engineering. *Journal of Geotechnical Engineering*, 110(2), pp.143–188.
- Zhang Y, Mitri HS (2008) Elastoplastic stability analysis of mine haulage drift in the vicinity of mined stopes. *Int J Rock Mech Min Sci* 45:574–593 . doi: 10.1016/j.ijrmms.2007.07.020
- Zhao, H., Li, Z., Kong, C.S., (2016). Probabilistic method to determine the overall rock block failure based on failure mode. *Engng. Trans.* 64 (1), 105–113.
- Zniber H, Mouhabbis E (2013) Effect of stope construction parameters on ore dilution in narrow vein mining. MSc thesis. McGill University, Montreal, Canada.

Chapter 3 - Assessing the effect of open stope geometry on the rock mass brittle damage in Canadian underground mines using response surface methodology¹

3.1. Abstract

Sublevel open stoping is a common method of underground mining in Canada. Therefore, assessing the stability of underground stopes has become a challenging issue for engineers in order to reduce the risk of fatalities and considerable financial loss. The stability of an underground stope is dependent on a number of factors including rock mass properties, *in situ* stress state and stope geometry. Considering the importance of the effect of geometry on open stope stability; this study aims to provide a comprehensive evaluation of the effect of open stope geometrical parameters on the brittle damage of the rock mass in hard rock mines. A dataset consisting of geometrical parameters of 150 open stopes in Canadian underground mines is utilized as a reference to provide realistic data on the range of input parameters. By applying the “*K*-means” clustering technique on the dataset, three different geometry clusters are defined and the corresponding range of each geometrical parameter (including stope strike length, stope width, stope height and stope hanging wall dip) within the clusters are determined accordingly. Subsequently, a response surface methodology (RSM) with a Box–Behnken Design is employed to evaluate the individual and interaction effects of the aforementioned input parameters on the “Brittle Shear Ratio” (BSR) of the rock mass surrounding a stope. A stability analysis is performed using *FLAC3D* numerical modelling software, for each cluster of stope geometry at three different mining depths, and

¹ Heidarzadeh S, Saeidi A, Rouleau A. Assessing the effect of open stope geometry on rock mass brittle damage using a response surface methodology. *International Journal of Rock Mechanics and Mining Sciences*. 2018; 106:60–73

distributed values of BSR are obtained. A statistical analysis using ANOVA allows to determine a set of individual and interactive parameters having a significant effect on the BSR of stopes for each geometry cluster at each mining depth.

KEYWORDS: Stope Stability, Stope Geometrical Parameters, Brittle Damage, Brittle Shear Ratio, Response Surface Methodology, Numerical Modelling, Sub-Level Open Stopping.

3.2. Introduction

Over the past decades, the mining of deep underground resources has greatly expanded due to the shortage of easily minable, near-surface mineral deposits, (Govett 1976 ; Potvin 2000). Among numerous underground excavation techniques, sublevel stoping is the most widely practiced method in Canadian underground mines (Hudson 1993; Wang 2004; Zhang and Mitri 2008; Abdellah et al. 2014b). Underground open stope stability is of significant concern to rock mechanics engineers as it directly affects mining production capacity and the safety of workers and equipment (Einstein 1996; Idris 2011; Abdellah et al. 2014b).

Three general approaches are commonly used to analyze the stability of underground excavations: analytical, empirical, and numerical methods. Analytical methods cannot accurately represent complex mining problems (Idris 2014). Common empirical methods (e.g., the stability graph method) (Mathews 1981; Potvin 1988) also have certain limitations, such as not considering the tensile mode of failure and the oversimplification of irregular geometries, thereby restricting the functionality these methods (Idris 2014). Numerical methods, on the other hand, circumvent the limitations of the two other methods and, therefore, have been widely used to analyze the stability of underground excavations.

The instability of underground open stopes is influenced by many factors including rock mass geomechanical parameters, natural and mining-induced stresses, and stope geometrical parameters (Diederichs and Kaiser 1996; Chen et al. 1997; Henning and Mitri 2007; Idris et al. 2013; Villaescusa 2014). Among these factors, the effect of stope geometry has been identified particularly important (Aglawe 1999) (Zhang and Mitri 2008) (Villaescusa 2014), although the detailed effects of these parameters on stope stability are not as of yet fully understood.

In general, the effects of geometry on the stability of an underground excavation have been addressed in almost all empirical stability analysis systems (Germain and Hadjigeorgiou 1997), but not through numerical approaches. For instance, in tunnel design, Terzaghi (1946) was the first to study the influence of excavation form in terms of the height and width on stability (Germain and Hadjigeorgiou 1997). Similarly, the notion of an unsupported span and its stand-up time was explained by Lauffer (1958) (Germain and Hadjigeorgiou 1997). Moreover, conventional rock mass classification systems (e.g., RMR, Q) commonly used to evaluate the stability of underground excavations, consider rock mass quality and excavation geometry (Germain and Hadjigeorgiou 1997). Furthermore, the effects of open stope geometry in terms of the hanging wall hydraulic radius (HR) or radius factor (RF) have been incorporated in stability graph methods (Mathews 1981) (Potvin 1988) (Milne 1996) (Wang 2004).

Numerical modeling, as a commonly used approach for the evaluation of open stope stability, has been mostly applied to assessing the effect of stope geometrical parameters on low confinement tensile (gravity-driven) modes of failure. Several significant publications related to numerical modeling of stope geometrical parameters effects on stability are summarized here. In a pioneering study, Chen et al. (1983) assessed the effect of open stope height using a finite element method and found it to be a critical design parameter. Pakalnis et al. (1995) reported that the mining

of narrow stopes increased the rate of dilution. Milne (1997) linked the hanging wall geometry of an open stope with measured deformation to provide an indicator of instability and successfully substituted the hanging wall HR with the RF term to analyze more complex geometries. Germain and Hadjigeorgiou (1997) defined an index for stope geometry by dividing the volume of a stope by its real surface area (RVS) as a measure of stope geometrical complexity to assess the applicability of the stability graph method. Clark (1998) then introduced a new parameter (ELOS - equivalent linear overbreak or slough) to evaluate the amount of dilution of a stope hanging wall. They reported that an increased HR of the stope hanging wall contributed to an increased extent of hanging wall overbreak. Perron (1999) demonstrated that stope height and geometry complexity adversely affected the stability of the hanging wall and suggested that stopes being 60 m high at the Langlois Mine (Québec) be re-designed to reduce dilution. Aglawe (1999) concluded that the geometry of excavations was the most significant factor influencing the occurrence of strainburst in highly stressed ground. Wang (2004) developed a method to correlate stope geometry and induced stress state through design graphs to evaluate stress relaxation-related dilution. Afterwards, Wang et al. (2007) examined the effect of stope geometrical parameters on the extent of the zone of relaxation.

Henning and Mitri (2007) assessed the effect of orebody dip on unplanned dilution and reported that a shallower hanging wall dip caused greater dilution due to the increased depth of overbreak. Hughes (2011) examined the effect of stope strike length on ore dilution in a narrow vein mined longitudinally. Using a finite element method they determined that longer stope strike lengths generate larger volumes of dilution, while shorter strike lengths are less prone to dilution. In a more recent study, El Mouhabbis (2013) investigated the effects of stope geometry on ore dilution and concluded that stope construction geometry has a significant effect on overbreak as a

greater stope strike length increases overbreak, a shallower ore dip enhances hanging wall overbreak, and that narrower stopes exhibit higher dilution. Therefore, the existing literature provides many studies that investigate the effect of excavation geometry on low confinement tensile (gravity-driven) modes of failure. Nevertheless, the influence of open stope geometrical parameters on rock mass brittle damage (ultimately causing spalling and slabbing failure) has not yet been fully determined.

One of the most efficient tools for evaluating the effect of parameters on open stope stability is the use of probabilistic methods combined with numerical modeling. (Idris et al. 2011). Among numerous probabilistic approaches used in rock mechanic problems, response surface methodology (RSM), as a discrete sampling probabilistic method, can assess individual and interactive effects of input parameters on single or multiple response variables. RSM consists of a set of mathematical and statistical tools used to generate an implicit mathematical expression between a dependent output response and a collection of input variables (Idris 2014) (Ahmadi et al. 2014). The aim of using RSM is to design, improve, and optimize different operational processes (Anderson and Whitcomb 2005). Through this approach, we can evaluate the effects and relative significance of individual input variables the interactive effect(s) of two or more variables, as well as the optimal conditions for the desired responses. The RSM approach generally applies two steps: the first step is to generate a mathematical expression that determines the input parameters and interactions having a significant influence on the response. The second step is to optimize the significant individual parameters and obtain the desired response value. RSM, in conjunction with numerical modeling, has been used to evaluate the stability of underground rock excavations (Mollon and Dias 2009; Lü and Low 2011; Pytel and Świtoń 2013).

The present research attempts to provide a comprehensive evaluation of the effect of stope geometrical parameters (i.e., stope strike length, stope width, stope height, and stope hanging wall dip) on the potential of brittle damage of the rock mass surrounding a stope at three different mining depths. This study applies geometrical parameters derived from a survey of numerous open stopes (Wang 2004) from the Canadian Shield. We use an RSM with a Box–Behnken design in conjunction with the finite difference code *FLAC3D* (Itasca 2015) to evaluate the individual and interactive effects of the aforementioned input parameters. Response surface optimization techniques are then used to obtain the most stable stope states by determining the optimal values for the stope geometrical parameters.

3.3. Methodology

Our proposed methodology to use numerical analysis for evaluation of the effect of open stope geometrical parameters on the state of stability, consists of a sequential procedure. Firstly, the required input parameters for numerical analysis, including the values of rock mass geomechanical parameters, magnitude of *in situ* stress components and the range of values for open stope geometrical parameters should be determined. Secondly, by adopting an appropriate probabilistic approach, various numerical modelling scenarios are generated as a combination of different open stope geometry setups. Finally, by accomplishing the numerical analysis and assessing the degree of rock mass brittle damage, the significant individual and interaction effects of open stope geometrical parameters on the rock mass brittle damage, are determined by applying an appropriate series of statistical analysis.

3.3.1. Determination of rock mass parameters

Deep mineral deposits in the Canadian Shield are commonly located in metamorphic and igneous Precambrian rocks (e.g., andesite, rhyolite, basalt, and granite). As such, these underground mines report moderate to strong rock mass quality (Zhang and Mitri 2008; Abdellah et al. 2014b). Given this typical rock mass quality for the Canadian Shield, we assigned the deterministic values for unconfined compressive strength (UCS) of intact rock, Young's modulus of intact rock, the Hoek-Brown material constant (m_i), and Poisson's ratio respectively as equal to 100 (MPa), 80 (GPa), 13 and 0.2. Using the GSI chart, we chose the "very blocky" structural class as the reference for the rock mass and a deterministic value of 60, was assigned to the rock mass parameter GSI.

By using the UCS and m_i values of the intact rock and the GSI value for the rock mass, we obtained the geomechanical rock mass properties through the following equations (Eqns. 3-1–3-6) (Hoek 2007):

$$m_b = m_i e^{\left(\frac{GSI-100}{28-14D}\right)} \quad (3-1)$$

$$s = e^{\left(\frac{GSI-100}{9-3D}\right)} \quad (3-2)$$

$$a = \frac{1}{2} + \frac{1}{6} \left(e^{\frac{-GSI}{15}} - e^{\frac{-20}{3}} \right) \quad (3-3)$$

$$\sigma_{cm} = \sigma_{ci} s^a \quad (3-4)$$

$$\sigma_t = \frac{s\sigma_{ci}}{m_b} \quad (3-5)$$

$$E_{rm} = E_i \left(0.02 + \frac{1 - \frac{D}{2}}{1 + e^{\frac{60 + 15D - GSI}{11}}} \right) \quad (3-6)$$

where D stands for the degree of disturbance of the rock mass caused by the excavation method and stress relaxation—it varies from 0 for undisturbed *in situ* rock masses to 1 for very disturbed rock masses (Hoek 2007). The value of 0.8 is assigned to D in this study, as the rock mass is assumed to be disturbed due to blasting. The parameters m_b and a are the Hoek-Brown failure criteria constants that reflect the characteristics of the rock mass; σ_{cm} and σ_t are, respectively, the compressive and tensile strengths of the rock mass; and E_{rm} is the rock mass deformation modulus. The parameter σ_{ci} is the uniaxial compressive strength (UCS) of the intact rock. The average values of rock mass strength and deformability parameters are obtained as: Bulk modulus $K = 2.733$ (GPa), Shear modulus $G = 5.695$ (GPa), $\sigma_t = 0.194$ (MPa), $m_b = 1.2$, $s = 0.002$ and $a = 0.502$.

3.3.2. State of *in situ* stress

Before any underground excavation, the rock mass is already subjected to *in situ* stresses. These stresses are due to the weight of overlying strata, locked-in because of tectonic activities, or related to local topography. Because of excavation, the *in situ* stress regime of the rock mass surrounding an opening is perturbed. The magnitude of the *in situ* stress components plays a critical role in the stability of any underground excavation (Hoek 2007). According to Arjang and Herget (1997), the major and the intermediate principal stress components (σ_1 and σ_2) in the Canadian Shield are nearly horizontal, plunging by 10° or less, whereas the minor principal stress component (σ_3) is near vertical. Moreover, as explained by Zhang *et al.* (2008), as a common characteristic for near vertical deposits in the Canadian Shield, the maximum horizontal stress component is at

an angle of 90° to the strike of the ore body and the minimum horizontal stress component is parallel to the ore strike.

For this study, to observe the behavior of significant geometrical parameters as a function of depth, we estimated the state of *in situ* stress at three levels of mining depth corresponding to 250-m-thick slices from 1000 m to 1750 m depth. We wished to clarify whether increased mining depth modifies the number or impact of significant geometry parameters. Three separate mining depths (1125 m, 1375 m and 1625 m) were considered as representative for *in situ* stress determination; the magnitudes of maximum and minimum horizontal components, and the vertical component of *in situ* stress for each depth were calculated (Table 3-1) based on the equations 3-7, 3-8, and 3-9 as proposed by Maloney *et al.* (2006) :

$$\sigma_1 \text{ (MPa)} = 0.026z \text{ (m)} + 23.636 \quad (3-7)$$

$$\sigma_2 \text{ (MPa)} = 0.016z \text{ (m)} + 17.104 \quad (3-8)$$

$$\sigma_3 \text{ (MPa)} = 0.020z \text{ (m)} + 1.066 \quad (3-9)$$

Table 3-1- The values of *in situ* stress components at three mining depths.

Depth (m)	σ_H (MPa)	σ_h (MPa)	σ_V (MPa)
1125	52.9	35.1	23.6
1375	59.4	39.1	28.6
1625	65.9	43.1	33.6

3.3.3. Determination of model geometry

We selected strike length, stope width, stope height, and stope hanging wall dip as appropriate input parameters, since they are comprehensive enough to define the stope geometry. To assign a realistic range of values to each parameter, we selected the database compiled by Wang (Wang 2004) as the reference of the common stope geometries of Canadian underground mines. The database consists of stope geometry information of 150 open stopes in Canadian underground mines, including eight cases from the Ruttan Mine, 45 cases from the Callinan Mine, and 97 cases from the Trout Lake Mine. Due to the wide range of values for each geometrical parameter in the database, we used cluster analysis to partition the data into groups to determine more appropriate parameter variations. This method of analysis is very efficient and useful for rock engineering, particularly when classifying rocks and grouping orientation data (Chen 1994).

For cluster analysis, we used a standard K -mean non-hierarchical algorithm. This algorithm requires the number of clusters—referred as “ K ”—to be determined in advance by the user. The K -mean algorithm was first introduced by Harrison (1992) for use in rock mechanics-related problems (Hammah and Curran 1999). This algorithm is based on the notion of seed points for each cluster. These points are selected at random and are assumed as the initial centroids of the clusters. The closest observations to the different centroids are linked to the seeds to form different clusters. Each time an observation is gained or removed from a cluster, the algorithm calculates new centroids. The process continues until every observation is placed as close as possible to a cluster centroid (Ellefmo 2005).

By examining various number of clusters, we observed that a number of three results in more clearly distinct clusters. Therefore, the number of clusters was set in advance to three. The K -mean algorithm was applied to 150 open stope cases using the “stope hanging wall dip” and the “stope

hanging wall hydraulic radius (HR)” as clustering parameters. We selected these clustering parameters, as opposed to other stope geometric elements, to simplify our statistics as HR captures simultaneously the effect of size and shape of the stope, (Villaescusa 2014) while the stope hanging wall dip represents the orientation.

The obtained *F*-values equal to 95.62 and 80.99, respectively for hanging wall dip and HR, indicate that the selected clustering parameters are clearly responsible for more significant differences between the clusters than within the clusters. Moreover, the number of members for cluster I, II and III are determined to be 36, 38 and 76 respectively. The stope geometrical input parameters and their corresponding range for each cluster are presented in Table 3-2.

Table 3-2- Stope geometry classes used in numerical modeling. HW: hanging wall.

Parameter	Cluster I	Cluster II	Cluster III
Strike length (m)	11–36	23.5–57	12.8–42
Stope height (m)	10–45.2	22–85	15–56
Stope width (m)	2.2–20.4	1.9–24	2.6–52
Stope HW dip (°)	24–54	41–90	53–85
Stope HW HR	2.7–9.6	7–14.4	4.4–10.8

The values of stope hanging wall HR and dip indicate that the obtained clusters can also be classified qualitatively. Accordingly, Cluster I corresponds to stopes having a “low to moderate” hanging wall HR and dip; while clusters II & III, represent steeply dipping stopes, having “moderate to high” and “moderate” ranges of hanging wall HR, respectively. These qualitative measures of stope size and inclination for the different clusters not only facilitates

comparisons between clusters, but also provides a clearer understanding of the relationship between slope geometry and stability.

3.3.4. Selecting failure criteria

In the case of underground open stopes located in deep hard rock mines or for a brittle rock mass context, the high magnitude of mining-induced stresses could cause rock mass damage initiation and sometimes failure in the areas close to the excavation walls (Diederichs 1999b; Castro et al. 2012; Shnorhokian et al. 2015). Under low confinement conditions, stress-induced instability occurs by two dominant processes, namely (1) stress-induced spalling and slabbing failure; and (2) structurally-controlled, gravity-driven failures. Spalling failure is due to the magnitude of radial stress near those excavation walls showing considerable reduction while the tangential stress reaches its maximum (Castro et al. 2012).

The potential rock mass brittle damage surrounding an open stope can be estimated by the BSR (Castro et al. 2012). The BSR (Eqn. 3-10) is obtained by dividing the differential induced stress ($\sigma_1 - \sigma_3$) around the stope by the unconfined compressive strength (UCS) of an intact rock.

$$BSR = \frac{\sigma_1 - \sigma_3}{UCS_{intact}} \quad (3-10)$$

The level of rock mass damage and the potential of strainburst occurrence has been tabulated by Castro et al. (2012) based on the BSR ratio. The deviatoric stress ($\sigma_1 - \sigma_3$) at each point around the excavation was determined by 3D numerical modeling. To calculate the value of BSR for each point of the model, we developed a built-in program in the FISH-language code (Itasca 2015) that uses the maximum shear stress of each zone.

3.3.5. Experimental Design

We used an RSM to evaluate the variability of effects of selected parameters associated with open slope geometry on the obtained maximum BSR value around the slope. One important advantage of using RSM, is its ability to approximate the implicit mathematical relationship between the input parameters and the response variable. In fact, RSM determines the aforementioned mathematical equations, through applying appropriate regression models (e.g. full quadratic polynomial model) and defining the significant input parameters (Mollon and Dias 2009). We employed a 3-level, 4-factor Box–Behnken design (BBD) to evaluate the individual or combined effects of the selected parameters on the response variable (BSR). The four geometrical parameters affecting slope stability, namely slope strike length (X1), slope height (X2), slope width (X3), and slope hanging wall dip (X4), were considered as independent input variables; while the maximum value of BSR of the rock mass surrounding the slope was selected as the response variable. We converted variables to coded values according to Eqn. 3-11:

$$x_i = \frac{X_i - X_0}{\Delta X_i} \quad (3-11)$$

where x_i and X_i are the coded and the real value of input variable, respectively, X_0 is the real value of input variable at the center point, and ΔX_i is the value between steps. In geotechnical problems, to obtain more accurate response surfaces having a better fit (Idris 2014), evaluation points normally should scatter ± 1 standard deviation around the mean value for the RSM designs (Table 3-3) (Langford and Diederichs 2013).

Table 3-3- Actual and coded values of the input parameters for each geometry class. HW: hanging wall.

Geometry cluster		Cluster I			Cluster II			Cluster III		
Parameter	Coded values	-1	0	1	-1	0	1	-1	0	1
Stope strike length (m)		11.00	23.50	36.00	23.50	40.25	57.00	12.80	27.40	42.00
Stope width (m)		2.20	11.30	20.40	1.90	12.95	24.00	2.60	27.30	52.00
Stope height (m)		10.00	27.60	45.20	22.00	53.50	85.00	15.00	35.00	56.00
Stope HW dip (°)		24.00	39.00	54.00	41.00	65.00	89.00	53.00	69.00	85.00

For each cluster, a set of 29 experimental runs were generated by Box–Behnken design (Tables 3-4–3-6). The obtained response values (maximum BSR value) were analyzed using *Design Expert 7.0* (Stat-Ease 2005) and a quadratic polynomial regression model was obtained as follows (Eqn. 3-12):

$$BSR = \alpha_0 + \sum \alpha_i X_i + \sum \alpha_{ii} X_i^2 + \sum \alpha_{ij} X_i X_j + \varepsilon \quad (3-12)$$

where α_0 represents the constant coefficient of the equation, α_i , α_{ii} , and α_{ij} are considered as the regression coefficients, and X_i , X_j stands for the significant input variables, while ε indicates the random error (Ahmadi et al. 2014).

Table 3-4- Box–Behnken design matrix for Cluster I and response values at three depths.

Experimental Run	Length (A)	Width (B)	Height (C)	Dip (D)	BSR- 1125 (m)	BSR- 1375 (m)	BSR- 1625 (m)
1	0.00	-1.00	0.00	-1.00	0.416	0.452	0.490
2	0.00	1.00	0.00	-1.00	0.398	0.434	0.456
3	-1.00	0.00	1.00	0.00	0.458	0.485	0.534
4	0.00	0.00	0.00	0.00	0.429	0.452	0.476
5	-1.00	1.00	0.00	0.00	0.470	0.495	0.527
6	1.00	-1.00	0.00	0.00	0.429	0.455	0.489
7	0.00	1.00	-1.00	0.00	0.432	0.461	0.489
8	0.00	0.00	0.00	0.00	0.429	0.452	0.476
9	0.00	0.00	0.00	0.00	0.429	0.452	0.476
10	0.00	0.00	0.00	0.00	0.429	0.452	0.476
11	-1.00	-1.00	0.00	0.00	0.430	0.478	0.510
12	1.00	0.00	0.00	1.00	0.447	0.483	0.535

13	-1.00	0.00	-1.00	0.00	0.470	0.540	0.550
14	0.00	-1.00	0.00	1.00	0.424	0.450	0.485
15	0.00	0.00	1.00	-1.00	0.402	0.435	0.460
16	0.00	-1.00	-1.00	0.00	0.424	0.457	0.492
17	1.00	0.00	0.00	-1.00	0.411	0.445	0.475
18	1.00	0.00	-1.00	0.00	0.457	0.510	0.530
19	1.00	0.00	1.00	0.00	0.422	0.448	0.497
20	0.00	-1.00	1.00	0.00	0.418	0.456	0.493
21	1.00	1.00	0.00	0.00	0.405	0.434	0.490
22	-1.00	0.00	0.00	-1.00	0.435	0.482	0.521
23	0.00	0.00	-1.00	1.00	0.432	0.454	0.479
24	0.00	0.00	-1.00	-1.00	0.408	0.444	0.481
25	0.00	1.00	0.00	1.00	0.488	0.542	0.564
26	0.00	0.00	0.00	0.00	0.429	0.452	0.476
27	0.00	1.00	1.00	0.00	0.441	0.470	0.506
28	0.00	0.00	1.00	1.00	0.432	0.464	0.494
29	-1.00	0.00	0.00	1.00	0.490	0.553	0.580

Table3- 5- Box-Behnken design matrix for Cluster II and response values at three depths.

Experimental Run	Length (A)	Width (B)	Height (C)	Dip (D)	BSR- 1125 (m)	BSR- 1375 (m)	BSR- 1625 (m)
1	0.00	0.00	-1.00	-1.00	0.416	0.458	0.489
2	0.00	1.00	0.00	1.00	0.450	0.472	0.518
3	1.00	0.00	0.00	1.00	0.427	0.452	0.481
4	1.00	0.00	-1.00	0.00	0.475	0.492	0.506
5	-1.00	0.00	0.00	-1.00	0.430	0.476	0.507
6	0.00	1.00	-1.00	0.00	0.481	0.501	0.546
7	1.00	0.00	1.00	0.00	0.423	0.448	0.480
8	-1.00	-1.00	0.00	0.00	0.450	0.479	0.522
9	0.00	0.00	-1.00	1.00	0.467	0.491	0.518
10	0.00	0.00	0.00	0.00	0.426	0.455	0.483
11	-1.00	0.00	0.00	1.00	0.468	0.493	0.515
12	0.00	1.00	0.00	-1.00	0.435	0.486	0.527
13	-1.00	1.00	0.00	0.00	0.489	0.540	0.580
14	0.00	-1.00	-1.00	0.00	0.420	0.465	0.528
15	0.00	-1.00	0.00	1.00	0.403	0.436	0.490
16	1.00	1.00	0.00	0.00	0.431	0.463	0.493
17	1.00	-1.00	0.00	0.00	0.420	0.471	0.500
18	0.00	0.00	0.00	0.00	0.426	0.455	0.483
19	-1.00	0.00	-1.00	0.00	0.476	0.505	0.528
20	0.00	0.00	1.00	1.00	0.428	0.464	0.490
21	1.00	0.00	0.00	-1.00	0.424	0.454	0.488
22	0.00	-1.00	1.00	0.00	0.435	0.463	0.488
23	0.00	1.00	1.00	0.00	0.453	0.486	0.529
24	0.00	-1.00	0.00	-1.00	0.417	0.455	0.510
25	0.00	0.00	0.00	0.00	0.426	0.455	0.483
26	-1.00	0.00	1.00	0.00	0.470	0.505	0.530
27	0.00	0.00	1.00	-1.00	0.452	0.492	0.532
28	0.00	0.00	0.00	0.00	0.426	0.455	0.483
29	0.00	0.00	0.00	0.00	0.426	0.455	0.483

Table 3-6- Box–Behnken design matrix for Cluster III and response values at three depths.

Experimental Run	Length (A)	Width (B)	Height (C)	Dip (D)	BSR- 1125 (m)	BSR- 1375 (m)	BSR- 1625 (m)
1	0.00	0.00	1.00	1.00	0.501	0.541	0.579
2	0.00	0.00	-1.00	-1.00	0.487	0.506	0.512
3	-1.00	-1.00	0.00	0.00	0.441	0.464	0.497
4	0.00	0.00	0.00	0.00	0.519	0.552	0.592
5	-1.00	0.00	0.00	-1.00	0.578	0.615	0.593
6	0.00	0.00	0.00	0.00	0.519	0.552	0.592
7	0.00	1.00	-1.00	0.00	0.571	0.636	0.575
8	1.00	-1.00	0.00	0.00	0.422	0.472	0.526
9	1.00	1.00	0.00	0.00	0.461	0.49	0.508
10	1.00	0.00	0.00	-1.00	0.475	0.499	0.544
11	0.00	0.00	0.00	0.00	0.520	0.552	0.592
12	0.00	1.00	1.00	0.00	0.580	0.626	0.587
13	1.00	0.00	-1.00	0.00	0.474	0.493	0.524
14	-1.00	0.00	-1.00	0.00	0.545	0.585	0.619
15	0.00	0.00	0.00	0.00	0.520	0.552	0.592
16	0.00	-1.00	0.00	-1.00	0.422	0.451	0.488
17	0.00	1.00	0.00	1.00	0.480	0.55	0.540
18	-1.00	0.00	1.00	0.00	0.563	0.617	0.669
19	1.00	0.00	1.00	0.00	0.448	0.476	0.519
20	0.00	-1.00	-1.00	0.00	0.429	0.463	0.493
21	0.00	0.00	-1.00	1.00	0.480	0.517	0.544
22	-1.00	0.00	0.00	1.00	0.575	0.621	0.660
23	-1.00	1.00	0.00	0.00	0.643	0.693	0.734
24	0.00	1.00	0.00	-1.00	0.536	0.563	0.574
25	0.00	-1.00	0.00	1.00	0.447	0.471	0.487
26	0.00	0.00	0.00	0.00	0.520	0.552	0.592
27	0.00	-1.00	1.00	0.00	0.454	0.487	0.515
28	1.00	0.00	0.00	1.00	0.472	0.51	0.541
29	0.00	0.00	1.00	-1.00	0.493	0.527	0.552

3.3.6. Numerical Modeling

The finite difference code *FLAC3D* (Itasca 2015) was used to construct models based on the geometry setup designed by RSM (Fig. 3-1). The planar symmetrical models were built based on a transverse stope configuration (Villaescusa 2014), containing multiple neighboring primary stopes having identical dimensions excavated in sequence. A constant value of 0.4 was assigned to the rib pillar W/H ratio, based on a database reported by Hudyma (1988) that contains 135 rib

pillar size parameters observed from 17 different Canadian open stope mines. Various mesh sizes were tested to obtain valid and stable numerical results. A finer mesh was generated for enhancing accuracy near the stopes and pillars, while the mesh becomes coarser for the rock mass surrounding the area of interest. Considering different stope sizes for each model, the conditions of external boundaries in displacement (roller conditions) have been positioned far enough to avoid any undesirable effect on the results obtained in the region of interest. For each mining depth, the *in situ* stress components were applied in an identical manner to the models of all three clusters according to the magnitudes reported in Table 3-1. Each stope was excavated in a single step, from left to right, and after each stope excavation, the rock mass was allowed to reach equilibrium.

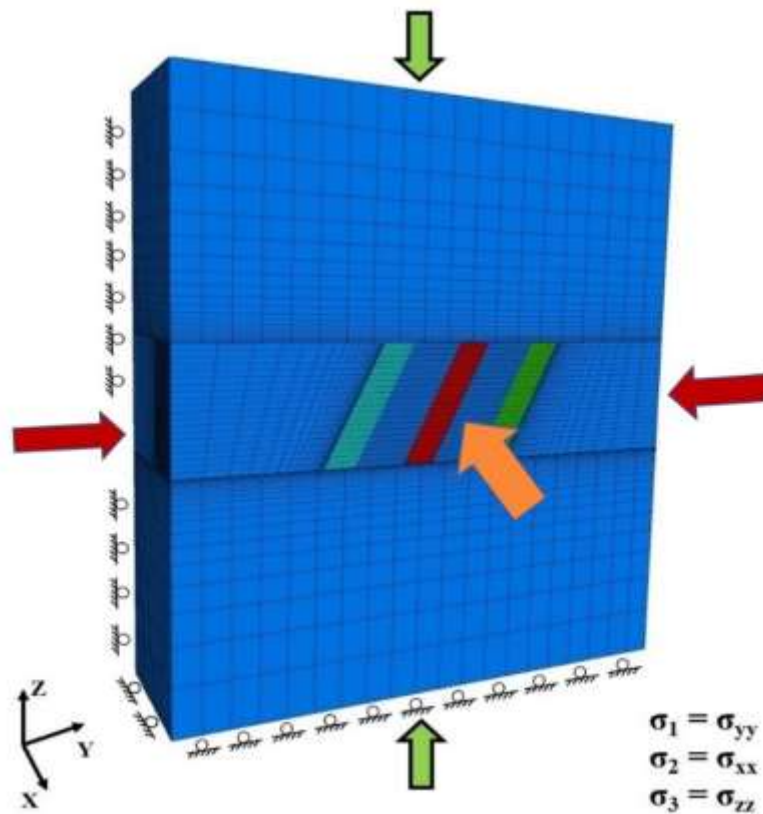


Figure 3-1 - Model boundary conditions and the state of *in situ* stresses.

3.4. Results and discussion

The value of BSR for each model zone, was obtained by using a FISH-language code generated to find the maximum shear stress (as an output parameter in *FLAC3D*) of each zone and to calculate the BSR value (Figs. 3-2 and 3-3).

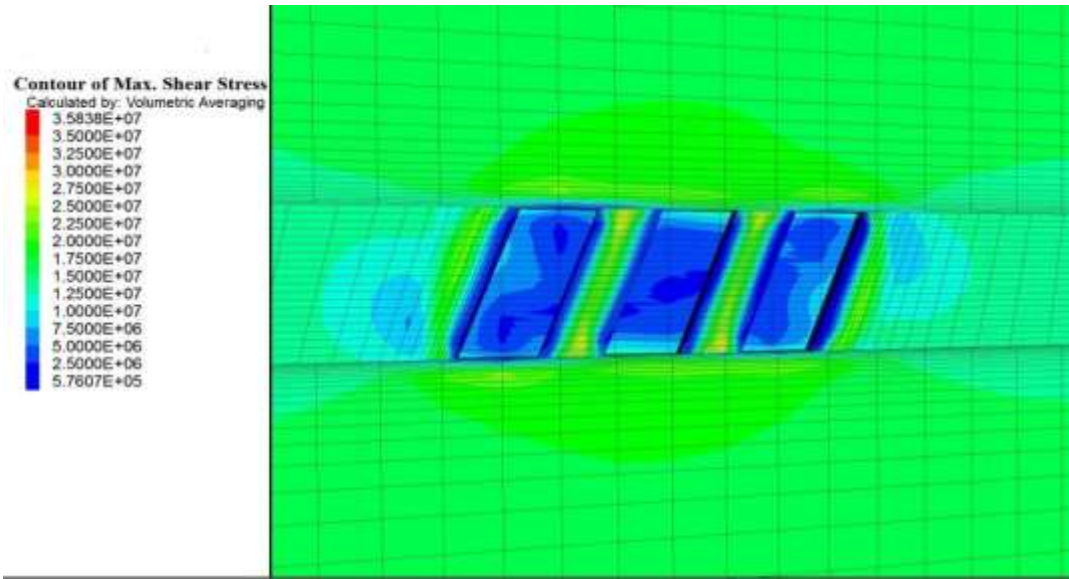


Figure 3-2 - Contour of maximum shear stress (Pa).

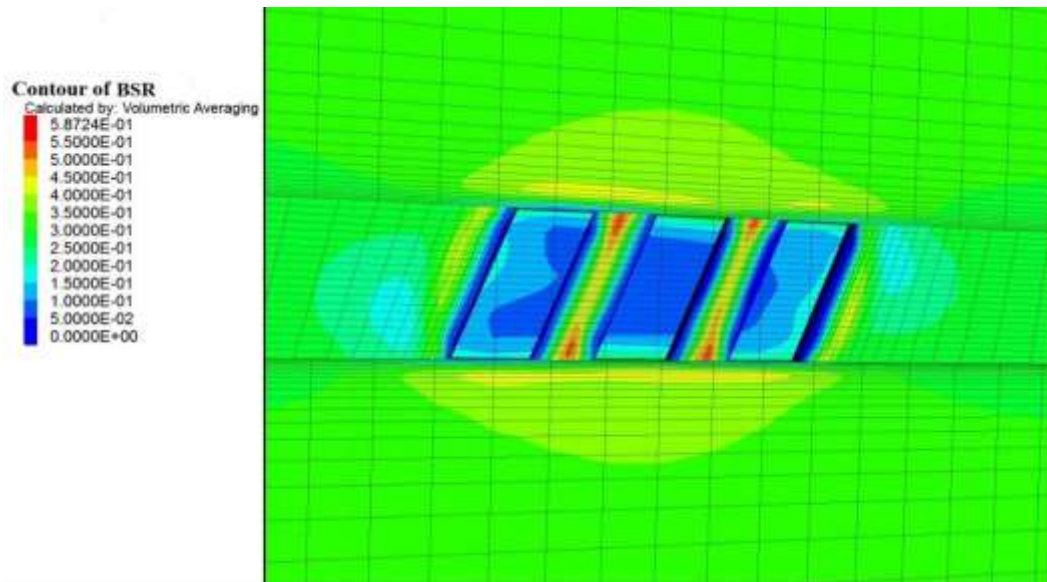


Figure 3-3 - Contour of the brittle stress ratio (BSR).

A statistical analysis by RSM was applied to determine the best-fit regression model for BSR values. The BSR results obtained for each cluster at three mining depths were fitted to different regression models (i.e., linear, interactive, quadratic, 2FI, and cubic) to find the corresponding equations. For each cluster at each of three mining depths, ANOVA was utilized to determine the level of significance for the applied regression models. The final equation for each cluster expresses the relationship between the BSR value (response variable) and individual/interactive effects of independent variables; the resulting nine equations are presented in Eqns. 3-13–3-21 for the three mining depths.

$$\text{BSR1 (1125 m)} = +0.43 -0.015 \times A + 7.750 \times 10^{-3} \times B + 0.020 \times D - 0.016 \times AB + 0.020 \times BD + 0.017 \times A^2 \quad (3-13)$$

$$\text{BSR2 (1125 m)} = +0.43 -0.015 \times A + 0.016 \times B - 6.167 \times 10^{-3} \times C - 0.011 \times AC - 0.011 \times BC - 0.019 \times CD + 0.017 \times A^2 + 0.018 \times C^2 \quad (3-14)$$

$$\text{Log}_{10}\text{BSR3 (1125 m)} = -0.29 -0.041 \times A + 0.047 \times B - 0.031 \times AB - 0.018 \times BD - 0.023 \times B^2 - 0.012 \times D^2 \quad (3-15)$$

$$\text{BSR1 (1375 m)} = +0.46 -0.025 \times A + 0.022 \times D + 0.025 \times BD + 0.022 \times A^2 \quad (3-16)$$

$$\text{BSR2 (1375 m)} = +0.45 -0.018 \times A + 0.015 \times B - 0.017 \times AB - 0.011 \times AC - 0.015 \times CD + 0.018 \times A^2 + 0.010 \times B^2 + 0.017 \times C^2 \quad (3-17)$$

$$\text{BSR3 (1375 m)} = +0.55 -0.055 \times A + 0.063 \times B - 0.053 \times AB - 0.017 \times B^2 - 0.016 \times D^2 \quad (3-18)$$

$$\text{BSR1 (1625 m)} = +0.49 -0.019 \times A + 0.020 \times D + 0.028 \times BD + 0.031 \times A^2 \quad (3-19)$$

$$\text{BSR2 (1625 m)} = +0.49 -0.020 \times A + 0.013 \times B - 0.016 \times AB - 0.018 \times CD + 0.012 \times A^2 + 0.024 \times B^2 + 0.016 \times C^2 \quad (3-20)$$

$$\text{BSR3 (1625 m)} = +0.59 -0.051 \times A + 0.043 \times B + 0.013 \times C - 0.064 \times AB - 0.018 \times AD - 0.038 \times B^2 - 0.017 \times C^2 - 0.027 \times D^2 \quad (3-21)$$

where BSR1, BSR2, and BSR3 are the “brittle shear ratio” values of the clusters I, II, and III, respectively; A, B, C, and D refer to the coded values of stope strike length, stope width, stope height, and stope HW dip, respectively. ANOVA results for clusters I, II, and III at the three different mining depths are presented in Tables 3-7–3-9, respectively.

Table 3-7- ANOVA results of the regression model for Cluster I at three depths.

Depth	Source	Coefficient estimate	Sum of squares	Degree of freedom	Mean square	F-value	p-value
1125 (m)	Model	0.43	0.013	6	2.175×10^{-3}	20.03	< 0.0001
	A	- 0.015	2.760×10^{-3}	1	2.760×10^{-3}	25.42	< 0.0001
	B	$+7.750 \times 10^{-3}$	7.208×10^{-4}	1	7.208×10^{-4}	6.64	0.0172
	D	0.020	4.921×10^{-3}	1	4.921×10^{-3}	45.32	< 0.0001
	AB	- 0.016	1.024×10^{-3}	1	1.024×10^{-3}	9.43	0.0056
	BD	0.020	1.681×10^{-3}	1	1.681×10^{-3}	15.48	0.0007
	A ²	0.017	1.940×10^{-3}	1	1.940×10^{-3}	17.87	0.0003
	Residual		2.389×10^{-3}	22	1.086×10^{-4}		
	Lack-of-fit		2.389×10^{-3}	18	1.327×10^{-4}		
	Pure error		0.000	4	0.000		
Cor total			0.015	28			
1375 (m)	Model	0.46	0.020	5	3.924×10^{-3}	15.27	< 0.0001
	A	- 0.025	7.400×10^{-3}	1	7.400×10^{-3}	28.81	< 0.0001
	B	$+6.500 \times 10^{-3}$	5.070×10^{-4}	1	5.070×10^{-4}	1.97	0.1734
	D	0.022	5.808×10^{-3}	1	5.808×10^{-3}	22.61	< 0.0001
	BD	0.025	2.500×10^{-3}	1	2.500×10^{-3}	9.73	0.0048
	A ²	0.022	3.405×10^{-3}	1	3.405×10^{-3}	13.25	0.0014
	Residual		5.909×10^{-3}	23	2.569×10^{-4}		
	Lack-of-fit		5.909×10^{-3}	19	3.110×10^{-4}		
	Pure error		0.000	4	0.000		
	Cor total			0.026	28		
1625 (m)	Model	0.49	0.020	5	3.921×10^{-3}	20.29	< 0.0001
	A	- 0.019	4.256×10^{-3}	1	4.256×10^{-3}	22.03	< 0.0001
	B	$+6.917 \times 10^{-3}$	5.741×10^{-4}	1	5.741×10^{-4}	2.97	0.0982
	D	0.020	4.961×10^{-3}	1	4.961×10^{-3}	25.68	< 0.0001
	BD	0.028	3.192×10^{-3}	1	3.192×10^{-3}	16.52	0.0005
	A ²	0.031	6.620×10^{-3}	1	6.620×10^{-3}	34.26	< 0.0001
	Residual		4.443×10^{-3}	23	1.932×10^{-4}		
	Lack-of-fit		4.443×10^{-3}	19	2.339×10^{-4}		
	Pure error		0.000	4	0.000		
	Cor total			0.024	28		

Table 3-8- ANOVA results of the regression model for Cluster II at three depths.

Depth	Source	Coefficient estimate	Sum of squares	Degree of freedom	Mean square	F-value	p-value
1125 (m)	Model	0.43	0.013	10	1.315×10^{-3}	13.80	< 0.0001
	A	- 0.015	2.791×10^{-3}	1	2.791×10^{-3}	29.28	< 0.0001
	B	0.016	3.136×10^{-3}	1	3.136×10^{-3}	32.90	< 0.0001
	C	- 6.167×10^{-3}	4.563×10^{-4}	1	4.563×10^{-4}	4.79	0.0421
	AC	- 0.011	5.290×10^{-4}	1	5.290×10^{-4}	5.55	0.0300
	BC	- 0.011	4.622×10^{-4}	1	4.622×10^{-4}	4.85	0.0409
	CD	- 0.019	1.406×10^{-3}	1	1.406×10^{-3}	14.75	0.0012
	A ²	0.017	1.890×10^{-3}	1	1.890×10^{-3}	19.83	0.0003
	C ²	0.018	2.280×10^{-3}	1	2.280×10^{-3}	23.91	0.0001
	Residual					9.532×10^{-5}	
	Lack-of-fit					1.226×10^{-4}	
	Pure error					0.000	
Cor total					0.015		
1375 (m)	Model	0.45	0.013	10	1.319×10^{-3}	19.47	< 0.0001
	A	- 0.018	3.960×10^{-3}	1	3.960×10^{-3}	58.46	< 0.0001
	B	0.015	2.640×10^{-3}	1	2.640×10^{-3}	38.98	< 0.0001
	AB	- 0.017	1.190×10^{-3}	1	1.190×10^{-3}	17.57	0.0005
	AC	- 0.011	4.840×10^{-4}	1	4.840×10^{-4}	7.14	0.0155
	CD	- 0.015	9.302×10^{-4}	1	9.302×10^{-4}	13.73	0.0016
	A ²	0.018	2.176×10^{-3}	1	2.176×10^{-3}	32.12	< 0.0001
	B ²	0.010	7.045×10^{-4}	1	7.045×10^{-4}	10.40	0.0047
	C ²	0.017	1.912×10^{-3}	1	1.912×10^{-3}	28.22	< 0.0001
	Residual					6.774×10^{-5}	
	Lack-of-fit					8.709×10^{-5}	
	Pure error					0.000	
Cor total					0.014		

1625 (m)	Model	0.49	0.055	9	6.072×10^{-3}	16.68	< 0.0001
	A	- 0.020	0.017	1	0.017	47.12	< 0.0001
	B	0.013	7.194×10^{-3}	1	7.194×10^{-3}	19.76	0.0003
	AB	- 0.016	3.568×10^{-3}	1	3.568×10^{-3}	9.80	0.0055
	CD	- 0.018	4.890×10^{-3}	1	4.890×10^{-3}	13.43	0.0016
	A ²	0.012	3.390×10^{-3}	1	3.390×10^{-3}	9.31	0.0066
	B ²	0.024	0.015	1	0.015	41.13	< 0.0001
	C ²	0.016	6.639×10^{-3}	1	6.639×10^{-3}	18.23	0.0004
	Residual		6.918×10^{-3}	19	3.641×10^{-4}		
	Lack-of-fit		6.918×10^{-3}	15	4.612×10^{-4}		
	Pure error		0.000	4	0.000		
Cor total		0.062	28				

Table 3-9- ANOVA results of the regression model for Cluster III at three depths.

Depth	Source	Coefficient estimate	Sum of squares	Degree of freedom	Mean square	F-value	p-value
1125 (m)	Model	- 0.29	0.057	7	8.097×10^{-3}	33.39	< 0.0001
	A	- 0.041	0.020	1	0.020	84.01	< 0.0001
	B	0.047	0.027	1	0.027	110.67	< 0.0001
	AB	- 0.031	3.930×10^{-3}	1	3.930×10^{-3}	16.21	0.0006
	BD	- 0.018	1.329×10^{-3}	1	1.329×10^{-3}	5.48	0.0292
	B ²	- 0.023	3.547×10^{-3}	1	3.547×10^{-3}	14.63	0.0010
	D ²	- 0.012	1.055×10^{-3}	1	1.055×10^{-3}	4.35	0.0494
	Residual		5.093×10^{-3}	21	2.425×10^{-4}		
	Lack-of-fit		5.092×10^{-3}	17	2.995×10^{-4}	1428.56	< 0.0001
	Pure error		8.386×10^{-7}	4	2.097×10^{-7}		
Cor total		0.062	28				
1375 (m)	Model	0.55	0.097	6	0.016	38.48	< 0.0001
	A	- 0.055	0.036	1	0.036	84.85	< 0.0001
	B	0.063	0.047	1	0.047	111.25	< 0.0001
	AB	- 0.053	0.011	1	0.011	26.42	< 0.0001
	B ²	- 0.017	1.958×10^{-3}	1	1.958×10^{-3}	4.65	0.0423
	D ²	- 0.016	1.816×10^{-3}	1	1.816×10^{-3}	4.31	0.0498
	Residual		9.270×10^{-3}	22	4.214×10^{-4}		
	Lack-of-fit		9.270×10^{-3}	18	5.150×10^{-4}		
Pure error		0.000	4	0.000			
Cor total		0.11	28				
1625 (m)	Model	0.59	0.089	10	8.949×10^{-3}	32.24	< 0.0001

A	- 0.051	0.031	1	0.031	111.71	< 0.0001
B	0.043	0.022	1	0.022	78.70	< 0.0001
C	0.013	1.976×10 ⁻³	1	1.976×10 ⁻³	7.12	0.0157
AB	- 0.064	0.016	1	0.016	58.56	< 0.0001
B ²	- 0.038	9.366×10 ⁻³	1	9.366×10 ⁻³	33.74	< 0.0001
C ²	- 0.017	1.986×10 ⁻³	1	1.986×10 ⁻³	7.16	0.0154
D ²	- 0.027	4.641×10 ⁻³	1	4.641×10 ⁻³	16.72	0.0007
Residual		4.996×10 ⁻³	18	2.776×10 ⁻⁴		
Lack-of-fit		4.996×10 ⁻³	14	3.569×10 ⁻⁴		
Pure error		0.000	4	0.000		
Cor total		0.094	28			

The applied regression models were statistically significant ($p \leq 0.0001$) for all three clusters at all three mining depths. The “adequate precision” ratio, a parameter that reflects the signal to noise ratio (Mollon and Dias 2009), has values well above the minimum desirable limit of 4.0 for all clusters at all these mining depths (Table 3-10).

Table 3-10- The values of determination coefficient (R^2), adjusted, and predicted determination coefficients.

Cluster	Depth (m)	Adequate precision	R^2	Adjusted R^2	Predicted R^2
Cluster I	1125	17.3	0.85	0.81	0.65
	1375	15.0	0.80	0.72	0.59
	1625	17.6	0.82	0.78	0.65
Cluster II	1125	12.8	0.89	0.83	0.63
	1375	16.6	0.92	0.87	0.70
	1625	16.5	0.89	0.84	0.64
Cluster III	1125	23.9	0.92	0.90	0.81
	1375	25.0	0.92	0.89	0.85
	1625	24.1	0.95	0.92	0.84

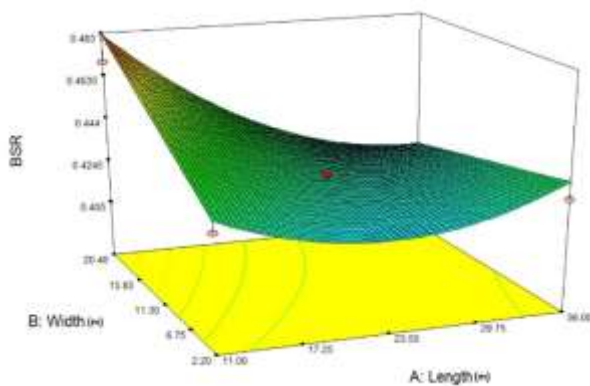
The similarity between the predicted determination coefficient (R^2) values and the adjusted R^2 (R^2_{adj}) is a valid indicator for eliminating unnecessary variables from the model. Values of these two parameters must be within approximately 0.20 of each other to be considered to be in reasonable agreement (Table 3-10) (Mollon and Dias 2009). The model R^2 values for all three

clusters at all three depths are above 0.80 indicating the goodness-of-fit of regression models for predicting the BSR results (Table 3-10).

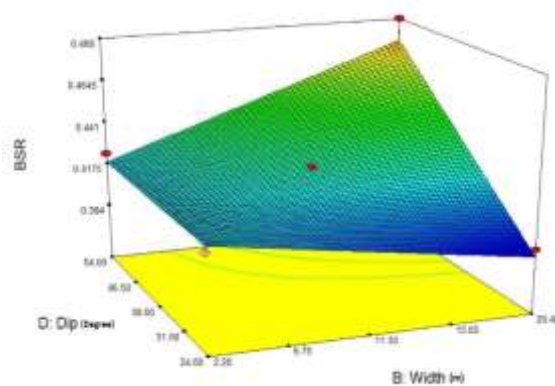
How each independent variable affects the response variable is determined through their regression coefficient values. Significant model terms for the BSR, for Cluster I, II and III at all three mining depths are presented in Tables 3-7-3-9, respectively.

3.4.1. Effects of geometrical parameters on BSR in cluster I

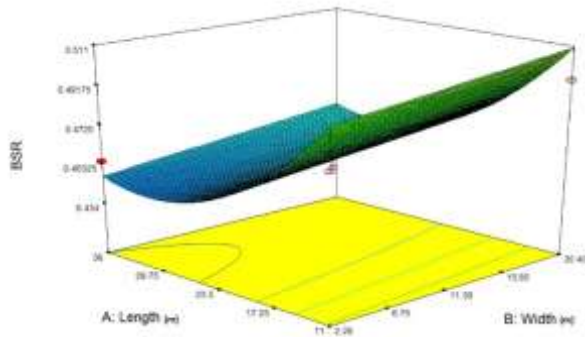
The increase in magnitude of *in situ* stress components at deeper mining levels is reflected by higher average values of BSR (Table 3-4), showing ranges from 0.398 to 0.490, 0.425 to 0.553, and 0.456 to 0.570 for mining depths of 1125, 1375, and 1625 m, respectively. Figs. 3-4 a-f, illustrate the response surface plots for the geometry Cluster I. In these plots, two factors vary while the others are kept constant at their mean values.



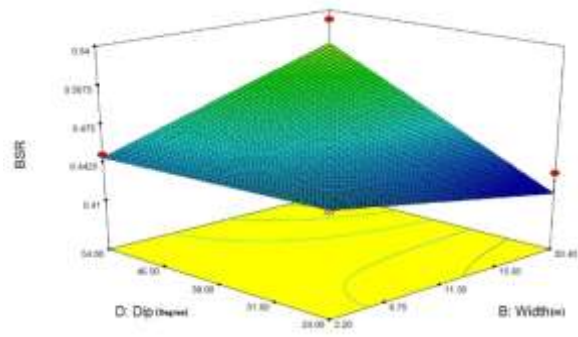
(a)



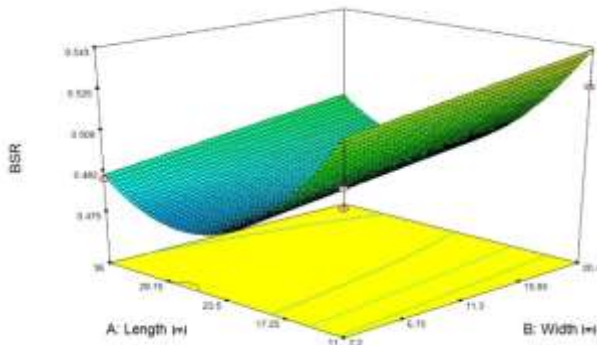
(b)



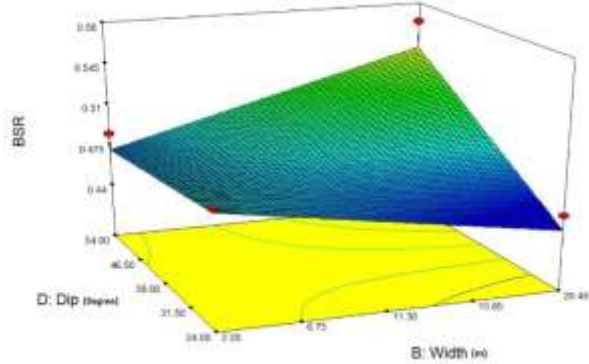
(c)



(d)



(e)



(f)

Figure 3-4 - Response surface plots for geometry Cluster I. (a) interaction between width/length at mining depth 1125 m; (b) interaction between HW dip/width at mining depth 1125 m; (c) interaction between width/length at mining depth 1375 m; (d) interaction between HW dip/width at mining depth 1375 m; (e) interaction between width/length at mining depth 1625 m; (f) interaction between HW dip/width at mining depth 1625 m.

The stope strike length has a negative effect on the BSR at all three mining depths (Fig. 3-4a, 4c, 4e) as indicated by the negative coefficient of A in Eqns. (3-13), (3-16), and (3-19), respectively. Yet, increasing the stope strike length to the higher values of its range (strike lengths above 29 m), showed a positive effect on the BSR, and was considered as the most significant parameter at 1625 m (the coefficient of A^2 in Eqns. (3-13), (3-16), and (3-19) being 0.017, 0.022, and 0.031, respectively).

These results are validated by a sensitivity analysis performed on the effect of stope strike length on principal stress components (Fig. 3-5). The negative effect of stope strike length on the

BSR can be explained as by increasing stope strike length up to 30 m, the magnitudes of maximum and minimum principal stresses (the tangential and the radial components of stress) on the region of model having maximum BSR values, decrease with differing rates so that the value of differential stress ($\sigma_1 - \sigma_3$) continues to be reduced.

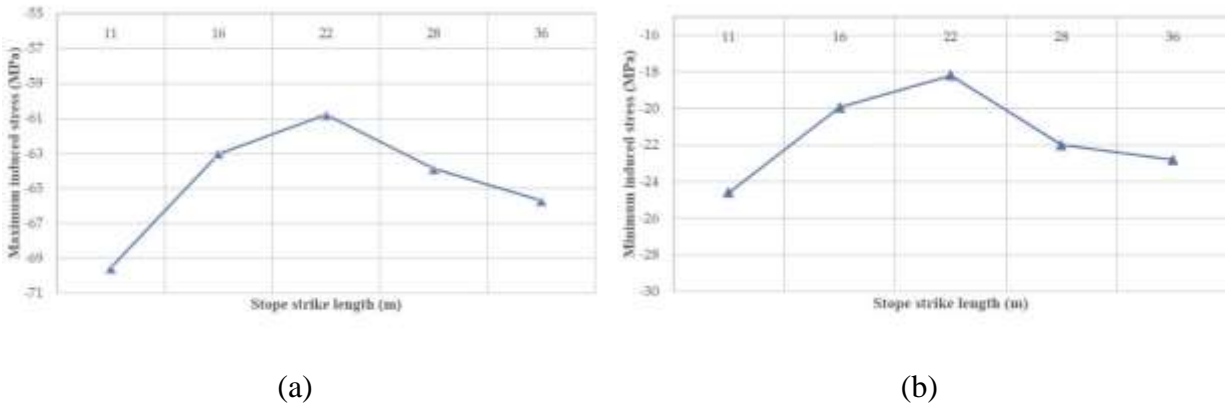


Figure 3-5 - Sensitivity analysis of the effect of stope strike length variation on (a) maximum and (b) minimum induced stress.

For strike lengths greater than 30 m, increasing the length causes the magnitude of principal stress components to be slightly more elevated and, consequently, the BSR value increases sharply.

On the other hand, variation in stope width shows a small positive effect on the BSR at all mining depths according to the positive coefficient of B in Eqns. (3-13), (3-16), and (3-19), respectively. This is expected as an increasing excavation width produces higher shear stress within excavation walls and consequently higher values of BSR.

Stope hanging wall dip also shows a significant positive effect on the BSR at all three depths (based on the positive coefficient of D in Eqns. (3-13), (3-16), and (3-19), respectively.). The results of evaluating the effect of stope hanging wall dip variation on the principal stress components for Cluster I, reveal that by increasing the hanging wall dip in the corresponding range, the magnitudes of maximum and minimum induced stress components increase with different rates, resulting in greater BSR values (Fig. 3-6).

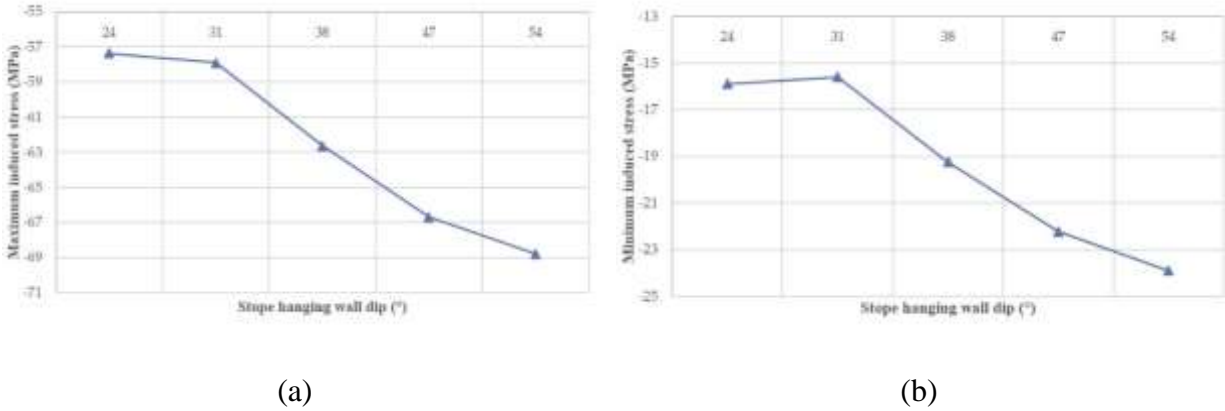


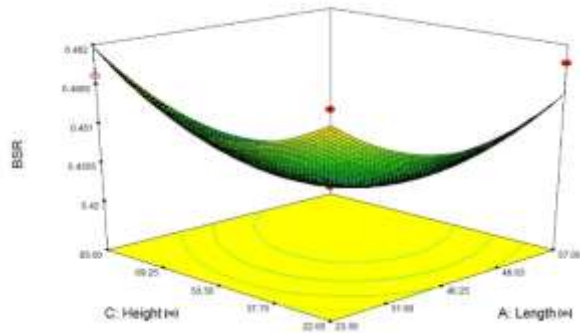
Figure 3-6 - Sensitivity analysis of the effect of stope hanging wall dip variation on (a) maximum and (b) minimum induced stress.

Fig. 3-4b illustrates the effects of stope width and stope hanging wall dip on the BSR. According to Eqn. (3-13), individual stope hanging wall dip and the interaction between stope width/stope hanging wall dip both have the most significant influence on the BSR. This indicates the absolute dominance of the effect of hanging wall dip over the stope width (the coefficients of D and BD in Eqn. (3-13) are identical at 0.020).

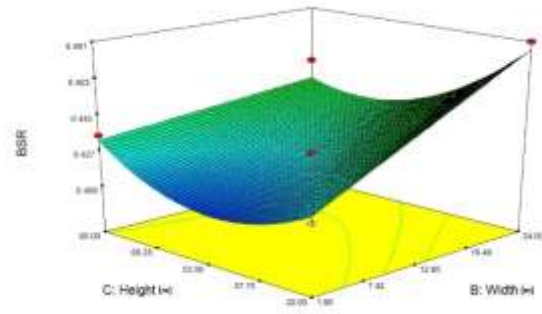
For mining depths at 1375 and 1625 m, the interacting effects of stope width/stope hanging wall dip have a significant positive influence on BSR values (according to the positive coefficient of BD in Eqns. (3-16) and (3-19), respectively). At increased mining depths, the interacting effect of stope width/stope hanging wall dip on the BSR becomes more pronounced; however, the interacting effect of stope strike length/stope width loses its significance on the BSR.

3.4.2. Effects of geometrical parameters on BSR in cluster II

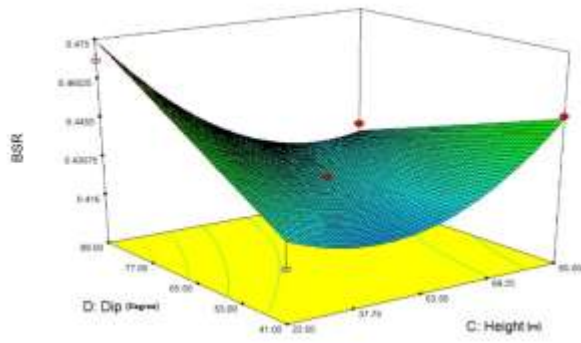
Figs. 3-7 a–h plot the effects of significant parameters on the BSR for Cluster II at the three mining depths.



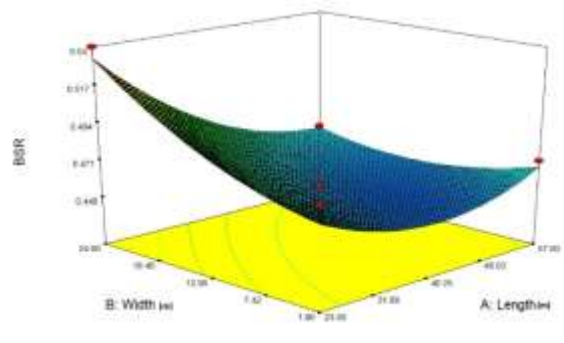
(a)



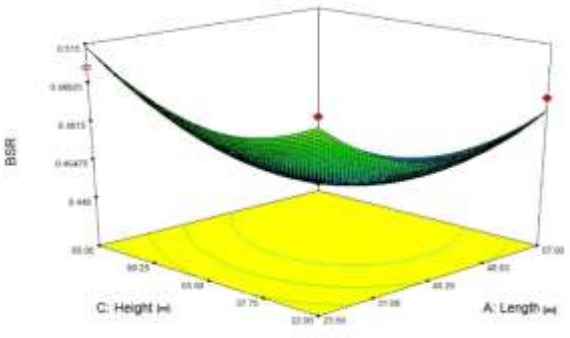
(b)



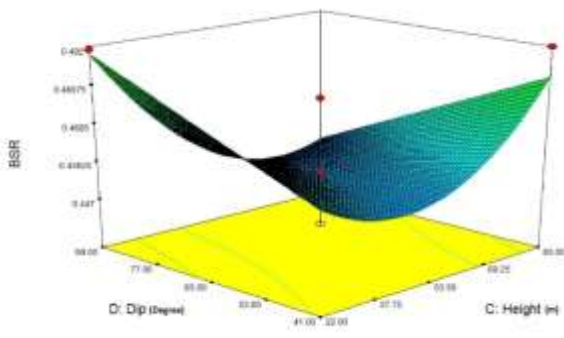
(c)



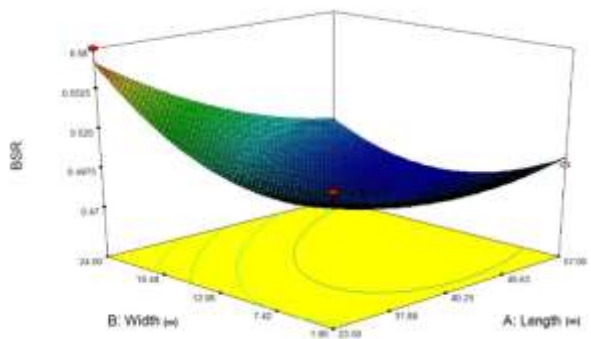
(d)



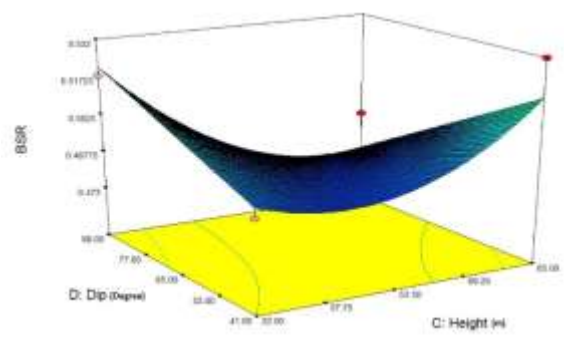
(e)



(f)



(g)



(h)

Figure 3-7 - Response surface plots for geometry Cluster II. (a) interaction between height/length at mining depth 1125 m; (b) interaction between height/width at mining depth 1125 m; (c) interaction between HW dip/height at mining depth 1125 m; (d) interaction between length/width at mining depth 1375 m; (e) interaction between height/length at mining depth 1375 m; (f) interaction between HW dip/height at mining depth 1375 m; (g) interaction between length/width at mining depth 1625 m; (h) interaction between HW dip/height at mining depth 1625 m.

The BSR shows high sensitivity to changes of the stope strike length at all three mining depths (the coefficient of A is -0.015, -0.018, and -0.020 in Eqns. (3-14), (3-17), and (3-20), respectively) in which an increased stope strike length from 23.5 m to 57.0 m results in a decreased BSR value at all mining depths (Fig. 3-7a, 7d, 7g).

At high strike length values in the corresponding range (values greater than 49 m), increased stope strike length leads to an increase in the BSR value at all three depths (based on the coefficient(s) of A^2 in Eqns. (3-14), (3-17), and (3-20), respectively). Decreasing the BSR value by enlarging stope strike length occurs as reduction of the magnitude of principal stress components occurs with unequal rates.

The positive effect of stope width on the BSR is presented in Figs. 3-7b, 3-7d, and 3-7g for the three mining depths 1125, 1375, and 1625 m, respectively. Therefore, increasing the stope width from 1.9 to 24.0 m at all three mining depths, increases the BSR value. The effect of changing stope width in high ranges is significant only in the two shallower depth levels, while for the deepest mining level (1625 m) the parameter B^2 is considered as the most significant parameter affecting the BSR value (the coefficient of B^2 is equal to 0.010 and 0.024 in Eqns. (3-17) and (3-20), respectively). It is evident that by increasing the excavation width, the shear stress around the excavation increases and results in higher values of BSR. A sensitivity analysis confirms the effect of stope width variation on the principal stress components (σ_1 and σ_3); it is observed that increasing stope width causes the maximum induced stress (σ_1) to increase at a higher rate than the minimum principal stress (σ_3), resulting in enhancement of the BSR value (Fig. 3-8).

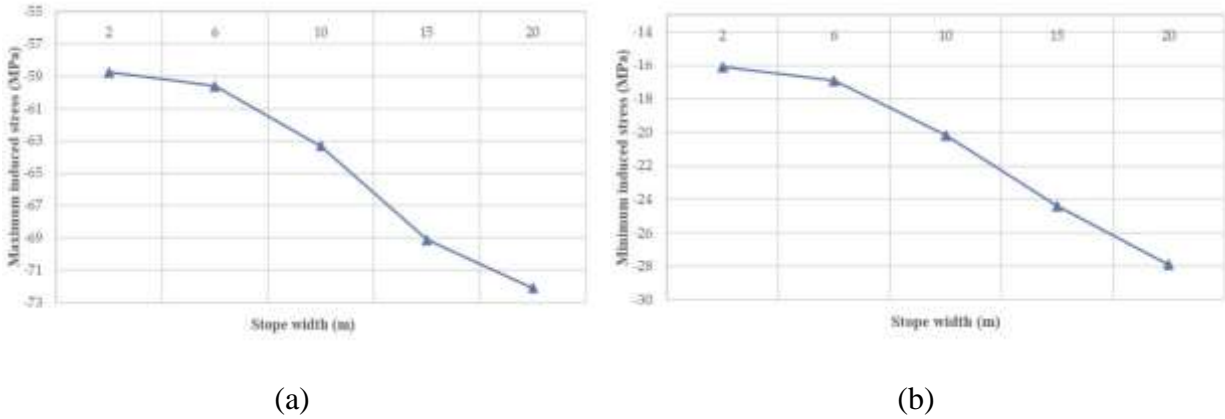


Figure 3-8 - Effect of slope width variation on (a) maximum and (b) minimum induced stress

The effect of slope height on the BSR is considered significant only at the mining depth of 1125 m showing a very small positive effect (coefficient of C in Eqn. (3-14)).

Following Eqns. (3-14) and (3-17), the interaction between two negative parameters, stope strike length and stope height, has a negative significant effect on the BSR at mining depths 1125 and 1375 m (Figs. 3-7a, 3-7e). From mining depth 1375 to 1625 m, interactive effect of stope strike length/stope width has a considerable negative synergistic influence on the target variable (Figs. 3-7d, 3-7g). This might be due to the powerful negative effect of strike length overcoming the small positive effect of stope width. Moreover, the parameter stope width also shows a significant negative effect interacting with stope height only at mining depth 1125 m (Fig 3-7b).

Finally, the BSR is significantly controlled by the interaction of stope height/stope hanging wall dip at all three depths (Fig. 3-7c, 3-7f, and 3-7h) in which this negative synergistic effect is considered as the most significant parameter at mining depth 1125 m (according to the coefficient of CD in Eqns. (3-14), (3-17), and (3-20)).

3.4.3. Effects of geometrical parameters on BSR in cluster III

The impacts of significant parameters on the BSR are presented in Figs. 3-9 a–f for Cluster III at the three mining depths. Stope strike length at all three depths has a significant negative effect

on the BSR (based on the negative coefficient of A in Eqns. (3-15), (3-18), and (3-21) respectively).

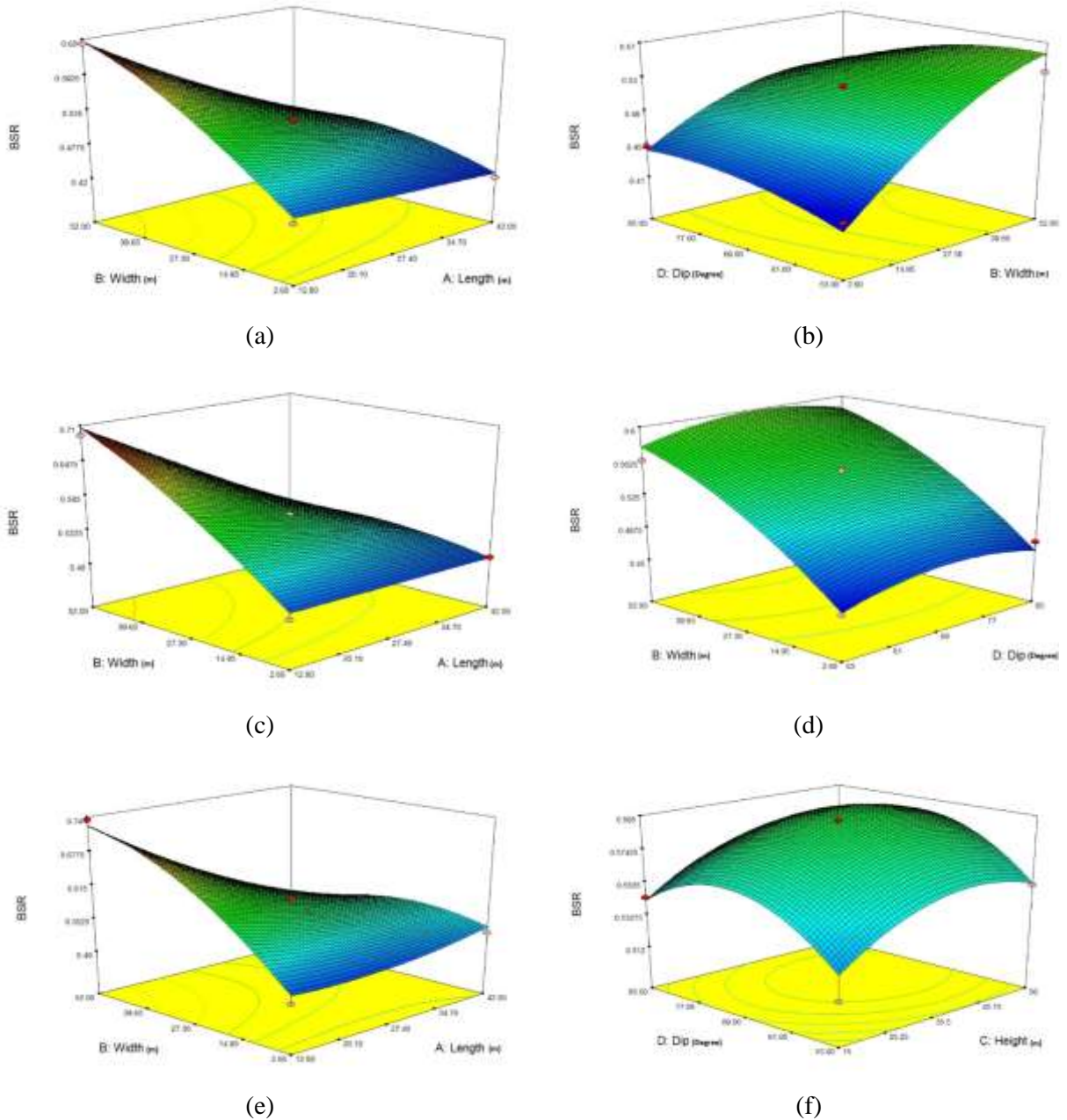


Figure 3-9 - Response surface plots for geometry Cluster III. (a) interaction between width/length at mining depth 1125 m; (b) interaction between HW dip/width at mining depth 1125 m; (c) interaction between width/length at mining depth 1375 m; (d) interaction between HW dip/width at mining depth 1375 m; (e) interaction between width/length at mining depth 1625 m; (f) interaction between HW dip/height at mining depth 1625 m.

In contrast, stope width has a positive effect on BSR at all three mining depths. It is considered as the most significant parameter at mining depths 1125 and 1375 m (with the B coefficient is 0.047, 0.063 and 0.043 in Eqns. (3-15), (3-18), and (3-21), respectively). Changing stope width to high ranges also has a significant negative effect at all three mining depths (coefficient of B^2 in Eqns. (3-15), (3-18), and (3-21) respectively).

The parameter stope height has a small positive effect on the BSR value, albeit only at the deepest mining level (1625 m), while the effect of stope height variations at higher ranges all has a significant negative effect on BSR at the mentioned mining depth (coefficient of C and C^2 in Eqn. (3-21)).

Stope hanging wall dip, by itself, does not show any significant effect but variations at the higher ranges of this parameter (between 77° to 85°) show a significant negative effect on the BSR at all three mining depths (according to the negative coefficients of D^2 in Eqns. (3-15), (3-18), and (3-21) respectively). The stope hanging wall dip also shows a significant negative effect interacting with stope width at mining depth of 1125 m.

The interaction between stope strike length and stope width presents a significant negative effect (following Eqn. (3-15), Eqn. (3-18), and Eqn. (3-21)) on the BSR at all mining depths and is considered as the most significant parameter for the depth 1625 m.

A comparison of the BSR results between the three geometry clusters at all mining depths, reveals that under such conditions of rock mass quality and *in situ* stress state, the BSR values are above the damage initiation threshold of 0.4 reported by Castro *et al.* (2012). However, only for the Cluster III at mining depth 1625 m do the values of BSR surpass the major damage limit of 0.7 that leads to failure of the rock mass. The obtained results indicate that for the assumed rock mass quality, stopes having low-moderate values of hanging wall HR and dip (Cluster I) are less

damaged and consequently more stable in terms of BSR. However, steeply dipping stopes having moderate hanging wall HR (Cluster III) experience major rock mass brittle damage and probable strainburst failure. The degree of brittle damage for stopes having geometries belonging to the second cluster (moderate-high hanging wall HR and dip) is highly influenced by strong interactions between geometrical parameters. This complicates a general conclusion about the effect of stope size and orientation. It seems that broad ranges for the values of each of the geometrical parameters cause a greater synergistic effect between the parameters when compared to situations having reduced variations for the geometrical parameters. Finally, it should be noted that the simulated models suggest that brittle failure is not the dominant mode of rock mass failure in such defined conditions of rock mass quality and *in situ* stress state.

3.4.4. Stope geometry optimization corresponding brittle rock mass failure

To determine the most stable (least damaged) open stope geometries in terms of brittle failure, a mathematical optimization is employed to define the optimal values for each geometrical parameter for all the clusters at all three mining depths. The minimum BSR and the suggested models were determined for each geometry cluster and the corresponding optimal conditions of input variables. Mathematical optimization is applied to determine a maximum point of the desirability function by adjusting the values of stope strike length, stope width, stope height, and stope hanging wall dip within their ranges for each cluster and minimizing the BSR value. Desirability is defined as an objective function which ranges from zero to one. The aim of numerical optimization is to find a combination of input parameter values which maximizes the desirability function (Stat-Ease 2005). The predicted optimal conditions are simulated by

FLAC3D. As illustrated in Table 3-11, the smallest value for minimum BSR predicted for Cluster I at a mining depth of 1125 m, corresponding to stope strike length of 33.2 m, stope width of 15.4 m, and the stope hanging wall dip of 25°. With this combination of input variables, the BSR is predicted as 0.395. In contrast, the largest value for a minimum BSR is modeled for Cluster III at mining depth of 1625 m, stope strike length of 31.3 m, stope width of 3.4 m, stope height of 18.2 m, and stope hanging wall dip of 79.6° producing a BSR value of 0.485. The desirability value is found to be 1.000 for the aforementioned cases and above 0.979 for all the cases (Table 3-11). The high degree of agreement between the predicted and repeated optimal results for all the cases indicates the efficiency and reliability of Box–Behnken design employed in combination with numerical modeling for evaluating and optimizing the effects of open stope geometrical parameters on the rock mass brittle damage.

Table 3-11- Numerical optimization of four independent variables and the responses based on the desirability value for three clusters at three mining depths.

Cluster/Depth	Length (m)	Width (m)	Height (m)	Dip (°)	BSR (Predicted)	BSR (Repeated)	Desirability
Cls1–1125 m	33.2	15.4	*	24.8	0.395	0.398	1.000
Cls1–1375 m	23.8	18.7	*	25.0	0.422	0.417	1.000
Cls1–1625 m	30.7	19.3	*	24.1	0.446	0.450	1.000
Cls2–1125 m	38.5	2.8	45.9	43.5	0.402	0.403	1.000
Cls2–1375 m	51.6	11.3	78.9	89.0	0.438	0.433	0.979
Cls2–1625 m	56.0	17.0	71.6	70.4	0.479	0.482	1.000
Cls3–1125 m	34.0	3.0	*	55.0	0.414	0.419	1.000
Cls3–1375 m	42.0	2.6	*	53.0	0.451	0.441	0.999
Cls3–1625 m	31.3	3.4	18.1	79.6	0.485	0.487	1.000

3.5. Conclusion

A response surface methodology combined with a finite difference code *FLAC3D* evaluated the individual and interactive effects of open stope geometrical parameters related to brittle damage of the surrounding rock mass of Canadian underground mines. A Box–Behnken design assessed the effects of stope strike length, stope width, stope height, and stope hanging wall dip belonging to three different geometry clusters on the BSR of the rock mass at three mining levels (1125, 1375, and 1625 m). The applied quadratic models provide an adequate fit to the obtained data. The mathematical relationship between the BSR and the geometrical parameters are accurately described by second-order polynomial equations. Results indicate that the BSR value increases for all three clusters with increasing mining depth, due to the increasing magnitude of *in situ* stress. The highest BSR values (independent from mining depth) were observed for Cluster III, having a moderate range of hanging wall HR and high range of hanging wall dip.

The lowest BSR values (independent from mining depth) were observed for Cluster I, having a low-moderate range of hanging wall HR and low-moderate range of hanging wall dip. The individual and interactive effects of stope geometrical parameter variations on the rock mass brittle damage are significant. Stope strike length and stope width show a negative and positive effect, respectively, on BSR values for all clusters at all three mining depths. Stope height changing from 69 m to 85 m showed a significant positive effect on BSR value. For shallow to moderately dipping stopes (up to 54°), increased hanging wall dip causes the BSR value to increase. For steeply dipping stopes, increasing hanging wall dip decreases the BSR value. For Cluster I, interaction between width and dip has a very significant positive effect; for Cluster II, the interaction between height and dip has a very significant negative effect; for Cluster III, interaction of length/width has a very significant negative effect on BSR.

It should be possible to apply a similar methodology to evaluate the effect of stope geometrical parameters on gravity-driven modes of rock mass failure caused by stress relaxation. Ultimately, by considering both the brittle and tensile modes of failure, a global conclusion can be obtained about optimal stope geometric conditions for ensuring stability.

Acknowledgements

This work was funded by a grant from Natural Sciences and Engineering Research Council of Canada (NSERC) and the authors would like to acknowledge the Niobec mine (Saint-Honoré, Québec).

3.6. References

- Abdellah W. (2013). Geotechnical risk assessment of mine haulage drifts during the life of a mine plan. PhD thesis, McGill University, Montreal, Canada.
- Abdellah W, Mitri HS, Thibodeau D, Moreau-verlaan L. (2014)a. Stability of mine development intersections — a probabilistic analysis approach. 195:184–95.
- Abdellah W, Raju GD, Mitri HS, Thibodeau D. (2014)b. Stability of underground mine development intersections during the life of a mine plan. *Int J Rock Mech Min Sci.* 72:173–181.
- Aglawe JP. (1999). Unstable, violent failure around underground openings in highly stressed ground. PhD thesis, Queen’s University at Kingston, Canada.
- Ahmadi A, Heidarzadeh S, Reza A, Darezereshki E, Asadi H. (2014). Optimization of heavy metal removal from aqueous solutions by maghemite ($\gamma\text{-Fe}_2\text{O}_3$) nanoparticles using response surface methodology. *J Geochemical Explor.* 147:151-158.
- Anderson MJ, Whitcomb PJ. (2005). *RSM Simplified Optimizing Processes Using Response Surface Methods for Design of Experiments.* Productivity Press.
- Arjang B, Herget G. (1997). *In situ* ground stresses in the Canadian hard rock mines: an update. *Int J Rock Mech Min Sci* 34:paper 015.
- Castro LAM, Bewick RP, Carter TG. (2012). An overview of numerical modelling applied to deep mining. In: Azevedo R, editor. *Innovative numerical modelling in geomechanics.* London: CRC Press — Taylor & Francis Group; p. 393–414.

- Chen D, Chen J, Zavodni ZM. (1983). Stability analysis of sublevel open stopes at great depth. The 24th U.S. Symposium on Rock Mechanics (USRMS).
- Chen D. (1994). Design of rock bolting systems for underground excavations. PhD thesis. University of Wollongong, New South Wales, Australia.
- Chen G, Jia Z, Ke J. (1997). Probabilistic analysis of underground excavation stability. *Int. J. Rock Mech. & Min. Sci.* 34:3-4, paper No. 051.
- Clark L. (1998). Minimizing dilution in open stope mining with a focus on stope design and narrow vein longhole blasting. MSc thesis, University British Columbia, Vancouver, Canada.
- Diederichs MS, Kaiser PK. (1996). Rock instability and risk analyses in open stope mine design. *Can Geotech J.* 33(3):431–439.
- Diederichs MS. (1999). Instability of hard rock masses: the role of tensile damage and relaxation. PhD Thesis. Waterloo, Ontario: University of Waterloo; Canada.
- Diederichs MS, Kaiser PK, Eberhardt E. (2004). Damage initiation and propagation in hard rock during tunneling and the influence of near-face stress rotation. *International Journal of Rock Mechanics and Mining Sciences* 41(5):785-812.48.
- Einstein HH (1996) Risk and Risk Analysis in Rock Engineering. *Risk Anal Tunn* 11:141–155 . doi: 10.1016/0886-7798(96)00014-4.
- Ellefmo S. (2005). A probabilistic approach to the value chain of underground iron ore mining. DEng thesis, Norwegian University of Science and Technology, Trondheim, Norway.
- Germain P, Hadjigeorgiou J (1997) Influence of stope geometry and blasting patterns on recorded overbreak. *Int J rock Mech Min Sci Geomech Abstr* 34:628.
- Govett GJS, Govett MH. (1976). World mineral supplies assessment and perspective. Volume 3. New York. Elsevier.
- Hammah RE, Curran JH. (1999). On distance measures for the fuzzy K-means algorithm for joint data. *Rock Mech Rock Eng* 32(1):1–27.
- Henning JG (2007) Evaluation of Long-Hole Mine Design Influences on Unplanned Ore Dilution. PhD thesis, McGill University, Montreal, Canada.
- Henning JG, Mitri HS (2007) Numerical modelling of ore dilution in blasthole stoping. *Int J Rock Mech Min Sci.*; 44:692–703.
- Hoek E (2007) Practical rock engineering. <http://www.rocscience.com/hoek/PracticalRockEngineering.asp>, World Wide Web edition.
- Hudson JA (1993) *Comprehensive Rock Engineering: Principles, Practice & Projects*. Vol 5. Pergamon Press.
- Hudyma MR (1998) Development of empirical rib pillar design criterion for open stope mining. PhD thesis, University of British Columbia. Vancouver, Canada.

- Hughes R (2011) Factors influencing overbreak in narrow vein longitudinal retreat mining. MSc thesis. McGill University, Montreal, Canada.
- Idris MA, Saiang D, Nordlund E (2011) Probabilistic analysis of open stope stability using numerical modelling. *Int. J. Min. Miner. Eng.* 3(3):194–219.
- Idris MA (2014) Probabilistic stability analysis of underground mine excavations. PhD thesis, Lulea University of Technology, Lulea, Sweden.
- Idris MA, Basarir H, Nordlund E, Wettainen T (2013) The Probabilistic Estimation of Rock Masses Properties in MalMBERGET Mine, Sweden. *Electron J Geotech Eng* 18:269–287
- Itasca Consulting Group, Inc. (2015). *FLAC3D – Fast Lagrangian Analysis of Continua in 3 Dimensions*, Ver. 5.0, User's Guide. Minneapolis: Itasca.
- Kaiser PK, Diederichs MS, Martin CD (2000) Underground works in hard rock tunnelling and mining. In: *GeoEng2000, Proceedings of the International Conference on Geotechnical and Geological Engineering*, Melbourne, Australia.
- Langford, J.C., Diederichs, M.S., (2013). Reliability based approach to tunnel lining design using a modified point estimate method. *International Journal of Rock Mechanics and Mining Sciences*. 60, pp. 263-276.
- Lü Q, Low BK. (2011). Probabilistic analysis of underground rock excavations using response surface method and SORM. *Comput Geotech* 38:1008–21.
- Mathews KE (1981) Prediction of stable excavations for mining at depth below 1000 metres in hard rock. Ottawa
- Maloney S, Kaiser P, Vorauer A. (2006). A re-assessment of *in situ* stresses in the Canadian Shield. In *Golden Rocks 2006, The 41st US Symposium on Rock Mechanics (USRMS)* American Rock Mechanics Association.
- Milne D. (1996). Underground design and deformation based on surface geometry. PhD Thesis, Mining Department, University of British Columbia, Vancouver, Canada.
- Mollon G, Dias D, Soubra AH. (2009). Probabilistic analysis of circular tunnels in homogeneous soil using response surface methodology. *J Geotech Geoenviron Eng* 135:1314–25.
- Pakalnis RC, Poulin R, Hadjigeorgiou J. (1995). Quantifying the cost of dilution in underground mines. *Mining Eng Dec*: 1136–41.
- Perron, J (1999) Simple solutions and employee's involvement reduced the operating cost and improved the productivity at Langlois mine. Proceeding 14th CIM Mine Operator's Conference. Bathurst, New Brunswick, Canada.
- Potvin Y. (1988). Empirical open stope design in Canada. PhD thesis, University of British Columbia, Vancouver, Canada.
- Potvin Y, Hudyma M. (2000). Open stope mining in Canada. In: *Proc MassMin 2000*, Brisbane, Australia, p. 661–74.

- Pytel W, Świtoń J (2013) Assessment of the Impact of Geomechanical Parameters Variability on Underground Excavations Stability Using Response Surface Method. *Stud Geotech Mech* 35: . doi: 10.2478/sgem-2013-0014
- Shnorhokian S, Mitri HS, Moreau-verlaan L (2015) assessment of stope sequence scenarios in a diminishing ore pillar. *Int J Rock Mech Min Sci* 74:103–118 . doi: 10.1016/j.ijrmms.2014.12.005.
- Stat-Ease, Inc. (2005). *Design-Expert 7.0.0* Minneapolis, USA.
- Villaescusa E. (2014). *Geotechnical design for sublevel open stoping*. CRC Press.
- Wang J (2004) Influence of stress, undercutting, blasting, and time on open stope stability and dilution. PhD thesis, University of Saskatchewan, Saskatoon, Canada.
- Wang J, Milne D, Wegner L, Reeves M (2007) Numerical evaluation of the effects of stress and excavation surface geometry on the zone of relaxation around open stope hanging walls. *Int J Rock Mech Min Sci* 44:289–298.
- Zhang Y, Mitri HS (2008) Elastoplastic stability analysis of mine haulage drift in the vicinity of mined stopes. *Int J Rock Mech Min Sci* 45:574–593 . doi: 10.1016/j.ijrmms.2007.07.020
- Zniber H, Mouhabbis E (2013) Effect of stope construction parameters on ore dilution in narrow vein mining. MSc thesis. McGill University, Montreal, Canada.

Chapter 4 - Evaluation of the effect of geometrical parameters on the stope probability of failure in the open stoping method using numerical modeling²

4.1. Abstract

Stress-induced failure is among the most common causes of instability in Canadian deep underground mines. Open stoping is the most widely practiced underground excavation method in these mines, and creates large stopes which are subjected to stress-induced failure. The probability of failure (POF) depends on many factors, of which the geometry of an open stope is especially important. In this study, a methodology is proposed to assess the effect of stope geometrical parameters on the POF, using numerical modelling. Different ranges for each input parameter are defined according to previous surveys on open stope geometry in a number of Canadian underground mines. A Monte-Carlo simulation technique is combined with the finite difference code *FLAC3D*, to generate model realizations containing stopes with different geometrical features. The probability of failure (POF) for different categories of stope geometry, is calculated by considering two modes of failure; relaxation-related gravity driven (tensile) failure and rock mass brittle failure. The individual and interactive effects of stope geometrical parameters on the POF, are analyzed using a general multi-level factorial design. Finally, mathematical optimization techniques are employed to estimate the most stable stope conditions, by determining the optimal ranges for each stope's geometrical parameter.

KEYWORDS: Stope stability, stope geometrical parameters, probability of failure, general factorial design, numerical modeling, Sublevel open stoping.

²Heidarzadeh S, Saeidi A, Rouleau A. Evaluation of the effect of geometrical parameters on stope probability of failure in the open stoping method using numerical modeling. *International Journal of Mining Science and Technology*; 2018

4.2. Introduction

Stability of underground excavations has become a critical issue in the mining industry due to the growing tendency to extract deep underground mineral resources. Open stoping underground excavation method is the most widely practiced technique in Canadian underground mines (Hudson 1993; Wang 2004; Zhang and Mitri 2008; Abdellah et al. 2014b). Open stoping creates large underground openings called “Stopes” whose level of stability must be assessed. Maintaining stope stability not only provides safety for the work force and underground equipment, but also contributes to the mine production capacity and profitability by minimizing unplanned ore dilution (Einstein 1996; Idris 2011; Brown 2012; Abdellah et al. 2014b).

Although the open stope stability state is significantly affected by external parameters such as the applied natural and mining-induced stresses, and the surrounding rock mass geomechanical characteristics (Diederichs and Kaiser 1996; Chen et al., 1997; Henning and Mitri 2007; Idris et al. 2013; Villaescusa 2014), stope geometry itself plays a key role in defining the level of stability (Zhang and Mitri 2008) (Villaescusa 2014) (Aglawe 1999).

Underground instability and the probable failure conditions, for open stopes located in deep hard rock, occur as a result of high magnitude mining-induced stresses. Low confinement stress-induced failure consists of the two dominant modes, namely; (1) stress-induced spalling and slabbing (brittle failure); and (2) structurally-controlled gravity-driven failures (i.e. tensile) (Castro et al. 2012).

Effects of open stope geometry (shape, size and inclination) on the state of stability, can be evaluated by using different analytical, empirical and numerical approaches. Numerical methods offer more advantages and less drawbacks compared to the other two methods (Idris 2014), therefore they are widely used to analyze the stability of underground open stopes.

Numerical evaluation of the effects of stope geometrical parameters on various instability modes has been investigated by several important studies. The effect of open stope height on the stability was studied by (Chen et al. 1983) , (Perron 1999), (Yao *et al.* 1999), and (Henning and Mitri 2007). These studies have indicated that increasing the stope height results in increasing the overbreak of stope walls and consequently contributes to unplanned ore dilution. The effect of stope strike length variations on stability were also studied by (Henning and Mitri 2007), (Hughes et al. 2011) and (Zniber EL Mouhabbis 2013), showing that longer strike lengths create greater ore dilution compared to shorter strike lengths, thereby reducing the stability level. Studies on the effect of stope span width variations on stability have demonstrated that narrower stopes result in higher dilutions, thus increasing the stope span width provides more stability (Zniber El Mouhabbis 2013) and (Pakalnis et al. 1995). Many studies also investigated the effect of stope hanging wall dip on stability (Henning and Mitri 2007), (Yao et al. 1999), (Hughes 2011), (Zniber El Mouhabbis 2013) and (Urli 2015) and concluded that a shallower hanging wall dip contributes to a larger overbreak extent due to the significant effect of gravity on hanging wall at low inclinations. Moreover, the effect of stope hanging wall size and shape [defined through the parameter hydraulic radius (HR)] on the stope stability was assessed by some comprehensive studies (Milne 1996), (Germain and Hadjigeorgiou 1997), (Clark 1998) and (Wang et al. 2007). It was reported that increasing the stope hanging wall HR adversely affected the hanging wall stability, by generating a greater extent of overbreak.

In a review of previous studies, (Villaescusa 2014) identified a general assumption that open stopes with high vertical and short horizontal dimensions, and/or long horizontal and short vertical dimensions have a higher degree of wall stability compared to square-shaped geometries, which are considered to generate the most unstable open stopes.

Nevertheless, no comprehensive evaluation has been made of the combined effects of open stope size, shape and inclination on their state of stability. In other words, the previous studies mainly focused on the effects of individual parameters while not considering the simultaneous variation of other geometrical parameters. Therefore, the aforementioned studies and their corresponding assumptions present a number of drawbacks. Firstly, most of the previous studies were case specific, and the variation ranges for selected geometric parameters were limited. Therefore, obtaining a comprehensive interpretation of the effect of selected geometric parameters on the stope stability seemed to be difficult. Secondly, in previous studies, single or multiple parameter(s) were evaluated individually, and therefore the interferences caused by variation of other stope geometric parameters have been underestimated. Finally, in previous studies either relaxation-related tensile failure, or rock mass brittle mode of failure, was selected to evaluate the state of stability; however, in real conditions the occurrence of different modes of stress-driven failure are possible depending on the applied *in situ* stress regime and rock mass geomechanical characteristics. Thus it would be more reasonable to consider all possible failure scenarios when evaluating the state of stope stability.

The present study uses a methodology to assess the individual and combined effects of stope geometrical parameters [i.e., stope hanging wall HR, stope span width and stope hanging wall dip] on the “probability of failure” (POF). The POF is calculated considering both relaxation-related gravity driven (tensile) failure, and rock mass brittle failure mode, respectively through stability indicators of (1) minimum principal induced stress (σ_3) and (2) rock mass BSR. The variation range of each geometrical parameter is derived from a survey of numerous open stopes (Wang 2004) located in the Canadian Shield. A Monte-Carlo simulation technique combined with the finite difference code *FLAC3D* (Itasca 2015) are utilized to simulate a large number of stopes,

grouped in categories with different ranges of span width, hanging wall HR and hanging wall dip. The individual and interactive effects of the aforementioned geometrical parameters are evaluated by using a general multi-level factorial analysis. Mathematical optimization techniques are ultimately used to predict the most stable slope states (in terms of the POF) by determining the optimal ranges for each geometrical input parameter.

4.3. Methodology

Figure. 4-1 proposes the methodology and the sequential steps we utilize to evaluate the individual and combined effects of slope geometrical parameters on the POF.

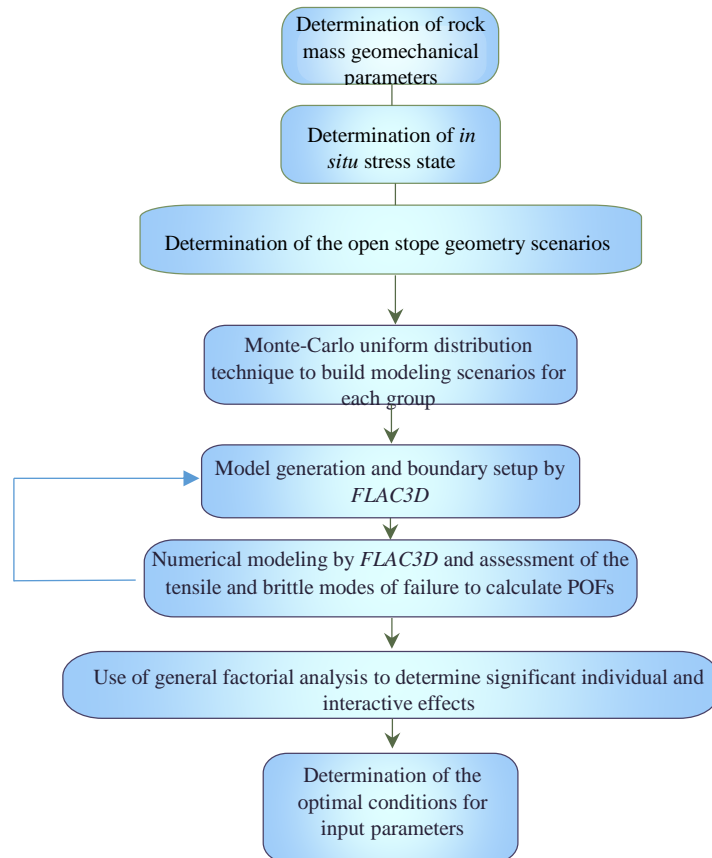


Figure 4-1 - The methodology and the sequential steps to evaluate the individual and combined effects of slope geometrical parameters on the POF.

4.3.1. Determination of rock mass parameters

The objective of this study is to evaluate the effect of open stope geometrical parameters on the POF by numerical modeling, and as such the rock mass geomechanical parameters should be assigned deterministically. To determine the rock mass geomechanical parameters, the unconfined compressive strength (UCS) of intact rock, the Hoek-Brown material constant (m_i) and the Geological Strength Index (GSI) of the rock mass are defined in accordance with the typical rock mass quality of the Canadian Shield. Deep underground mines in the Canadian Shield are generally located in moderate to high strength metamorphic and igneous Precambrian rocks (e.g. andesite, rhyolite, basalt and granite) (Zhang and Mitri 2008) (Abdellah et al. 2014b). Hence, the mean value of the parameters GSI, UCS and m_i are assigned accordingly (Tables 4-1 – 4-2).

Table 4-1 - Intact rock properties.

Property (units)	Value
UCS (MPa)	120
Young's modulus (GPa)	80
m_i	13
Poisson's ratio	0.2

The UCS and m_i values of the intact rock and the GSI value for the rock mass, are used to calculate the geomechanical rock mass properties using the following equations (Eqns. 4-1–4-6) (Hoek 2007):

$$m_b = m_i e^{\left(\frac{GSI-100}{28-14D}\right)} \quad (4-1)$$

$$s = e^{\left(\frac{GSI-100}{9-3D}\right)} \quad (4-2)$$

$$a = \frac{1}{2} + \frac{1}{6} \left(e^{\frac{-GSI}{15}} - e^{\frac{-20}{3}} \right) \quad (4-3)$$

$$\sigma_{cm} = \sigma_{ci} s^a \quad (4-4)$$

$$\sigma_t = \frac{s \sigma_{ci}}{m_b} \quad (4-5)$$

$$E_{rm} = E_i \left(0.02 + \frac{1 - \frac{D}{2}}{1 + e^{\frac{60 + 15D - GSI}{11}}} \right) \quad (4-6)$$

where D represents the degree of disturbance of the rock mass due to the excavation method and blasting; ranging from 0 for undisturbed *in situ* rock masses to 1 for highly disturbed rock masses (Hoek 2007). The value of 0.8 is selected for the parameter D in this study, as the rock mass is assumed to be disturbed by blasting effects. The parameters m_b , s and a are the Hoek-Brown failure criteria constants defining the rock mass properties; σ_{cm} and σ_t stand for the compressive and tensile strengths of the rock mass respectively; and E_{rm} is deformation modulus of the rock mass. The parameter σ_{ci} represents the uniaxial compressive strength (UCS) of the intact rock. Rock mass strength and deformability parameters with their corresponding values are given in Table 4-2.

Table 4-2 - Rock mass geomechanical parameters.

Property (units)	Value
GSI	70
Bulk modulus, K (GPa)	4.684
Shear modulus, G (GPa)	9.760
Tensile strength, σ_t (MPa)	0.57
m_b	2.18
s	0.01
a	0.501

4.3.2. State of *in situ* stress

Excavating an opening causes the existing *in situ* stress regime of the surrounding rock mass to be perturbed. The magnitude and orientation of the *in situ* stress components have a significant influence on the stability of any underground excavation (Hoek 2007). Arjang *et al.* (1997), stated that the major and intermediate principal stress components (σ_1 and σ_2) in the Canadian Shield are oriented almost horizontally, plunging by 10° or less, while the minor principal stress component (σ_3) is vertical. For near vertical deposits in the Canadian Shield, Zhang and Mitri (2008), mentioned that the maximum horizontal stress component is normally inclined perpendicular to the strike of the ore body and the minimum horizontal stress component oriented parallel to the ore strike.

In this study, the average mining depth of 1400 m is considered as representative of deep underground stopes for estimating the deterministic values of *in situ* stress components (Table 4-3).

Table 4-3 - The values of *in situ* stress components.

Depth (m)	σ_H (MPa)	σ_h (MPa)	σ_V (MPa)
1400	60.0	39.5	29.0

The magnitudes of *in situ* stress components are estimated using the Eqns. 4-7- 4-9 as suggested by Maloney and Kaiser. (2006):

$$\sigma_1(\text{MPa}) = 0.026z(m) + 23.636 \quad (4-7)$$

$$\sigma_2(\text{MPa}) = 0.016z(m) + 17.104 \quad (4-8)$$

$$\sigma_3(\text{MPa}) = 0.020z(m) + 1.066 \quad (4-9)$$

4.3.3. Determination of model geometry

The stope hanging wall hydraulic radius (HR), the stope span width and the stope hanging wall dip are selected as appropriate input parameters, to define stope size, shape and inclination (Fig. 4-2).

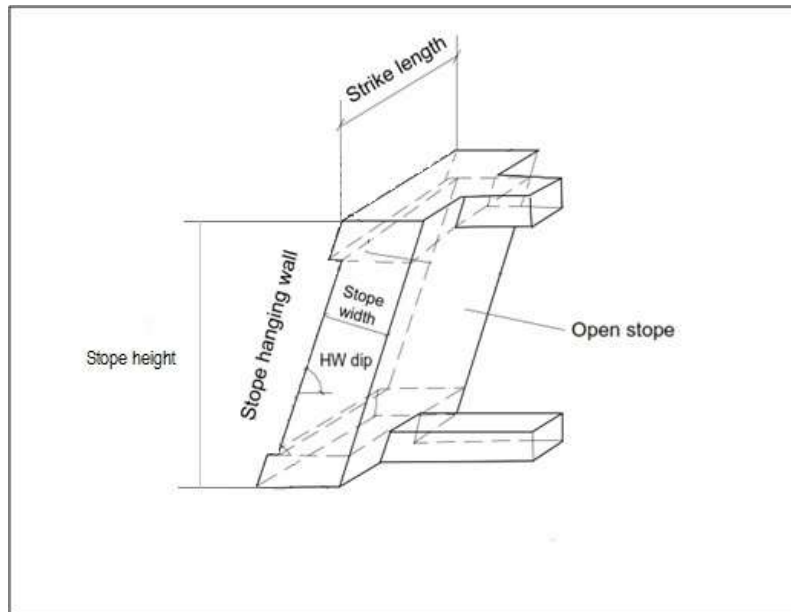
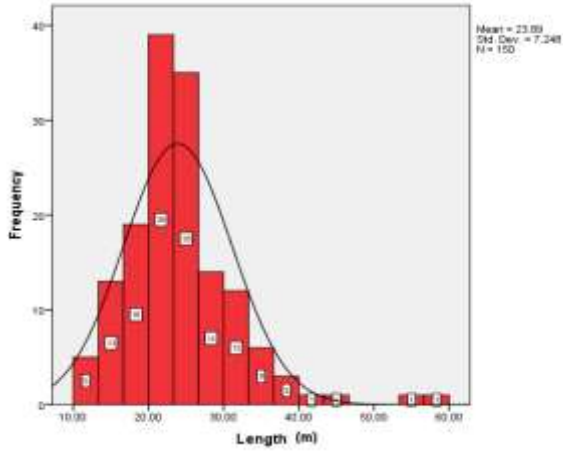
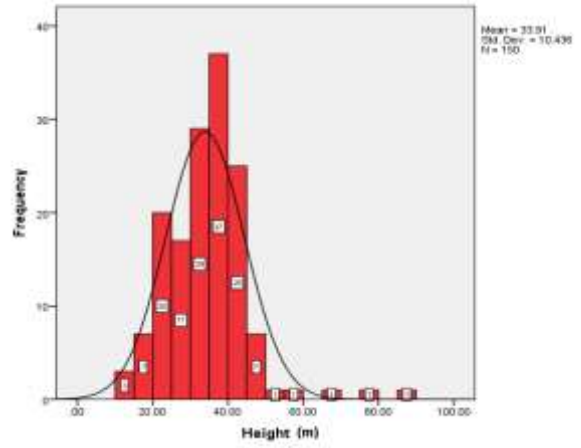


Figure 4-2 - An open stope geometrical parameters (Adopted from Wang [2]).

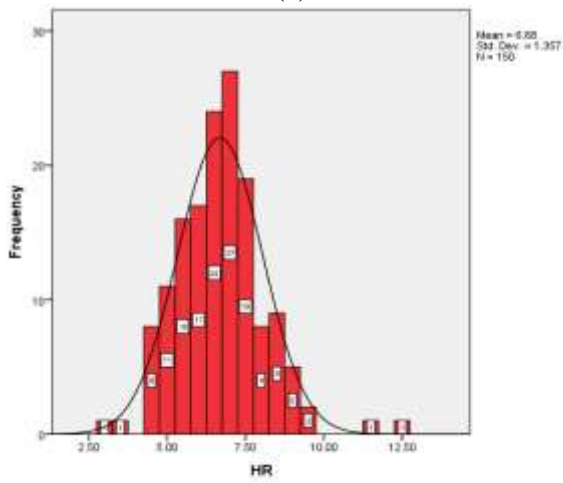
Realistic ranges of values for each parameter, are obtained from the database compiled by Wang (2004) and the study by Zhang and Mitri (2008), reporting the typical open stope dimensions and inclinations in Canadian underground mines. According to the provided distribution functions for stope span width, hanging wall HR and dip in our reference datasets (Fig. 4-3), three categories of stopes are defined having hanging wall HR ranges of below 5 m, between 5 and 7 m and between 7 and 10 m. Although, it should be noted that the minimum reported value for hanging wall HR in our reference dataset, is equal to 2.5 m; therefore first hanging wall HR category is defined having the range between 2.5 to 5 m. For each category of hanging wall HR, four classes of stopes are considered, respectively having hanging wall dip ranges of 20° - 45° , 45° - 60° , 60° - 75° and 75° - 90° .



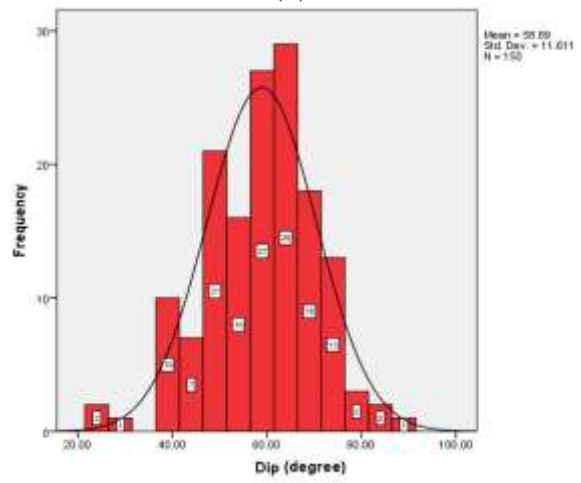
(a)



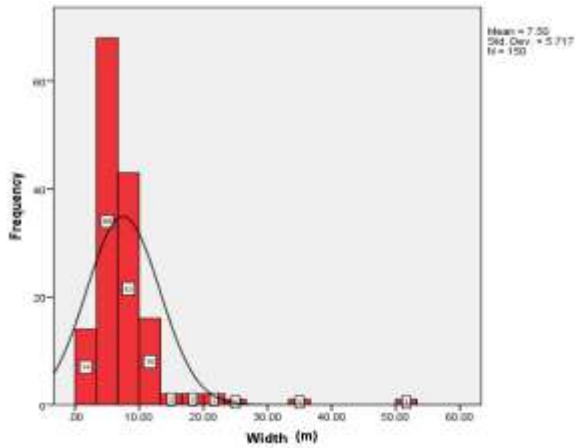
(b)



(c)



(d)



(e)

Figure 4-3 - Distribution plots of (a) slope strike length, (b) slope height, (c) slope hanging wall HR, (d) slope hanging wall dip and (e) slope span width; for 150 open slope cases adopted from Wang [(Wang 2004)].

For each class of hanging wall dip in each hanging wall HR category, Monte-Carlo simulation with uniform distribution function is utilized to generate 100 realizations as a combination of random stope geometrical parameters respecting the predefined ranges of hanging wall HR and dip. Monte-Carlo simulation is reported as the most accurate method of its kind in the case of a large number of realizations of a simulation model (Idris 2014). However, as reported by Idris (2014) a small number of realizations (e.g. 100 realizations) is also able to provide a fair approximation of the output variables. Therefore, a total of 400 realizations (mining scenarios) are generated for each hanging wall HR category, i.e. 100 realizations for each one of the four classes of hanging wall dip (Table 4-4). All 1200 realizations for three hanging wall HR categories are repeated for three mean values of stope span width equal to 4 m, 8 m and 12 m (Table 4-4). Ultimately, 3600 realizations are generated for numerical analysis.

Table 4-4 - Stope geometrical categories the corresponding number of Monte-Carlo simulation for each category.

Number of simulations	Stope span width (m)	Stope HW HR (m)	Stope HW dip range (°)			
400	4	2.5-5	20-45	45-60	60-75	75-90
400	4	5-7	20-45	45-60	60-75	75-90
400	4	7-10	20-45	45-60	60-75	75-90
400	8	2.5-5	20-45	45-60	60-75	75-90
400	8	5-7	20-45	45-60	60-75	75-90
400	8	7-10	20-45	45-60	60-75	75-90
400	12	2.5-5	20-45	45-60	60-75	75-90
400	12	5-7	20-45	45-60	60-75	75-90
400	12	7-10	20-45	45-60	60-75	75-90

4.3.4. Selecting failure criteria

In the case of underground open stopes located in deep, hard rock mines or for a brittle rock mass context, the high magnitude of mining-induced stresses could cause rock mass damage initiation and sometimes failure in the areas close to the excavation walls (Castro et al., 2012) (Diederichs 1999a) (Shnorhokian et al. 2015). Failure as a generic term, could be identified in many forms [e.g., plastic yielding, macroscopic boundary cracks, spalling or complete collapse of the excavation] (Idris 2014). Hence, recognizing the damage process and subsequent failure modes plays an important role in assessment of underground stope instability. In general, under low confinement conditions, stress-induced instability occurs by two dominant processes, namely; (1) stress-induced spalling and slabbing failure, and; (2) structurally-controlled, gravity-driven failure (Castro et al., 2012). The damage process commences with the creation of extension micro fractures within the intact rock bridges in the rock mass as a result of high compressive stress regime. These compression-induced tension cracks normally form parallel to the major principal induced stress (σ_1). Accumulation and propagation of these cracks finally leads to the development of macro-fractures and release surfaces. As a result, tangential and radial stresses decrease drastically, creating an unconfined area, or a relaxation zone, around the opening. In the case of spalling failure, the magnitude of the minor principal induced stress (σ_3) near the excavation walls undergoes a significant reduction, whereas the tangential stress increases to its maximum. However, in the case of gravity-driven, structurally-controlled failures, relaxation in the walls reduces the minor principal induced stress to zero or less and creates tensile stress (Castro et al., 2012) (Diederichs 1999a) (Kaiser et al. 2000). It should be noted that according to Kaiser *et al.* (2000), relaxation in excavation walls is attributed to the reduction of tangential stresses (the major

and/or intermediate principal stress) parallel to the walls, not to the radial stress component which leads to low confinement (Henning 2007).

Therefore, in this study, two different stability indicators are used to determine the brittle and tensile modes of failure in the rock mass. The potential rock mass brittle damage surrounding an open stope can be estimated by the “brittle shear ratio” (BSR) (Castro et al., 2012) (Shnorhokian et al. 2015). The BSR (Eq. 4-10) is defined as the ratio of differential induced stress ($\sigma_1 - \sigma_3$) around the stope over the uniaxial compressive strength (UCS) of an intact rock.

$$BSR = \frac{\sigma_1 - \sigma_3}{UCS_{intact}} \quad (4-10)$$

Castro *et al.* (2012) described the rock mass damage level based on the BSR. To obtain the maximum BSR value of each model, a built-in program in the FISH-language code (Itasca 2015) was developed to use the maximum shear stress of each zone and calculate the BSR for each zone of the model. The maximum BSR value around the stope for each model was selected as the output variable.

The potential of gravity-driven failure due to the presence of tensile stress near the opening surface, is determined by comparing the magnitude of minor principal induced stress (σ_3) to the rock mass tensile strength. Since the tension is positive in *FLAC3D*, if the magnitude of σ_3 exceeds the tensile strength threshold, the excavation is considered to be failed.

4.3.5. Determination of the probability of failure

The probability of stope failure (POF) is selected as the parameter of interest to assess the effect of stope size, shape and inclination on its stability.

In a deterministic approach, the POF can be calculated as the proportion of stopes having either the magnitude of minimum principal induced stress (σ_3), and/or the maximum BSR value exceeded the corresponding allowable threshold, when considering either the relaxation-related gravity driven or the brittle failure mode. The stability thresholds (maximum allowable limit) for the BSR was reported to be equal to 0.7 by Castro *et al.* (2012). The threshold for tensile stress is considered to be the tensile strength of the rock mass, estimated by Eq. 4-5 as equal to 0.57 (MPa). Thus, the number of failed models for each hanging wall dip class of every hanging wall HR category, are counted and the probability of failure is calculated using Eq. 4-11.

$$POF (\%) = \frac{\text{Number of failed models } (\sigma_3 \geq \sigma_t(\text{rock mass}) \text{ or } BSR \geq 0.7) \text{ in each class}}{\text{Total number of models in each class}} \times 100 \quad (4-11)$$

4.3.6. Numerical modeling

The finite difference code *FLAC3D* (Itasca 2015) is employed to build models based on the geometry setup obtained by Monte-Carlo simulation (Fig. 4-4). The transverse stope configuration (Villaescusa 2014) is selected to generate planar symmetrical models, with multiple neighboring primary stopes having identical dimensions. Stopes are excavated in sequence. The rib pillar W/H ratio is set at 0.4 for all the models according to a database reported by Hudyma (1998) that contains 135 rib pillar size parameters observed from 17 different Canadian open stope mines. Different mesh sizes are tested to obtain the most reliable and accurate numerical results. To increase accuracy, a finer mesh size is adopted near the stopes and pillars, while the coarser mesh is applied for the homogeneous isotropic rock mass surrounding the area of interest. To avoid any adverse effect on the obtained results, the roller conditions for external boundaries are

positioned far enough from the region of interest, based on different slope dimensions for each model. The identical *in situ* stress state is applied to the models of all geometrical categories using the magnitudes reported in Table 4-3. The slopes in each model are excavated in separate single steps from left to right, and after each excavation step, the model is allowed to reach equilibrium.

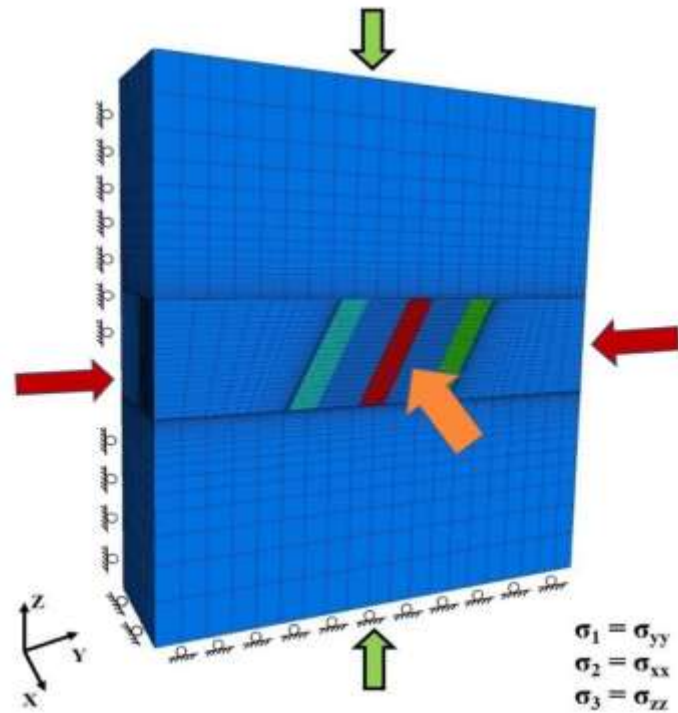


Figure 4-4 - Model boundary conditions and the state of *in situ* stress.

4.4. Results and discussion

The POF is calculated for each class of hanging wall dip in all categories of hanging wall HR for the two considered failure modes. The possibility of brittle failure for each model is evaluated by plotting BSR contours and determining the zone with maximum BSR value (Fig. 4-5); and the possibility of structurally-controlled gravity driven failure is assessed by comparing the highest magnitude of minimum principal induced stress of each model (as an output of *FLAC3D*), with the obtained value of rock mass tensile strength (Fig. 4-6 a–b). The ratio of the

number of failed model realizations, over 100 realizations for each hanging wall dip class, provides the POF in percentage. It should be noted that for the presumed state of *in situ* stress and rock mass quality, no brittle failure condition is observed. Thus, the main failure mechanism is determined to be the structurally-controlled gravity driven (i.e. tensile) failure.

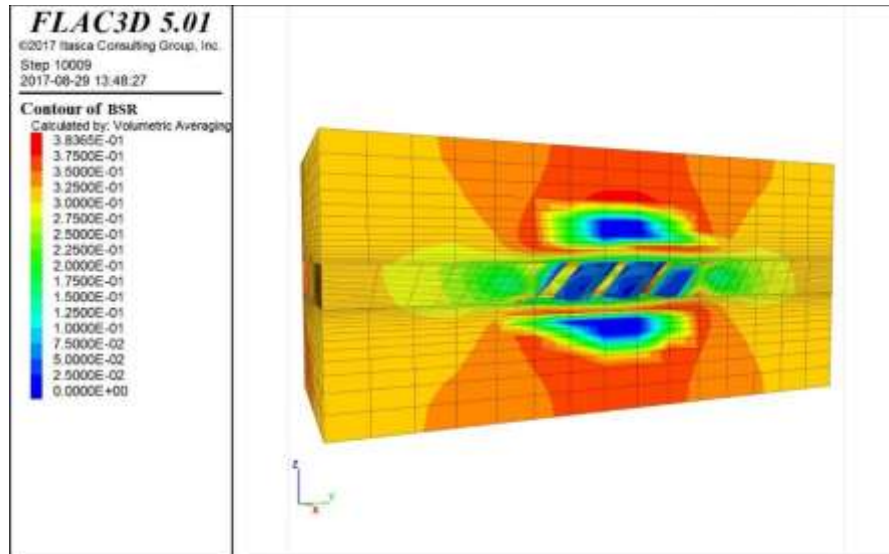


Figure 4-5 - Contour of the brittle shear ratio (BSR).

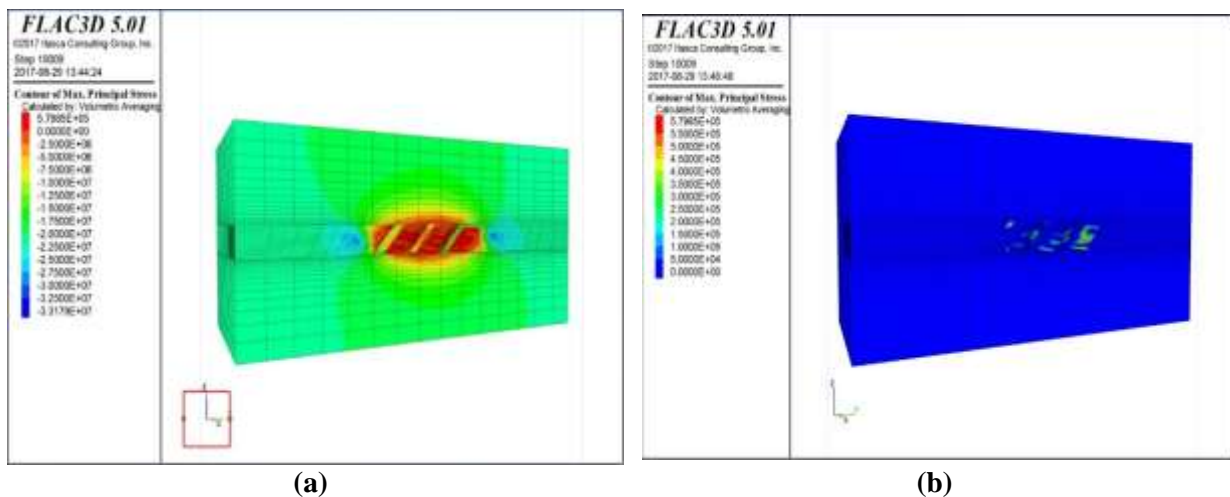


Figure 4-6 - Contour of (a) minimum principal induced stress $-\sigma_3$ (MPa), (b) minimum principal induced stress $-\sigma_3 \geq 0$.

In order to have a better understanding about the way each input parameter affects the POF, and/or whether interaction effect exists between the parameters or not, a general factorial design with 36 experiments is generated by *Design Expert 7.0* (Stat-Ease 2005) trial software. The general (multi-level) factorial design allows categorical factors to be defined with different numbers of levels and creates an experiment that includes all possible combinations of factor levels. The 36-experiment design and the values of response (POF), obtained from numerical modellings, are presented in Table 4-5. The process takes place by fitting different regression models (i.e., mean, main effects, 2FI and 3FI) to the response data (POFs). Consequently, ANOVA is used to determine the level of significance for the applied regression models. The final equation (Eq. 4-12) expresses the relationship between the POF value (response variable), and the individual/interactive effects of independent variables:

$$POF (\%) = f(A[1], A[2], B[1], B[2], B[3], C[1], C[2], A[1]C[1], A[2]C[1], A[1]C[2], A[2]C[2], B[1]C[1], B[2]C[1], B[3]C[1], B[1]C[2], B[2]C[2], B[3]C[2])$$

(4-12)

Where POF is the “probability of failure” in percentage; A, B and C refer to the coded values of stope span width, stope hanging wall dip and stope hanging wall HR, respectively; [n] represents the corresponding level (range) for each input variable.

Table 4-5 - The 36-full factorial experimental runs and the corresponding values of POF obtained from numerical modellings.

Run	Span width (m)	HW dip (°)	HW HR (m)	POF (%)
1	8	75-90	7-10	49
2	8	45-60	7-10	47
3	8	60-75	2.5-5	21
4	4	75-90	7-10	14
5	4	60-75	5-7	26
6	8	60-75	7-10	36
7	4	60-75	7-10	6
8	8	60-75	5-7	49
9	4	45-60	7-10	26
10	4	45-60	5-7	32
11	8	20-45	5-7	43
12	4	60-75	2.5-5	23
13	12	75-90	7-10	56
14	8	45-60	2.5-5	55
15	12	60-75	5-7	45
16	8	20-45	2.5-5	36
17	12	45-60	2.5-5	76
18	8	45-60	5-7	34
19	12	20-45	7-10	36
20	4	20-45	2.5-5	28
21	4	20-45	7-10	15
22	12	75-90	2.5-5	50
23	8	75-90	5-7	59
24	12	75-90	5-7	64
25	12	45-60	5-7	37
26	12	60-75	7-10	50
27	8	20-45	7-10	29
28	12	20-45	2.5-5	47
29	12	45-60	7-10	47
30	12	20-45	5-7	40
31	4	45-60	2.5-5	48
32	4	75-90	5-7	42
33	8	75-90	2.5-5	44
34	12	60-75	2.5-5	25
35	4	20-45	5-7	36
36	4	75-90	2.5-5	34

ANOVA results of the general factorial design are presented in Table 4-6. The applied regression model is statistically significant ($p \leq 0.0001$), and the parameter “adequate precision” which reflects the signal to noise ratio (Ahmadi et al. 2014), has the value well above the minimum desirable limit of 4.0 (Table 4-7).

Table 4-6 - ANOVA results of the regression model applied to POF data.

Source	Sum of squares	Degree of freedom	Mean square	F-value	p-value
Model	6823.97	17	401.41	10.61	< 0.0001
A	2602.06	2	1301.03	34.39	< 0.0001
B	1433.64	3	477.88	12.63	0.0001
C	427.56	2	213.78	5.65	0.0125
AC	613.61	4	153.40	4.05	0.0162
BC	1747.11	6	291.19	7.70	0.0003
Residual	681.00	18	37.83		
Cor total	7504.97	35			

The model regression coefficient (R^2) equals 0.91, and thus indicates the goodness-of-fit of the regression model for predicting the POF results (Table 4-7). Another validation of the assigned model is the proximity of the predicted determination coefficient (R^2) value and the adjusted R^2 (R^2_{adj}), which indicates that unnecessary variables are eliminated from the model. If the values of these two parameters fall within approximately 0.20 of each other, a reasonable agreement would be achieved (Table 4-7).

Table 4-7 - The values of determination coefficient (R^2), adjusted and predicted determination coefficients.

Adequate precision	R^2	Adjusted R^2	Predicted R^2
14.0	0.91	0.82	0.64

Regression coefficient values reflect the way each independent variable impacts the response variable; however, it should be noted that in the case of a general factorial design with multi-level categorical factors, these coefficients do not imply a physical meaning. Since these coefficients are calculated according to a mathematical algorithm, it is strongly recommended

(Stat-Ease 2005) to use the model graphs, instead of coefficient values, to develop a better interpretation of the model. Significant model terms influencing the POF are individual parameters of A (span width), B (hanging wall dip), C (hanging wall HR) and interactions of $A*C$ and $B*C$ (Table 4-6).

4.4.1. Effect of open stope hanging wall HR on the probability of failure

Dimensions of the stope hanging wall “exposed surface” is one of the most important factors influencing the hanging wall stability, since it directly contributes to the extent of the hanging wall relaxation zone (Clark 1998). The stope strike length and height characterize the exposed surface of a hanging wall. According to previous studies (Henning and Mitri 2007) (Hughes 2011) (Zniber El Mouhabbis 2013) longer strike lengths cause a greater degree of relaxation-related dilution, whereas, decreasing the strike length provides more stability. It is also reported (Henning and Mitri 2007) (Chen et al. 1983) (Perron 1999) that increasing the stope height contributes to greater instabilities and according to Henning (2007), even imposes a stronger effect on hanging wall overbreak, compared to the strike length. Furthermore, to account for the combined effect of hanging wall size and shape, the hydraulic radius (HR) is used as a common measure, and as reported by many studies, increasing the hanging wall HR leads to a higher extent of hanging wall instability (Villaescusa 2014) (Clark 1998) (Urli 2015).

Despite the aforementioned assumptions corresponding to the effect of hanging wall size and shape on stability, the actual role of hanging wall HR has not been fully understood yet, since the interferences caused by variation of other stope geometric parameters such as span width and hanging wall dip have been largely underestimated. Therefore, the effect of the stope hanging wall HR is investigated for three categories of stope with different values of span width; each category

contains model realizations with four different classes of hanging wall dip. Figures. 4-7 a–d illustrate the POFs corresponding to HR variations for each stope hanging wall dip class.

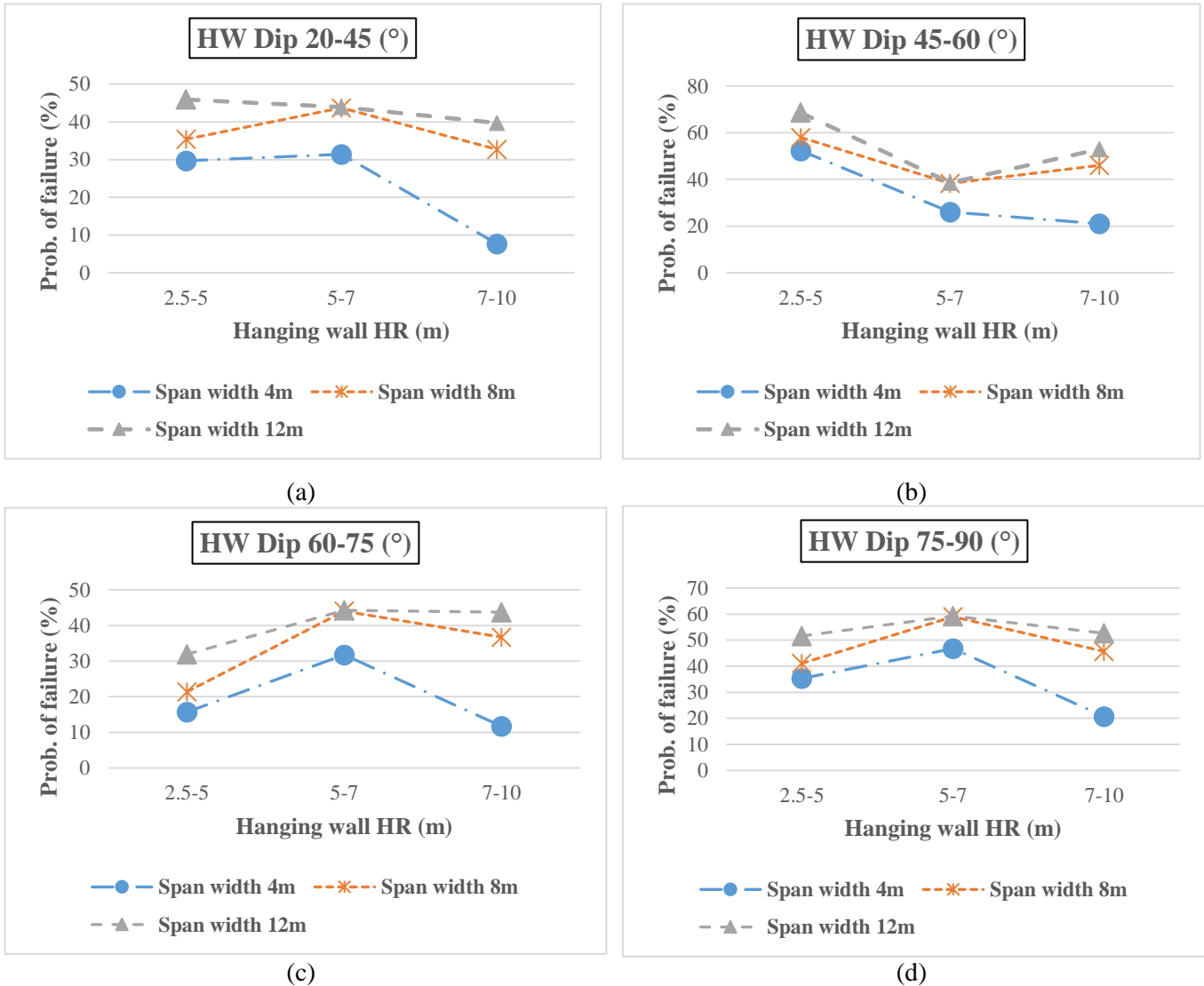


Figure 4-7 - POF plots for hanging wall HR variations for three average span width groups. (a) hanging wall dip range 20-45°; (b) hanging wall dip range 45-60°; (c) hanging wall dip range 60-75°; (d) hanging wall dip range 75-90°.

In the case of shallow dipping stopes having hanging wall dip ranging between 20-45°, and span width between 4 m and 8 m, increasing the hanging wall HR range from 2.5-5 m to 5-7 m increases the POF from 30% to 32%, and from 36% to 44%, respectively. Whereas, increasing the HR to its ultimate range (7-10 m), decreases the POF dramatically to 8% and 33%, respectively.

However, for slopes with 12 m of span width, increasing the hanging wall HR range, causes the POF to reduce from 46% to 40% (Fig. 4-7a).

For shallow to moderately dipping slopes ($45-60^\circ$), with a span width equal to 8 m and 12 m, increasing the hanging wall HR range from 2.5-5 m to 5-7 m, decreases the POF from 58% to 38% and from 69% to 39%, respectively, while increasing the HR to its maximum range (7-10 m), increases the POF to 46% and 53%. However, slopes having span width equal to 4 m became more stable by increasing the hanging wall HR range, resulting in a decrease of the POF from 52% to 21% (Fig. 4-7b).

In the case of moderately to steeply dipping slopes ($60-75^\circ$) with a span width of 4 m, increasing the hanging wall HR range from 2.5-5 m to 5-7 m, significantly increases the POF (from 16% to 32%), while increasing the hanging wall HR to its highest range (7-10 m), causes a rapid reduction in the POF (decreased to 12%). For the slopes with a span width equal to 8 m, the POF increases first (from 21% to 44%) by increasing the range of hanging wall HR from 2.5-5 m to 5-7 m, and then decreases to 37% while HR reaches its maximum range (7-10 m). In addition, 12 m-wide slopes have their POF continuously increasing (from 32% to 44%), by increasing the hanging wall HR range (Fig. 4-7c).

Finally, increasing the range of hanging wall HR from 2.5-5 m to 5-7 m for steeply dipping ($75-90^\circ$) slopes increases the POF from 35% to 47%, 41% to 59% and 52% to 60%, for span width of 4 m, 8 m and 12 m, respectively, while increasing the HR range to 7-10 m, causes the POF to decrease to 21%, 46% and 53%, for span widths of 4 m, 8 m and 12 m, respectively (Fig. 4-7d).

The obtained results of the slope hanging wall HR effect on the POF, challenges the conventional previous assumptions, since hanging wall HR variation does not show similar patterns of effect depending on differences in span width and hanging wall dip ranges. Thus, these observations

strongly suggest the presence of significant interaction effects between hanging wall HR and the two other aforementioned parameters.

4.4.2. Effect of open stope span width on the probability of failure

The effect of open stope span width on relaxation-related dilution has previously been investigated by some studies, and accordingly as a general notion, it is reported that narrower stopes undergo a larger extent of dilution and therefore are more prone to be unstable (Pakalnis et al. 1995; Zniber El Mouhabbis 2013). However, to obtain a clearer understanding about the effect of span width on stope stability, a more comprehensive assessment is accomplished by considering the influence of other geometric parameters in different ranges.

Figures. 4-8 a–c plot the effects of stope span width on the POF for three hanging wall HR categories in different hanging wall dip classes. As observed in Figure. 4-8a, stopes whose hanging wall HR ranges between 2.5 and 5 m, increasing the span width from 4 m to 12 m continuously increases the POF for all four hanging wall dip classes respectively from 30% to 46%, 52% to 69%, 16% to 32% and 35% to 52%. Where stopes had their hanging wall HR range between 5-7 m, increasing span width from 4 m to 8 m raises the POF in all four classes of hanging wall dip, respectively from 31% to 44%, 26% to 38%, 32% to 44% and 47% to 59%; whereas, increasing span width to 12 m causes almost no change in the values of POF for neither of the four hanging wall dip classes. It is also found that stopes with hanging wall dip ranges of 20-45° and 60- 75° have almost identical POFs in every stope span width category (Fig. 4-8b). Finally, increasing the span width from 4 m to 12 m for the large stopes with a hanging wall HR range of 7-10 m, increases the POF from 8% to 40%, 21% to 53%, 12% to 44% and 21% to 53%, respectively, for hanging wall dip classes of 20- 45°, 45- 60°, 60- 75° and 75- 90°. Here, almost identical POF values are

observed in hanging wall dip classes of 45-60° and 75- 90° (Fig. 4-8c). The results of the stope span width effect on the POF, do not support the previous reported assumptions, since wider stopes show less stability (in terms of POF) than narrower ones.

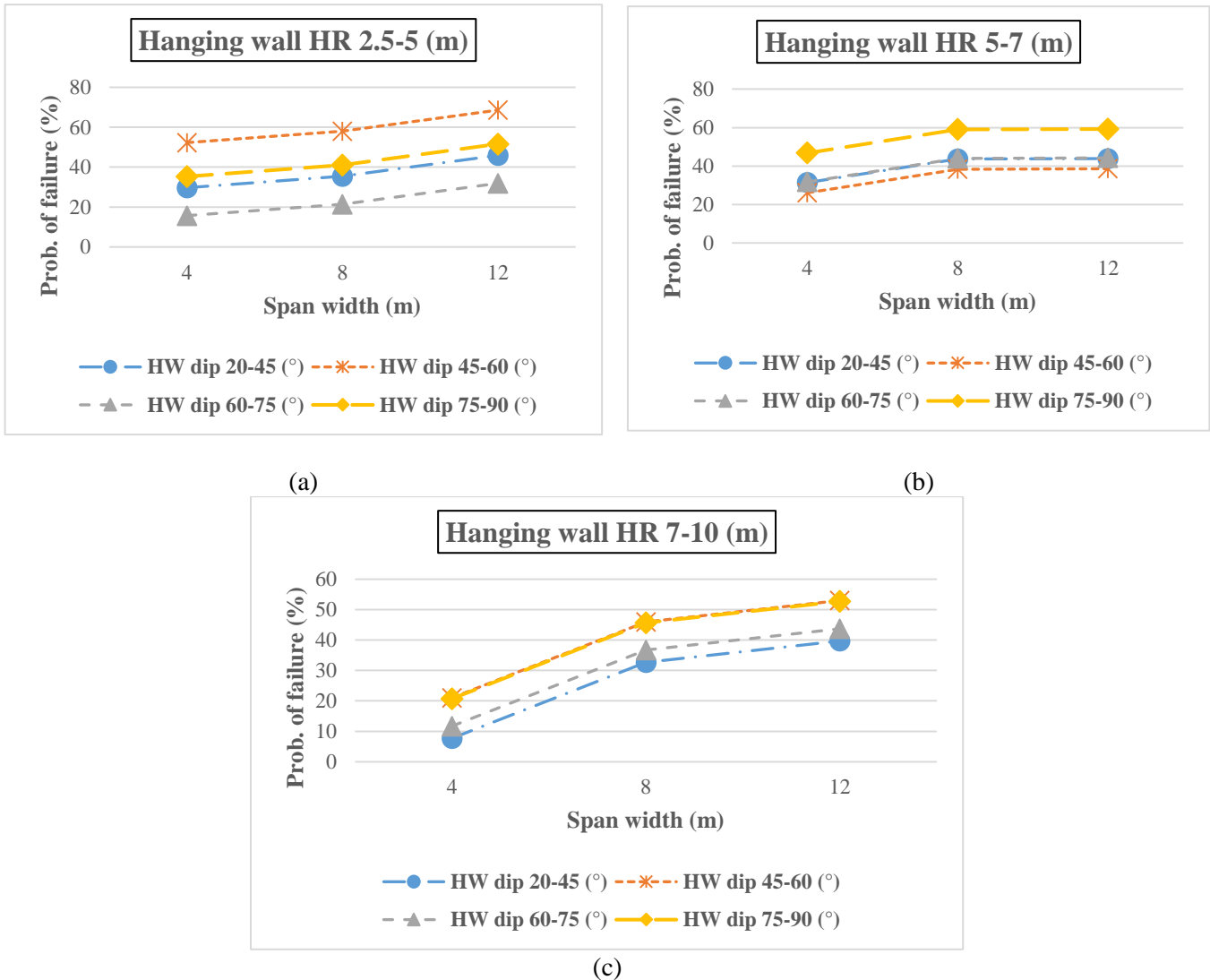


Figure 4-8 - POF plots for span width variations for four hanging wall dip classes. (a) hanging wall HR range 2.5-5 m; (b) hanging wall HR range 5-7 m; and (c) hanging wall HR range 7-10 m.

4.4.3. Effect of open stope hanging wall dip on the probability of failure

According to Henning (2007), greater hanging wall overbreak occurs for shallower dips, since vertical stresses (σ_3) are shed onto the surrounding orebody, leading to the creation of larger

relaxation zones. Hence, shallow dipping stopes are considered to be more unstable. However, the effect of hanging wall dip may be altered when it is combined with the effect of other stope geometric parameters.

The impacts of open stope hanging wall dip on the POF are presented in Figures. 4-9 a–c, with three values of span width, in various categories of hanging wall HR ranges. In stopes with a hanging wall HR in the range 2.5-5 m, increasing the hanging wall dip results in similar variation trends on the POF for all the span width groups. Accordingly, for stopes with span widths of 4 m, 8 m and 12 m, increasing the range of hanging wall dip from 20-45° to 45-60°, increases the POF from 30% to 52%, from 35% to 58% and from 46% to 69%, respectively. Moreover, increasing the hanging wall dip to the range of 60-75°, causes a significant decrease in the POF to 16%, 21% and 32%, respectively. Ultimately, reaching a hanging wall dip range of 75-90°, results in 35%, 41% and 52% of POF for stopes with span widths of 4 m to 12 m, respectively (Fig. 4-9a).

In the case of stopes having hanging wall HR ranging from 5 to 7 m, similar patterns of POF variation are observed for all the span width groups, especially for span widths of 8 m and 12 m, in which almost identical POFs are obtained for each hanging wall dip range. For stopes with a span width equal to 4 m, increasing the range of hanging wall dip from 20-45° to 45-60°, decreases the POF from 31% to 26%, while increasing the hanging wall dip range to 60-75° and ultimately 75-90°, increases the POF to 47%. For stopes with 8 m and 12 m span widths, POFs of 44%, 39%, 44.3% and 59% are obtained for dip ranges of 20-45° to 75-90°, respectively (Fig. 4-9b).

The effect of increasing the hanging wall dip on the POF shows a similar pattern for all three span width groups with 7-10 m hanging wall HR. Thus, for stopes having span widths of 4 m, 8 m and 12 m, increasing the range of hanging wall dip from 20-45° to 45-60°, increases the

POF from 8% to 21%, from 33% to 46% and from 40% to 53% respectively. Moreover, increasing the hanging wall dip range to 60-75°, reduces the POFs to 12%, 37% and 44% respectively. Ultimately, increasing the dip range to 75-90°, results in POFs of 21%, 46% and 53% for span width groups of 4 m to 12 m, respectively (Fig. 4-9c).

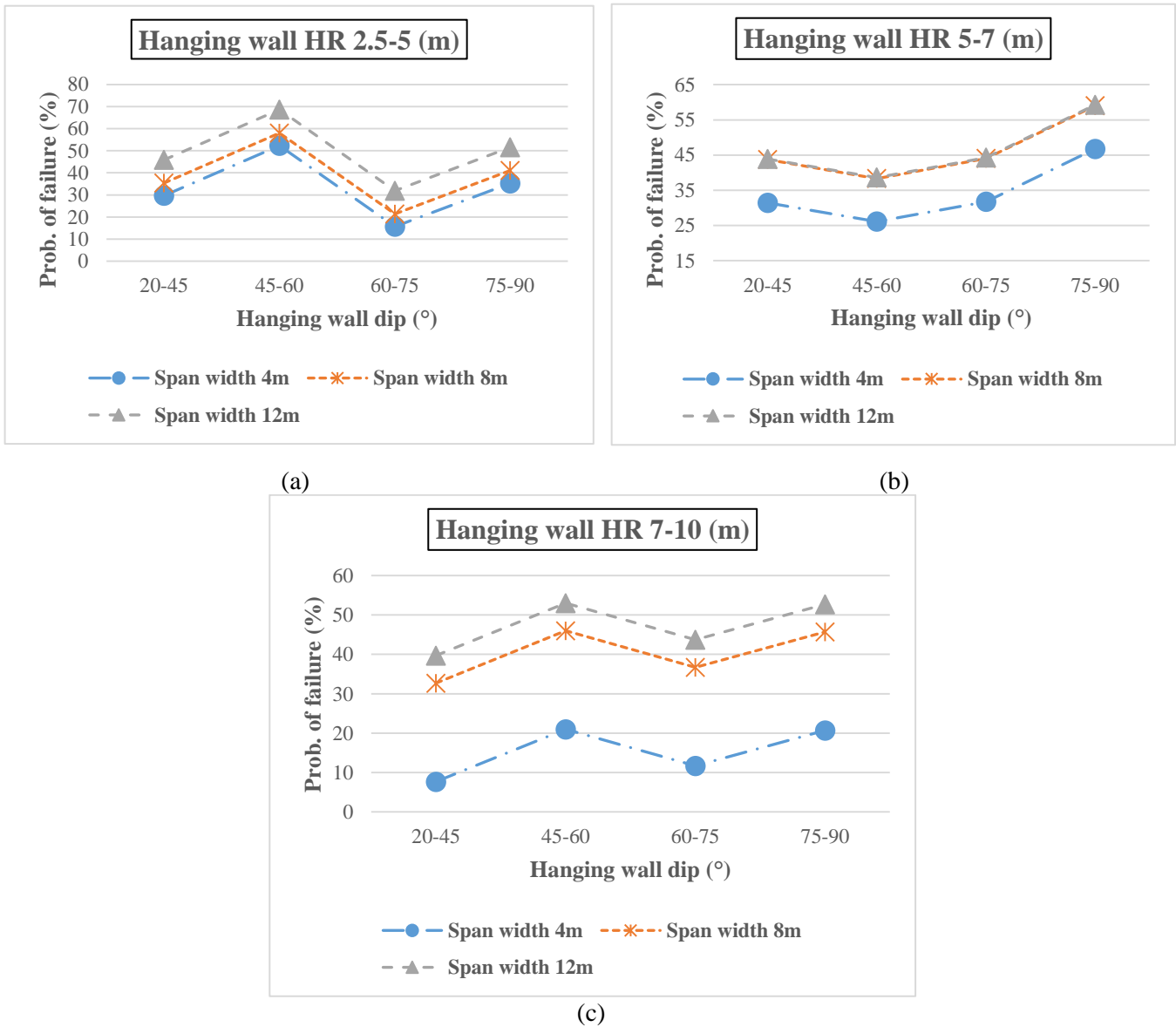


Figure 4-9 - POF plots for hanging wall dip variation for three span width groups. (a) hanging wall HR range 2.5-5 m; (b) hanging wall HR range 5-7 m; (c) hanging wall HR range 7-10 m.

4.4.4. Interaction effect of open slope geometric and inclination parameters on the probability of failure

As indicated by the results for individual parameters in previous sections, the POF is significantly controlled by strong interactions between certain geometrical parameters. The presence of synergistic effects between the geometrical parameters complicates a general conclusion on the influence of slope size, shape and inclination on the POF. Based on the results of previous studies, it can be assumed that slopes, either with high vertical and short horizontal dimensions or with long horizontal and short vertical dimensions, are considered more stable in comparison to square-shaped slopes (Villaescusa 2014).

Figures. 4-10 a–d illustrate the interaction effects of slope span width and slope hanging wall HR, for the hanging wall dip ranges of 20-45°, 45-60°, 60-75° and 75-90° respectively. As previously discussed, it is observed that regardless of the slope hanging wall dip range, increasing the slope span width increases the POF for all three hanging wall HR categories (Figs. 4-10 a–d). In shallow dipping slopes (HW dip between 20-45°), increasing the hanging wall HR for slopes with low and moderate span widths (4 m and 8 m), firstly elevates the POF and then reduces the POF to their minimums. However, for large span widths (12 m), a global decreasing trend of POF is observed (Fig. 4-10a). The most stable condition (POF = 8%) occurs with narrow slopes (span width of 4 m), having the maximum range of hanging wall HR (5-7 m). In contrast, when the horizontal dimensions of the slope becomes closer to its vertical dimension (the category of span width equal to 12 m and HR ranges between 2.5 and 5 m), the POF increases to its maximum level of 46%.

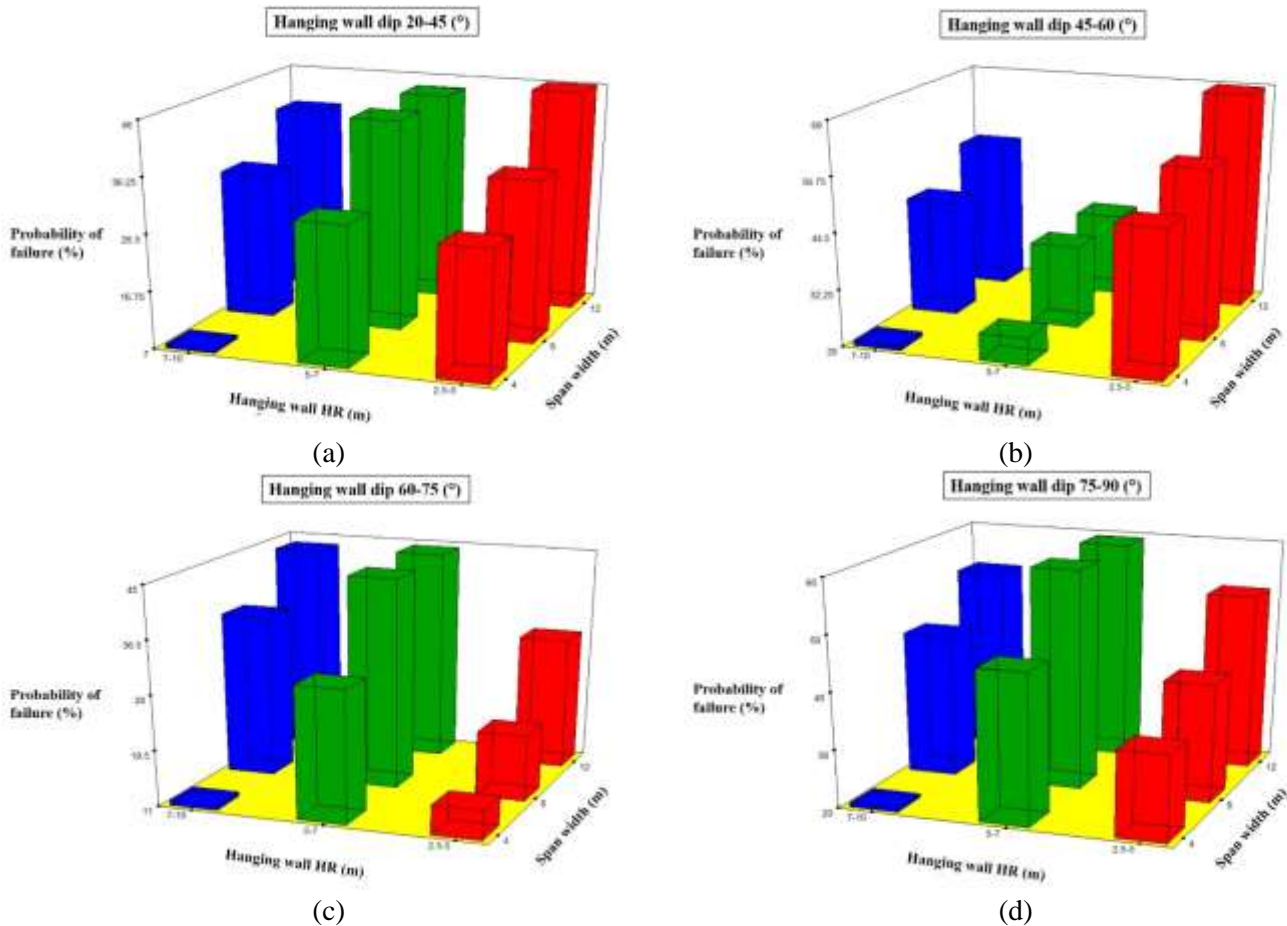


Figure 4-10 - General factorial analysis plots showing interaction effects between slope span width and slope hanging wall HR in (a) hanging wall dip range 20-45°; (b) hanging wall dip range 45-60°; (c) hanging wall dip range 60-75°; (d) hanging wall dip range 75-90°.

For shallow to moderately dipping stopes (HW dip between 45-60°) with the span width of 4 m; increasing the hanging wall HR, sharply decreases the POF. In this case, the most stable condition occurs in the group of stopes with span widths of 4 m and hanging wall HR between 7 and 10 m. For stopes with span widths of 8 m and 12 m, increasing the HR decreases the POF in the beginning (at HR range of 5-7 m), and then increases it considerably for larger HR values. It is also observed that reducing the difference between stope's horizontal and vertical dimensions (the category of span width equal to 12 m and HR ranges between 2.5 and 5 m), results in the most unstable condition in terms of POF (69%) (Fig. 4-10b).

In the case of moderately to steeply dipping stopes (HW dip between $60\text{-}75^\circ$), increasing the hanging wall HR first increases the POF (at HR range of 5-7 m), and then decreases it for all the span width categories. Again, the most stable condition in term of POF (11%) is achieved for stopes with hanging wall HR between 7 and 10 m and span width of 4 m (Fig. 4-10c).

A similar pattern of POF variation is observed for steeply dipping stopes (HW dip between $75\text{-}90^\circ$), in that increasing the hanging wall HR first increases the POF (at HR range of 5-7 m), and then decreases it across all span widths. In addition, the lowest POF (21%) was observed for stopes with high vertical (HR ranges between 7 and 10 m), and short horizontal (span width of 4 m) dimensions (Fig. 4-10d).

Across the hanging wall dip classes, the highest level of stability (the lowest POF values), is achieved for the category of stopes with the hanging wall HR ranging between 7-10 m, and span width of 4 m. This result supports the previously stated assumption that high vertical and short horizontal dimensioned stopes are more stable than square-shaped stopes. Moreover, it provides a general pattern for POF variations; where in all the hanging wall dip classes (except the dip class of $45\text{-}60^\circ$), increasing the hanging wall HR and span width simultaneously, causes the POF to increase. In stopes dipping between $45\text{-}60^\circ$, increasing the hanging wall HR and span width simultaneously, at first causes the POF to decrease significantly, and then to increase by the same value.

The interaction effect of stope hanging wall HR and stope hanging wall dip, for span widths of 4 m, 8 m and 12 m are presented in Figures. 11 a–c, respectively. Regardless of the stope span width, the POF for the stopes with hanging wall HR ranges between 2.5 and 5 m and 7 and 10 m, follows an increase/decrease/increase pattern as the stope hanging wall dip range is increased.

While for the stopes with a hanging wall HR range of 5-7 m, the POF decreases at first and then continuously increases with increasing stope hanging wall dip ranges (Figs. 4-11 a–c).

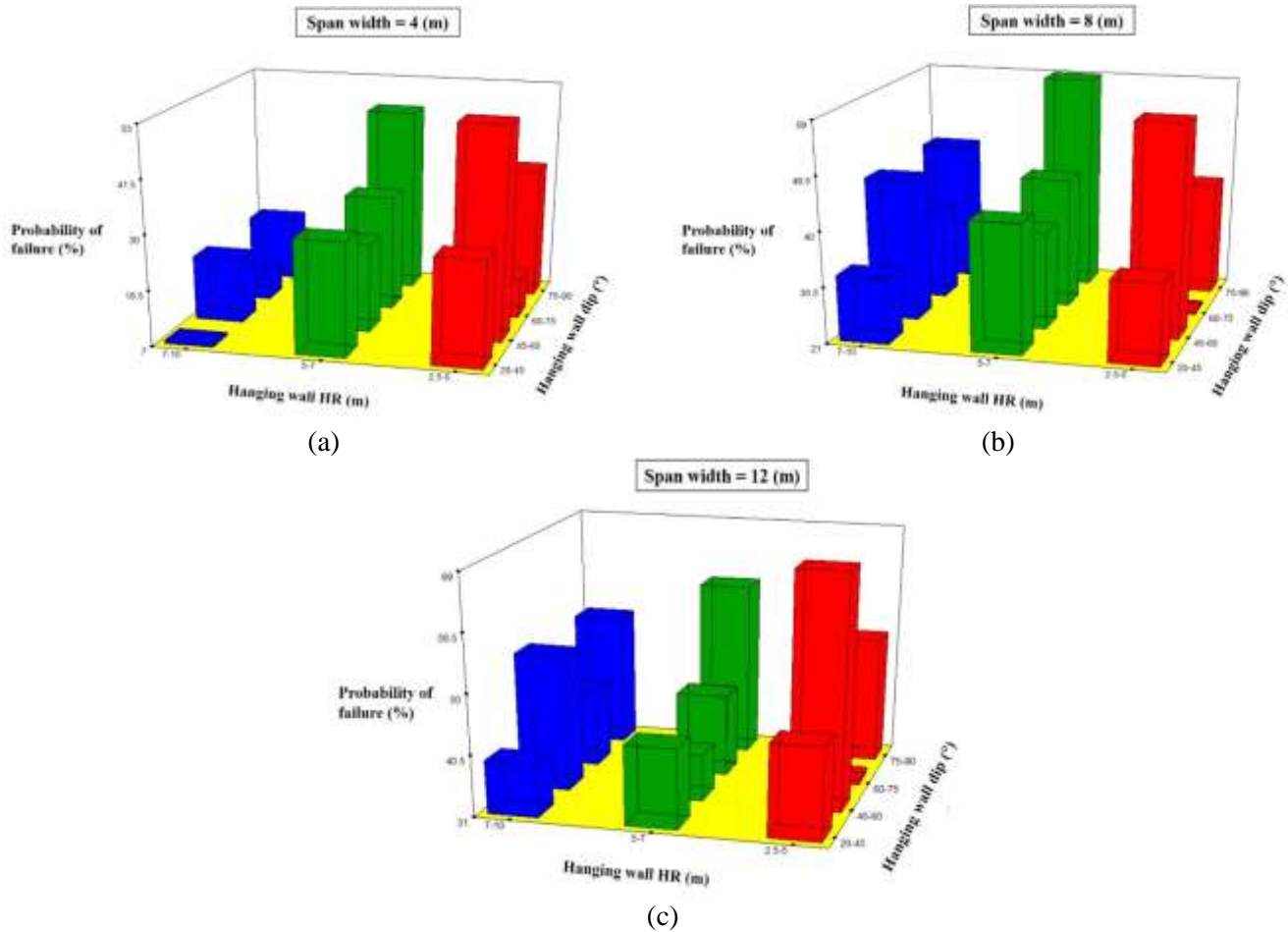


Figure 4-11 - General factorial analysis plots showing interaction effects between stope hanging wall dip and stope hanging wall HR for (a) span width of 4 m; (b) span width of 8 m; (c) span width of 12 m.

Where stope span widths equaled 4 m, the POF for the stopes with hanging wall dip ranges of 20-45°, 60-75° and 75-90°, increases to its highest level by increasing the hanging wall HR range from 2.5-5 m to 5-7 m. Consequently, the POF decreases to its minimum when the hanging wall HR is increased to 7-10 m range. However, for stopes with hanging wall dip ranges of 45-60°, the POF continuously decreases with increasing hanging wall HR ranges (Fig. 4-11a).

For 8 m-wide stopes with moderate to steeply dipping hanging walls ($60-75^\circ$ and $75-90^\circ$), increasing the HR range from 2.5-5 m to 5-7 m, increases the POF from their minimum value to their maximum value; however, when HR range is increased to 7-10 m, the POF decreases. For a hanging wall dip range of $20-45^\circ$, increasing the HR range to 5-7 m results in an increase of POF to its maximum value, while at the 7-10 m range of HR, the POF is decreased to its minimum value. POF for the stopes dipping between $45-60^\circ$, decreases from their maximum to minimum value by increasing the HR from 2.5-5 m to 5-7 m and increases when HR ranges between 7 and 10 m (Fig. 4-11b).

Finally, for 12 m-wide stopes dipping between $60-75^\circ$ and $75-90^\circ$, increasing the hanging wall HR range from 2.5-5 m to 5-7 m, enhances the POF from their minimum to the maximum value; whereas increasing HR to 7-10 m, causes the POF to decrease. The POF for stopes dipping between $45-60^\circ$, decreases from their maximum to minimum values by increasing the HR from 2.5-5 m to 5-7 m; in contrast, an increase in the POF value is observed, when the HR reaches the 7-10 m range. In stopes dipping $20-45^\circ$, increasing the HR range from 2.5-5 m to 7-10 m, decreases the POF (Fig. 4-11c).

4.5. Conclusions

The Monte-Carlo simulation approach combined with the finite difference code *FLAC3D*, are employed to assess the individual effects of open stope size, shape and inclination on the stope probability of failure. The effect of stope hanging wall HR, stope span width and stope hanging wall dip were evaluated for three groups of stopes, having different average values of span width (4 m, 8 m and 12 m), with every group divided in three hanging wall HR categories (2.5-5 m, 5-7 m and 7-10 m) and each category of HR varied the hanging wall dip in four classes of $20-45^\circ$, $45-$

60°, 60-75° and 75-90°. In order to calculate the POF as the response variable, the possibility of rock mass brittle failure and structurally-controlled gravity driven (tensile) failure were assessed for simulated stopes through the BSR parameter and the minimum principal induced stress, respectively. It was found that under the presumed state of *in situ* stress and rock mass quality; structurally-controlled gravity driven failure is the dominant mode of failure. Due to the presence of strong interaction effects between the parameters; a general multi-level factorial design with 36 experiments was utilized to determine the individual and interactive effects of the parameters. An appropriate quadratic model with an adequate fit was applied to the obtained POF results. The mathematical relationship between the POF and the geometrical parameters in their corresponding levels were adequately described by a polynomial equation. Results indicated that the three parameters stope hanging wall HR, stope span width and stope hanging wall dip have a strong influence on the stope stability state; while the probability of stope failure is significantly controlled by interaction effects between span width / hanging wall HR and hanging wall dip / hanging wall HR. The interaction between the parameters, alters the way each parameter affects the probability of stope failure; hence, the effect of each geometrical parameter on POF must be assessed by considering the variation level of other parameters. However, a key finding of this study is that whatever the stope hanging wall dip is, increasing the stope span width from 4 m to 12 m, increases the POF in all categories of stope hanging wall HR.

Moreover, aside from stope span width range, when the hanging wall HR ranged between 2.5-5 m, the most unstable condition occurs for hanging wall dip between 45-60°, while the most stable condition occurs for hanging wall dip between 60-75°. In contrast, for stopes having their hanging wall HR ranging between 5-7 m, the most stable condition occurs for the hanging wall dip range of 45-60°, while the maximum instability is observed for hanging wall dip between 75-90°.

Furthermore, it can be concluded that independent of stope span width, increasing the stope hanging wall HR range from 2.5-5 m to 7-10 m decreases the POF for the stopes dipping up to 60°. While stopes dipping greater than 60°, the most unstable condition occurs for the hanging wall HR range of 5-7 m for all span width groups.

The mathematical optimization performed with *Design Expert 7.0* (Stat-Ease 2005) trial software predicts that the maximum stability (in terms of POF) would be achieved for narrow stopes (span width of 4 m) whose hanging wall dip ranges between 20 and 45° and hanging wall HR ranges between 7 and 10 m. In contrast, the maximum instability would occur in wider stopes (span width equal to 12 m) whose hanging wall HR ranges between 2.5-5 m and hanging wall dip ranges between 45 and 60°.

Acknowledgements

This work was funded by a grant from Natural Sciences and Engineering Research Council of Canada (NSERC) and the authors would like to acknowledge the Niobec mine (Saint-Honoré, Québec).

4.6. References

- Abdellah W, Raju GD, Mitri HS, Thibodeau D (2014) Stability of underground mine development intersections during the life of a mine plan. *Int J Rock Mech Min Sci* 72:173–181 .
- Aglawe JP (1999) Unstable and Violent Failure around Underground Openings in Highly Stressed Ground. PhD thesis, Queen's University at Kingston, Ontario, Canada.
- Ahmadi A, Heidarzadeh S, Reza A, et al (2014) Optimization of heavy metal removal from aqueous solutions by maghemite (γ -Fe₂O₃) nanoparticles using response surface methodology. *J Geochemical Explor* 147:151–158.
- Arjang B, Herget G (1997) *In situ* ground stresses in the Canadian hard rock mines: an update. *Int J Rock Mech Min Sci* 1997; 34: paper 015.
- Brown ET (2012) Risk assessment and management in underground rock engineering—an overview. *Joural Rock Mech Geotech Eng* 2012:193–204.

- Castro LAM, Bewick RP, Carter TG (2012) An overview of numerical modelling applied to deep mining. In: Azevedo R, editor. Innovative numerical modelling in geomechanics. London: CRC Press — Taylor & Francis Group; p. 393–414.
- Chen D, Chen J, Zavodni ZM (1983) Stability analysis of sublevel open stopes at great depth. The 24th U.S. Symposium on Rock Mechanics (USRMS).
- Chen G, Jia Z, Ke J (1997) Probabilistic analysis of underground excavation stability. *Int. J. Rock Mech. & Min. Sci.*; 34:3–4, paper No. 051.
- Clark L (1998) Minimizing dilution in open stope mining with a focus on stope design and narrow vein longhole blasting. MSc thesis, University British Columbia, Vancouver, Canada.
- Design-Expert 7.0.0 Manual. Stat-Ease, Inc. (2012). Minneapolis, USA.
- Diederichs MS (1999) Instability of hard rock masses: the role of tensile damage and relaxation. PhD thesis, University of Waterloo, Canada.
- Diederichs MS, Kaiser PK (1996) Rock instability and risk analyses in open stope mine design. *Can Geotech J* 33:431–439 . doi: 10.1139/t96-064
- Einstein HH (1996) Risk and Risk Analysis in Rock Engineering. *Risk Anal Tunn* 11:141–155 . doi: 10.1016/0886-7798(96)00014-4
- Germain P, Hadjigeorgiou J (1997) Influence of stope geometry and blasting patterns on recorded overbreak. *Int J rock Mech Min Sci Geomech Abstr* 34:628.
- Henning JG (2007) Evaluation of Long-Hole Mine Design Influences on Unplanned Ore Dilution. PhD thesis, McGill University, Montreal, Canada.
- Henning JG, Mitri HS (2007) Numerical modelling of ore dilution in blasthole stoping. *Int J Rock Mech Min Sci.*; 44:692–703.
- Hoek E (2007) Practical rock engineering. <http://www.rocscience.com/hoek/PracticalRockEngineering.asp>, World Wide Web edition.
- Hudson JA (1993) *Comprehensive Rock Engineering: Principles, Practice & Projects*. Vol 5. Pergamon Press.
- Hudyma MR (1998) Development of empirical rib pillar design criterion for open stope mining. PhD thesis, University of British Columbia. Vancouver, Canada.
- Hughes R (2011) Factors influencing overbreak in narrow vein longitudinal retreat mining. MSc thesis. McGill University, Montreal, Canada.
- Idris MA, Saiang D, Nordlund E (2011) Probabilistic analysis of open stope stability using numerical modelling. *Int. J. Min. Miner. Eng.* 3(3):194–219.
- Idris MA (2014) Probabilistic stability analysis of underground mine excavations. PhD thesis, Lulea University of Technology, Lulea, Sweden.

- Idris MA, Basarir H, Nordlund E, Wettainen T (2013) The Probabilistic Estimation of Rock Masses Properties in Malmberget Mine, Sweden. *Electron J Geotech Eng* 18:269–287
- Itasca Consulting Group, Inc. (2015). *FLAC3D – Fast Lagrangian Analysis of Continua in 3 Dimensions*, Ver. 5.0, User’s Guide. Minneapolis: Itasca.
- Kaiser PK, Diederichs MS, Martin CD (2000) Underground works in hard rock tunnelling and mining. In: *GeoEng2000*, Proceedings of the International Conference on Geotechnical and Geological Engineering, Melbourne, Australia.
- Maloney S, Kaiser P, Vorauer A (2006) A re-assessment of *in situ* stresses in the Canadian Shield. In *Golden Rocks 2006*, The 41st US Symposium on Rock Mechanics (USRMS). American Rock Mechanics Association.
- Milne D (1996) Underground design and deformation based on surface geometry. PhD Thesis, Mining Department, University of British Columbia, Vancouver, Canada.
- Pakalnis RC, Poulin R, Hadjigeorgiou J (1995) Quantifying the cost of dilution in underground mines. *Mining Eng*; Dec: 1136–41.
- Perron, J (1999) Simple solutions and employee’s involvement reduced the operating cost and improved the productivity at Langlois mine. Proceeding 14th CIM Mine Operator’s Conference. Bathurst, New Brunswick, Canada.
- Shnorhokian S, Mitri HS, Moreau-verlaan L (2015) Stability assessment of stope sequence scenarios in a diminishing ore pillar. *Int J Rock Mech Min Sci* 74:103–118
- Stat-Ease, Inc. (2005). *Design-Expert 7.0.0* Minneapolis, USA.
- Urli V (2015) Ore-Skin Design to Control Sloughage in Underground Open Stope Mining by Ore-Skin Design to Control Sloughage in Underground Open.
- Villaescusa E (2014) *Geotechnical design for sublevel open stoping*. CRC Press.
- Wang J (2004) Influence of stress, undercutting, blasting, and time on open stope stability and dilution. PhD thesis, University of Saskatchewan, Saskatoon, Canada.
- Wang J, Milne D, Wegner L, Reeves M (2007) Numerical evaluation of the effects of stress and excavation surface geometry on the zone of relaxation around open stope hanging walls. *Int J Rock Mech Min Sci* 44:289–298.
- Yao, X., G. Allen, (1999) Dilution evaluation using the cavity monitoring system at HBSM-Trout Lake Mine. 101th Annual General Meeting, Calgary, Alberta, Canada.
- Zhang Y, Mitri HS (2008) Elastoplastic stability analysis of mine haulage drift in the vicinity of mined stopes. *Int J Rock Mech Min Sci* 45:574–593.
- El Mouhabbis HZ (2013) Effect of stope construction parameters on ore dilution in narrow vein mining. MSc thesis. McGill University, Montreal, Canada.

Chapter 5 - Use of probabilistic numerical modeling to evaluate the effect of geomechanical parameter variability on the probability of open stope failure: a case study of the Niobec Mine, Quebec (Canada) ³

5.1. Abstract

The inherent variability of the geomechanical parameters of a rock mass plays a critical role in affecting underground mine stability. Neglecting this characteristic of a rock mass oversimplifies stability assessment and provides potentially inaccurate results as the actual behavior of rock mass is not considered. Use of probabilistic methods in conjunction with numerical analysis is a reliable approach for evaluating the effect of geomechanical parameter variability on the different modes of underground instability. The degree of stability can be expressed by the probability of failure (POF) for different stress-induced instability modes. Here, we use probabilistic methods (Random Monte Carlo and Monte Carlo simulations) coupled with the finite difference code FLAC3D to incorporate the variability of rock mass geomechanical parameters into numerical analysis. We assess the stability of seven existing primary open stopes at mining levels V and VI at the Niobec Mine, Quebec, Canada. The stability around each open stope is evaluated by calculating the tensile and compressive probabilities of failure, based on the Hoek-Brown tensile and compressive safety factor, and the probability of brittle damage initiation (PDI), via the brittle shear ratio (BSR). For the evaluated open stopes, tensile and compressive failures share similar probabilities of

- ³Heidarzadeh S, Saeidi A, Rouleau A. Use of probabilistic numerical modeling to evaluate the effect of geomechanical parameter variability on the probability of open stope failure: a case study of the Niobec Mine, Quebec (Canada). *Journal of Rock Mechanics and Geotechnical Engineering* (Submitted)

occurrence. Considering the PDI values around all the open stopes, no brittle failure is expected to occur under the existing conditions of rock mass quality and in-situ stress regime at the Niobec Mine. Comparison of these probabilistic numerical model results with those run using a deterministic numerical approach highlights the effect of variability of rock mass geomechanical parameters on stope stability.

KEYWORDS: Numerical modeling, geomechanical variability, probability of failure, Hoek-Brown safety factor, brittle shear ratio, Niobec Mine.

List of Symbols and Abbreviations

m_i	Hoek-Brown material constant for intact rock
E_i	Young's modulus of intact rock
UCS	Uniaxial compressive strength of intact rock
m_b	Hoek-Brown material constant for rock mass
S	Material constant for the Hoek-Brown failure criterion
a	Material constant for the Hoek-Brown failure criterion
σ_{ci}	Uniaxial compressive strength of intact rock
σ_{cm}	Uniaxial compressive strength of rock mass
σ_t	Uniaxial tensile strength of intact rock
σ_1	Major principal stress
σ_2	Intermediate principal stress
σ_3	Minor principal stress
E_{rm}	Deformation modulus of rock mass
D	Degree of disturbance of the rock mass

K	Bulk modulus
G	Shear modulus
K_{\min}	Minimum horizontal to vertical stress ratio
K_{\max}	Maximum horizontal to vertical stress ratio
Z	Depth
σ_v	Vertical stress component
$\sigma_H(\min)$	Minimum horizontal stress component
$\sigma_H(\max)$	Maximum horizontal stress component
γ	The unit weight of the overburden
BSR	Brittle Shear Ratio
SF	Safety factor
POF	Probability of failure
RSM	Response Surface Methodology
SORM	Second-Order Reliability Method
PEM	Point-Estimate Method
ANN	Artificial Neural Network
FLAC3D	Fast Lagrangian Analysis of Continua in 3 Dimensions
GSI	The geological strength index
PDF	Probability density function
PDI	Probability of damage initiation
MCS	Monte Carlo Simulation
RMCS	Random Monte Carlo Simulation
Nb	Niobium

5.2. Introduction

The instability of underground openings remains a challenge for the mining industry. For open stoping as the most widely applied excavation technique in Canadian underground mines (Hudson 1993; Wang 2004; Zhang and Mitri 2008; Abdellah et al., 2014b), instability issues adversely affect mine production capacity and profitability as well as the safety of personnel and equipment (Einstein 1996; Idris et al., 2011; Brown 2012; Abdellah et al., 2014b). Therefore, ensuring underground stability is of primary importance; solving this issue relies on recognizing the key parameters that cause instability and determining their effects (Heidarzadeh et al., 2018a).

Open-stope stability is influenced by several factors including stope geometry (Zhang and Mitri 2008; Aglawe 1999; Villaescusa 2014; Heidarzadeh et al., 2018b), the state of in-situ stress, and the geomechanical characteristics of the rock mass (Villaescusa 2014; Diederichs and Kaiser 1996; Chen et al., 1997; Henning 2007; Idris et al., 2013). Among these factors, the effect of the geomechanical parameters of the rock mass is critical and cannot be neglected as it reflects the heterogeneous nature of the rock mass. The physico-mechanical properties of a rock mass are intrinsically variable (Idris et al., 2011); this affects its behavior in terms of both strength and stiffness (Idris 2014).

A conventional deterministic approach cannot capture the variability of rock mass properties and achieve a proper stability analysis. Probabilistic methods are more appropriate for incorporating the uncertainties associated with the inherent variability of the geomechanical parameters of a rock mass. Probabilistic methods consider these uncertainties by defining the geomechanical input variables of the rock mass as probability distribution functions (that consider the mean and standard deviation values) instead of assigning a single mean value to the parameters;

thus the actual behavior of the rock mass is reflected in the numerical stability analysis (Idris et al., 2011, Dong et al., 2017).

The application of probabilistic methods in underground stability problems have been investigated in several studies. Diederichs and Kaiser (1996), developed a methodology to take into account the variability and uncertainty in calibration and input data of the modified stability graph method for stability assessment of open stopes. Chen et al. (1997), applied the first-order second-moment approximation method to determine the probability of failure for two different underground excavations. The results highlighted the important role of the distribution of parameter values; higher dispersion of input parameter values resulted in changing the probability of failure. Langston and Kirsten (2001), assessed the probability of hanging wall failure in sublevel open stopes at the Stillwater Mine in Montana and provided a skeletal graph relating probability of failure to rock mass parameters and stope geometry. Griffiths et al. (2002) applied probabilistic methods (Random field theory and Monte Carlo simulation) with numerical analysis to evaluate the influence of spatial variation of compressive strength of intact rock on the stability of underground pillars; they concluded that the deterministic average value of rock strength is not a good indicator of the overall strength of the pillar. Lü and Low (2011) performed a probabilistic analysis using RSM (Response surface methodology) and SORM (Second-order reliability method) to evaluate the stability of underground rock excavations considering multiple failure modes. Guarascio and Oreste (2012) proposed a probabilistic approach to evaluate the degree of safety of a pillar in room and pillar mining method, which considered the typical uncertainty associated with the geomechanical parameters of the rock mass. Abdellah et al. (2013) used the Random Monte Carlo Simulation (RMCS) in conjunction with finite difference code FLAC to assess the effect of rock mass geomechanical parameter variability on the state of mine haulage

drifts stability. Pytel and Świtoń (2013) used RSM in conjunction with numerical modeling to assess the impact of rock mass geomechanical parameter variability on stability state of underground excavations. Abdellah et al. (2014a) proposed a methodology to assess the probability of instability of a mine development intersection at Vale's Garson Mine (Sudbury, Canada) by employing the modified Point-Estimate Method (PEM) in conjunction with the finite difference modeling software FLAC3D. Idris (2014), evaluated different probabilistic methods such as PEM, Artificial Neural Network (ANN) and RSM to determine the role of uncertainties in rock mass properties on underground stope stability. Zhao et al. (2016) used Monte Carlo simulation (MCS) to incorporate the variability of the cohesion and friction angle of rock mass for stochastic evaluation of overall rock block failure in a copper mine site in Australia. Among the various probabilistic approaches used in rock mechanics and geotechnical studies, Monte Carlo simulation (MCS) and Random Monte Carlo simulation (RMCS) offer a number of advantages (Abdellah et al., 2014a).

Probabilistic evaluation of the state of open-stope stability requires appropriate stability criteria to determine the potential of different probable types of underground failure. Various instability criteria have been used to investigate different modes of underground instability (Wang 2004; Zhang and Mitri 2008; Idris 2014; Henning and Mitri 2007; Shnorhokian et al., 2015; Heidarzadeh et al., 2018b). In reality, the applied in-situ stress regime and geomechanical characteristics of the rock mass determine the possibility of occurrence of different modes of stress-induced failure. Therefore, a comprehensive stability analysis requires adopting multiple failure criteria to address all possible failure mechanisms.

In this study, we apply numerical modeling to perform a probabilistic stability analysis of seven primary open stopes located in mining blocks V and VI at the Niobec underground mine

(Saint-Honoré, Quebec). The Niobec Mine was selected due to its unique features in terms of open-stope geometry setup, hard rock quality, and the reports of minor collapses and failures (Lavoie 2018). We combine probabilistic methods with the finite difference code *FLAC3D* (Itasca 2015) to evaluate the stability state of each studied stope, taking into consideration the inherent variability associated with the geomechanical parameters of the rock mass. The stability state is defined via the tensile and compressive probabilities of failure (POF) and the probability of brittle damage initiation (PDI), by using the Hoek-Brown tensile and compressive safety factor and the brittle shear ratio (BSR), respectively, as stability indicators. Monte Carlo simulation generates the probabilistic rock mass input parameters while Random Monte Carlo simulations are performed for 100 numerical modeling runs having a random spatial distribution of the geomechanical parameters of the rock mass. To clarify the role of the inherent variability of these parameters on the different modes of instability, we use a deterministic numerical model simulation to compare rock mass behavior under both a deterministic and a probabilistic stability analysis.

5.3. Niobec Mine

The Niobec underground mine is located 13 km northwest of the City of Saguenay within the limits of the municipality of Saint-Honoré, Quebec, Canada (Fig. 5-1). It is North America's single major Niobium (Nb) source and the world's only underground Nb mine (Dorion 2013). The commercial production of the Nb concentrate began in 1976. The deposit consists of a sub-vertical very late Precambrian intrusion of alkaline silicate rocks (syenite) and carbonatites (calcite and dolomite). The elliptical-shaped intrusion has a dolomitic and calcite-carbonatite core, surrounded by syenite; it is covered entirely by the flat-lying Paleozoic limestone of the Trenton group (Thivierge et al., 1983).

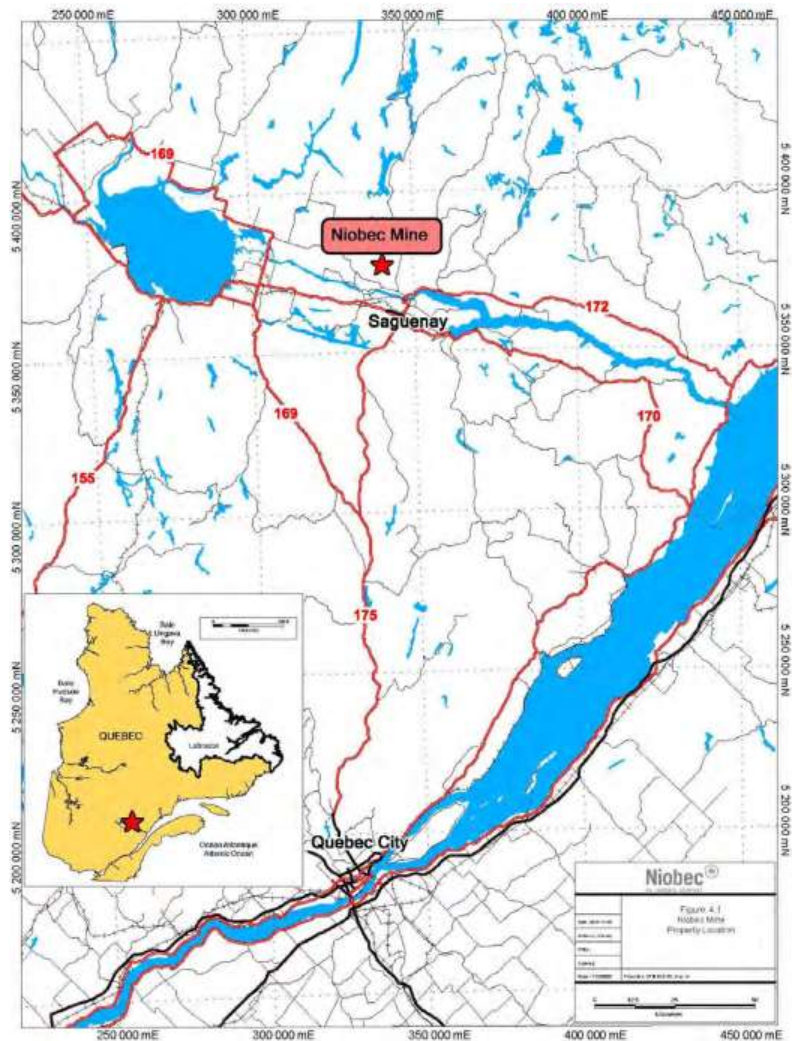


Figure 5-1 - Location of the Niobec Mine near Saguenay, Quebec (Canada) (Vallieres et al. 2013).

Open stoping is the underground excavation method currently used at the Niobec Mine. The average dimensions of the open stopes are 90-m-high, 61–73-m-long, and 25-m-wide. To maintain a natural stability, the roof of the stopes has a dome-shaped design. The deposit has been excavated at multiple mining blocks (levels) that are divided by crown pillars left between the levels. We focus our stability analysis on the primary stopes of mining blocks V and VI (from 564–732 m below the surface) as minor stability problems, such as seismic events caused by

blasting, collapses in active galleries, and minor rock falls in the walls and pillars, have been reported (Lalancette 2018).

5.4. Methodology

Fig. 5-2 presents the methodology and sequential steps that we use to assess the effect of the geomechanical variability of the rock mass on the state of open-stope stability.

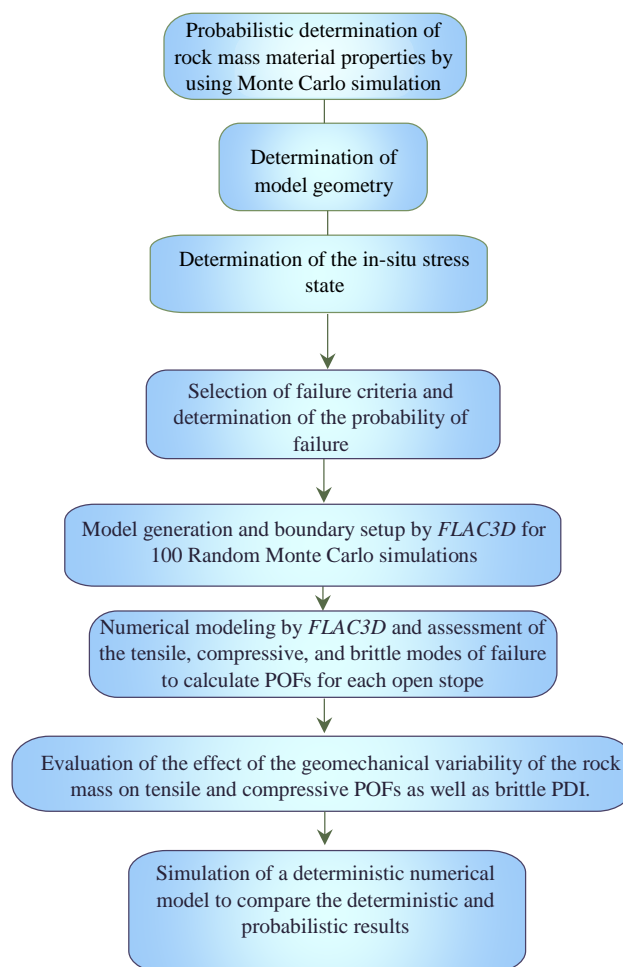
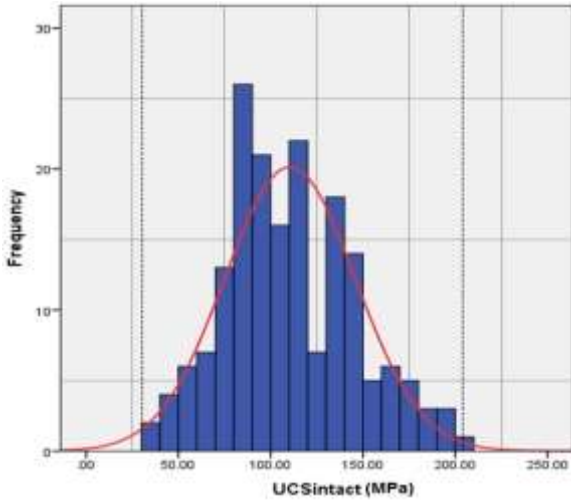


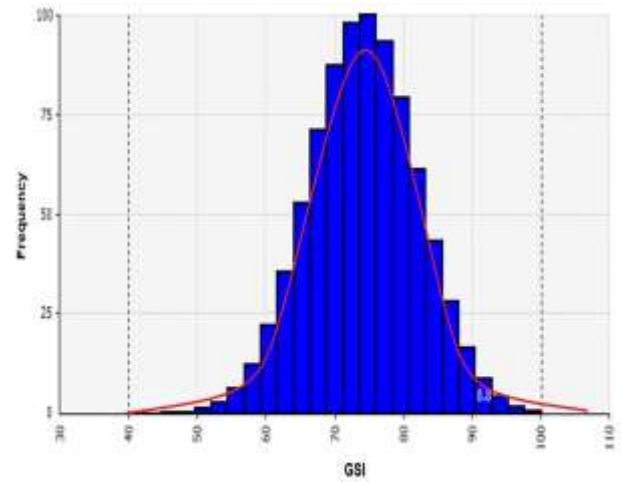
Figure 5-2 - The methodology used to evaluate the effect of geomechanical variability of the rock mass on open-stope stability.

5.4.1. Determining rock mass properties

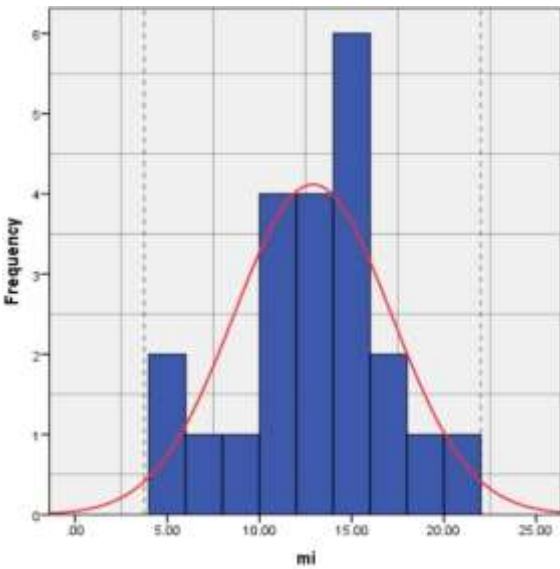
Laboratory testing of core samples extracted from various locations within the Niobec Mine have determined the physical and mechanical properties of the intact rock (Bétournay et al., 1986; Labrie 1987, 1997, 2005; Desbiens 1997; Corthésy 2000a; Lajoie 2010; Grenon 2013; Itasca 2014). Lavoie (2018) compiled all available rock property datasets to summarize the material properties of the combined syenite and carbonatite rock mass at the Niobec Mine. This approach is helpful for developing numerical models as it simplifies each model by defining a single type of material property for the entire rock mass rather than dealing with multiple rock types of variable properties. Accordingly, the mean and standard deviation values of the uniaxial compressive strength (UCS) of intact rock, the Hoek-Brown material constant (m_i), the Young's modulus of intact rock (E_i), and the geological strength index (GSI) of the combined syenite and carbonatite rock mass context are adopted from Lavoie (2018). These values are considered as random input parameters when calculating the geomechanical parameters of the rock mass. Normal probability density functions (PDFs) are assumed for these parameters since the normal distribution is recommended by several studies to be assigned to the intact rock and rock mass material properties (Hoek 2007, Cai 2011). To eliminate negative and/or false values, the normal PDFs are truncated by using the minimum and maximum values reported in the datasets. Figs. 5-3 a–d present the truncated PDF plots for intact rock material properties and the GSI of the rock mass. The black dashed lines in Fig. 5-3 a–d indicate the limits of the actual minimum and maximum values of the parameters.



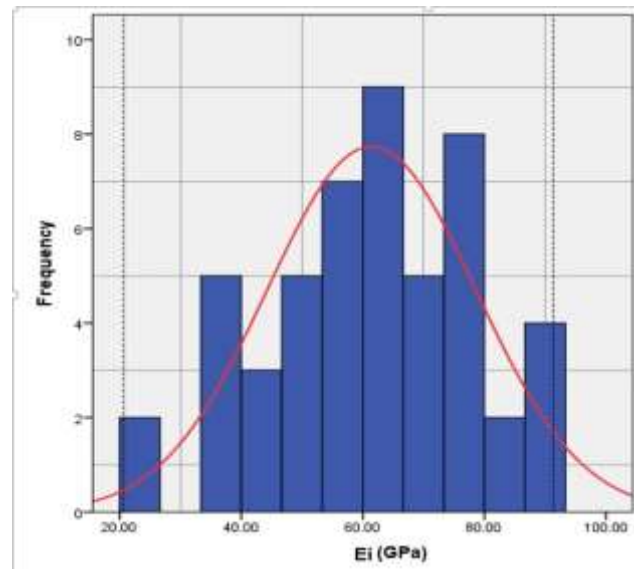
(a)



(b)



(c)



(d)

Figure 5-3 - The truncated normal probability distribution functions (PDFs) for (a) the uniaxial compressive strength (UCS) of the intact rock, (b) the geological strength index (GSI) of the rock mass, (c) the Hoek-Brown material constant m_i , and (d) Young's modulus E_i of the intact rock (data compiled by Lavoie 2018).

To account for the variability associated with the intact rock parameters, statistical moments (i.e. mean and standard deviation) of each parameter are determined and used in the subsequent calculations (Table 5-1).

Table 5-1 - Statistical moments for the intact rock parameters.

Property (units)	Mean value and standard deviation
UCS (MPa)	110.4 ± 35.5
E_i (GPa)	61.4 ± 17.2
m_i	12.8 ± 4.3
Poisson's ratio	0.26 ± 0.07

UCS: uniaxial compressive strength, E_i : Young's modulus, m_i : Hoek-Brown material constant

The MCS method then calculates the Hoek-Brown strength and deformability parameters of the rock mass through Eqns. 5-1–5-6 (Hoek 2007) by using the mean and standard deviation values of the random input parameters (i.e. UCS, GSI, and m_i).

$$m_b = m_i e^{\left(\frac{GSI-100}{28-14D}\right)} \quad (5-1)$$

$$s = e^{\left(\frac{GSI-100}{9-3D}\right)} \quad (5-2)$$

$$a = \frac{1}{2} + \frac{1}{6} \left(e^{\frac{-GSI}{15}} - e^{\frac{-20}{3}} \right) \quad (5-3)$$

$$\sigma_{cm} = \sigma_{ci} s^a \quad (5-4)$$

$$\sigma_t = \frac{s\sigma_{ci}}{m_b} \quad (5-5)$$

$$E_{rm} = E_i \left(0.02 + \frac{1 - \frac{D}{2}}{1 + e^{\frac{(60+15D-GSI)}{11}}} \right) \quad (5-6)$$

where D stands for the degree of disturbance of the rock mass (ranging between 0 to 1 for undisturbed in-situ rock masses to highly disturbed rock masses) (Hoek 2007). Since the rock mass

is assumed to be disturbed by blasting effects, the parameter D is considered equal to 0.8 for this study (Henning 2007). The parameters m_b , s , and a represent the Hoek-Brown failure constants, σ_{cm} and σ_t are the parameters defining the compressive and tensile strengths of the rock mass respectively, and E_{rm} is the deformation modulus of the rock mass. The parameter σ_{ci} is the UCS of the intact rock.

The MCS generates the range of each geomechanical parameter of the rock mass by performing 10000 iterations based on the Latin hypercube sampling algorithm to provide smoother resulting PDFs. Each output parameter's PDF is generated from 10000 calculations obtained from different combinations of randomly selected input parameter values in accordance with their produced PDF. The mean and standard deviation values of the rock mass strength and deformability parameters generated through the MCS are reported in Table 5-2.

Table 5-2 - Statistical moments of the geomechanical parameters of the rock mass.

Property (units)	Mean value and standard deviation
Geological strength index (GSI)	74.4 ± 8.2
Bulk modulus, K (GPa)	30.34
Shear modulus, G (GPa)	19.07
Tensile strength, σ_t (MPa)	1.7 ± 1.4
Compression strength σ_{cm} (MPa)	29.45 ± 17.1
Hoek-Brown failure constants	
m_b	5.4 ± 2.4
s	0.086 ± 0.08
a	0.501 ± 0.0008
Deformation modulus, E_{rm} (GPa)	47.15 ± 14.2

Furthermore, to incorporate the variability of the geomechanical parameters into numerical modeling, the RMCS method is used as it is one of the best-known probabilistic approaches. This method is capable of assigning spatially random values of geomechanical parameters within a given region of the rock mass in the model (Abdellah 2013).

5.4.2. Determining model geometry

The primary open stopes located in mining blocks V and VI of the Niobec Mine are modeled using the finite difference code FLAC3D (Itasca 2015). The developed models consist of the six primary stopes of mining block V (each being 25-m-wide, 34.7-m-high, 61–73-m-long) and the seven primary stopes of mining block VI (each being 25-m-wide, 94.7-m-high, 61–73-m-long). These primary stope dimensions were provided by the mine authorities. To improve the stability, the roof of the open stopes is dome-shaped. Undercut draw points having identical layouts are also present, while 25-m-wide rib pillars and 25-m-long transverse pillars are designed to be left between the stopes. Based on the existing open-stoping design at the Niobec Mine, no crown pillar was included between the primary stopes at mining blocks V and VI in the model; hence the upper and lower stopes were modelled combined together, resulted in seven primary stopes. The excavation sequence pattern was provided by the Niobec Mine authorities and was adjusted according to the ore mineralization and the interactions between the primary and secondary stopes (not considered in this study) in terms of overall stability (Lalancette 2018). The simulated primary stopes and their excavation sequence are shown in Fig. 5-4.

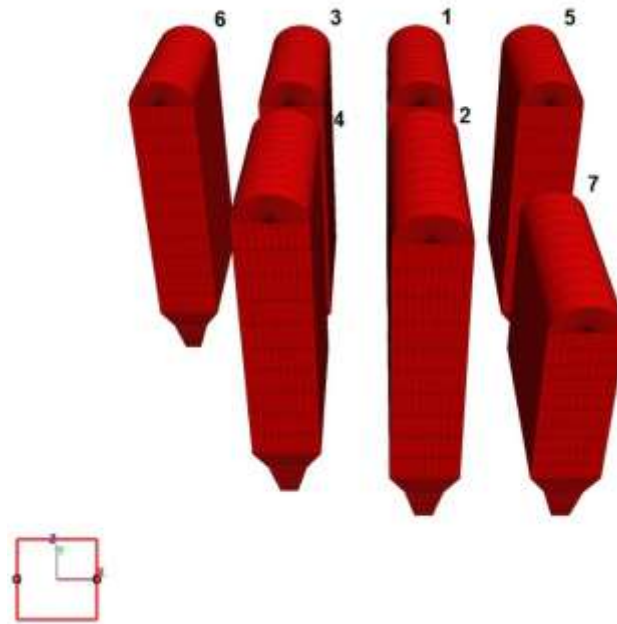


Figure 5-4 - The seven primary open stopes and the excavation sequence of mining blocks V and VI at the Niobec Mine.

5.4.3. State of in-situ stress

To determine the existing natural stress field within the rock mass, we could rely on the number of studies that have assessed the in-situ stress components at different mining levels of the Niobec Mine (Itasca 2014; Labrie 2005; Golder 2012; Corthésy 2000b, Corthésy et al., 2013a, 2013b). However, this data is highly dispersed and wide variations are observed in the orientation of the principal stresses within the rock mass. Consequently, Lavoie (2018) proposed an empirical relation to determine the principal stress components as a function of depth (Figs. 5-5a–b).

Power trend curves are applied (Fig. 5-5a) to the calculated values of the horizontal to vertical stress ratio K , at different depths; the obtained correlation coefficients support the validity of the resulting Eqns. 5-7–5-8. As a result, the range of the maximum and minimum horizontal in-

situ stress components as a function of depth are estimated by Eqns. 5-9–5-11 and are plotted in Fig. 5-5b (Lavoie 2018).

$$K_{\min} = 679.93z^{-1.101} \quad (5-7)$$

$$K_{\max} = 78205z^{-1.755} \quad (5-8)$$

$$\sigma_v = \gamma z \quad (5-9)$$

$$\sigma_{H(\min)} = \sigma_v \times K_{\min} \quad (5-10)$$

$$\sigma_{H(\max)} = \sigma_v \times K_{\max} \quad (5-11)$$

where K_{\max} and K_{\min} represent the maximum and minimum horizontal to vertical stress ratios, respectively, z (m) is the depth, σ_v (MPa) is the vertical stress component, γ is the unit weight of the overlying strata (considered equal to 0.027 MN/m³), and $\sigma_{H(\min)}$ (MPa) and $\sigma_{H(\max)}$ (MPa) are the minimum and maximum horizontal stress components, respectively.

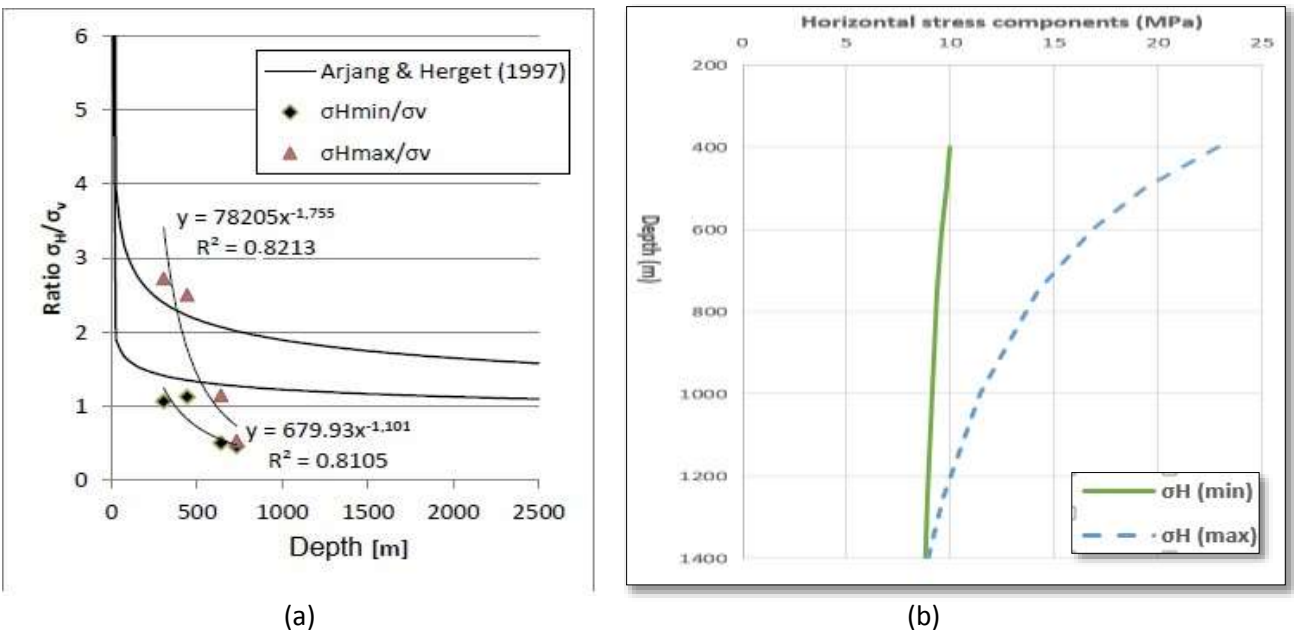


Figure 5-5 - (a) Power trend curves applied to the calculated horizontal to vertical stress ratio K at various depths and (b) variations of the maximum and minimum horizontal in-situ stress components as the function of depth (after Lavoie 2018).

The values for the applied vertical and horizontal stress components in the models are calculated for the upper and lower boundaries (Table 5-3). A linear variation gradient, as a function of depth, is developed for each stress component that is to be applied in the models (Figs. 5-6a–b).

Table 5-3 - The range of values for the in-situ stress components.

Depth (m)	$\sigma_{H(\max)}$ (MPa)	$\sigma_{H(\min)}$ (MPa)	σ_V (MPa)
511–805	19.0–29.9	9.8–15.4	13.8–21.7

Assuming that the orientation of the horizontal stress components are perpendicular to the boundaries of the model may not reflect the actual orientations in some areas of the mine. However, these simplifications allow the numerical simulations to be more straightforward and maximize the differential stresses induced on the largest walls of the excavations. Therefore, adopting these conditions constitutes a more conservative approach for evaluating the state of underground stability at the Niobec Mine.

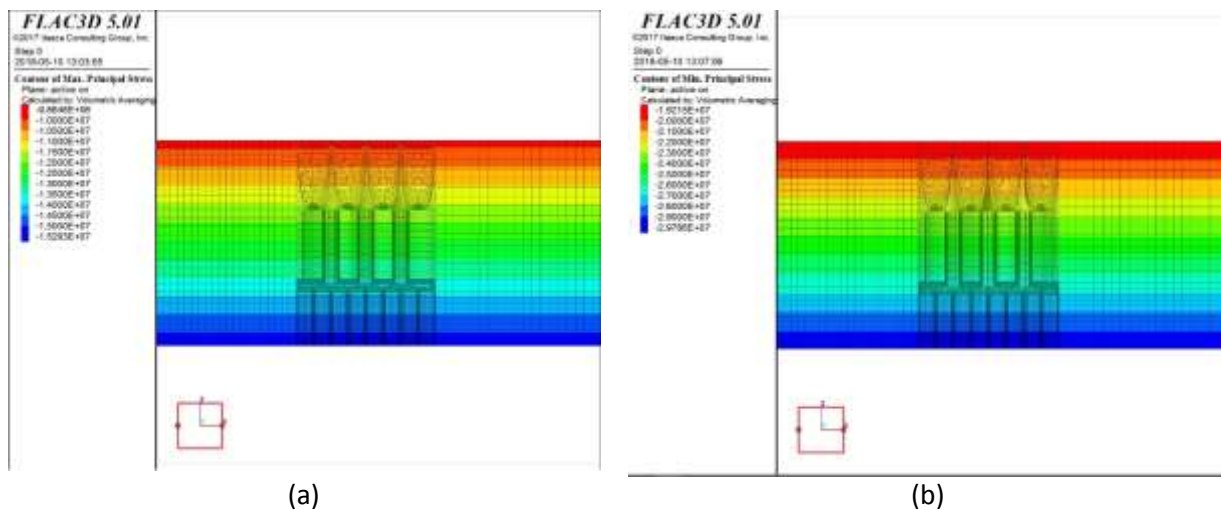


Figure 5-6 - The linear variation gradient of (a) the maximum horizontal in-situ stress component as a function of depth and (b) the vertical in-situ stress component as a function of depth.

5.4.4. Selecting failure criteria

In general, rock mass instability around an underground excavation occurs due to the perturbation of the in-situ stress regime that is defined via three major types, i.e. tensile, compressive, and shear failure (Shnorhokian et al. 2018). Depending on the level of confinement (low or high confinement), stress-induced instability is referred to as either an inner or an outer shell problem (Castro et al., 2012). In particular, under the low confinement conditions being addressed by this study, stress-induced damage to the rock mass leads to two dominant failure conditions, namely (1) stress-induced spalling and slabbing failure and (2) structurally controlled gravity-driven failure (Castro et al., 2012). To assess the level of damage and ultimate failure conditions associated with these instability modes, we used three different stability indicators. First, the potential brittle damage of the rock mass around the open stope is evaluated for each model zone by using the BSR described in Eqn. 5-12 (Shnorhokian et al., 2015):

$$BSR = \frac{\sigma_1 - \sigma_3}{UCS_{intact}} \quad (5-12)$$

As well, the potential of compressive and tensile failure around each open stope is evaluated using the Hoek-Brown safety factor (SF). For compressive conditions of instability, the Hoek-Brown compressive safety factor can be calculated by dividing the value of the Hoek-Brown maximum principal stress at the failure threshold by the maximum principal induced stress for each zone of the models (Eqn. 5-13). In the case of tensile failure ($\sigma_3 \leq 0$), the Hoek-Brown tensile safety factor is calculated by dividing the tensile strength of the rock mass (Eqn. 5-5) by the minimum principal induced stress of the rock mass (Eqn. 5-14).

$$SF = \frac{\sigma_3 + \sigma_{ci} \left(m_b \frac{\sigma_3}{\sigma_{ci}} + s \right)^a}{\sigma_1} \quad (5-13)$$

$$SF = \frac{\frac{s\sigma_{ci}}{m_b}}{\sigma_3} \quad (5-14)$$

5.4.5. Determining the probability of failure

The probability of slope failure (POF) for compressive and tensile instability modes (as well as the PDI) is selected as the output parameter to assess the state of stability. Accordingly, the compressive and tensile POFs are calculated through Eqns. 5-15 and 5-16, respectively, for each open slope, through obtaining the minimum values of Hoek-Brown compressive and tensile safety factors in the 100 simulated models and by including the proportion of values falling below the threshold of 1.00.

To calculate the PDIs, the maximum BSR value around each open slope is obtained for 100 simulated models, and the fraction of maximum BSR values exceeding a threshold of 0.4 (Castro et al., 2012) determines the PDI in percentage (Eqn. 5-17).

$$POF_{Comp.} (\%) = \frac{\text{Number of the obtained minimum Hoek-Brown compressive SF value} \leq 1.00 \text{ for each slope}}{\text{Total number of obtained minimum Hoek-Brown compressive SF for each slope}} \times 100 \quad (5-15)$$

$$POF_{Tens.} (\%) = \frac{\text{Number of the obtained minimum Hoek-Brown tensile SF value} \leq 1.00 \text{ for each slope}}{\text{Total number of obtained minimum Hoek-Brown tensile SF for each slope}} \times 100 \quad (5-16)$$

$$PDI (\%) = \frac{\text{Number of the obtained maximum BSR value} \geq 0.40 \text{ for each slope}}{\text{Total number of obtained maximum BSR values for each slope}} \times 100 \quad (5-17)$$

5.4.6. Numerical modeling

The finite difference code *FLAC3D* (Itasca 2015) is used to develop 100 simulated models having different randomly determined values for the geomechanical parameters of the rock mass (Figs. 5-7a–c). The dimensions of the modeled multiple neighboring stopes of mining blocks V and VI at the Niobec Mine remain identical for each simulation. Stopes are excavated according to a predetermined sequence. The Hoek-Brown plastic constitutive model is employed for the material of the models. Due to the sensitivity of the results to mesh size, different mesh sizes are examined and by comparing the resulting Hoek-Brown compressive and tensile safety factors, we selected the mesh sizes producing the most accurate numerical results. We observed that using a coarse mesh density results in relatively high safety factors and hence overestimating the state of stability for all the stopes. In contrast, using finer meshes decreased the values of both the Hoek-Brown tensile and compressive safety factors while increased the accuracy of the results. Subsequently, a finer mesh size (dense mesh) is adjusted near the stopes and pillars (target area), while a coarser mesh is adopted for the surrounding rock mass. It should be noted that a denser mesh increases the accuracy of the results by improving the resolution at high-stress gradients (Zhang and Mitri 2008). The roller conditions for external boundaries are positioned far enough from the region of interest to eliminate any probable adverse effect on the results. Also, an identical in-situ stress state and variation gradient are applied to all the models, using the values reported in Table 5-3. The stopes in each simulated model are excavated in separate single steps, and after each excavation step, the model is allowed to reach equilibrium.

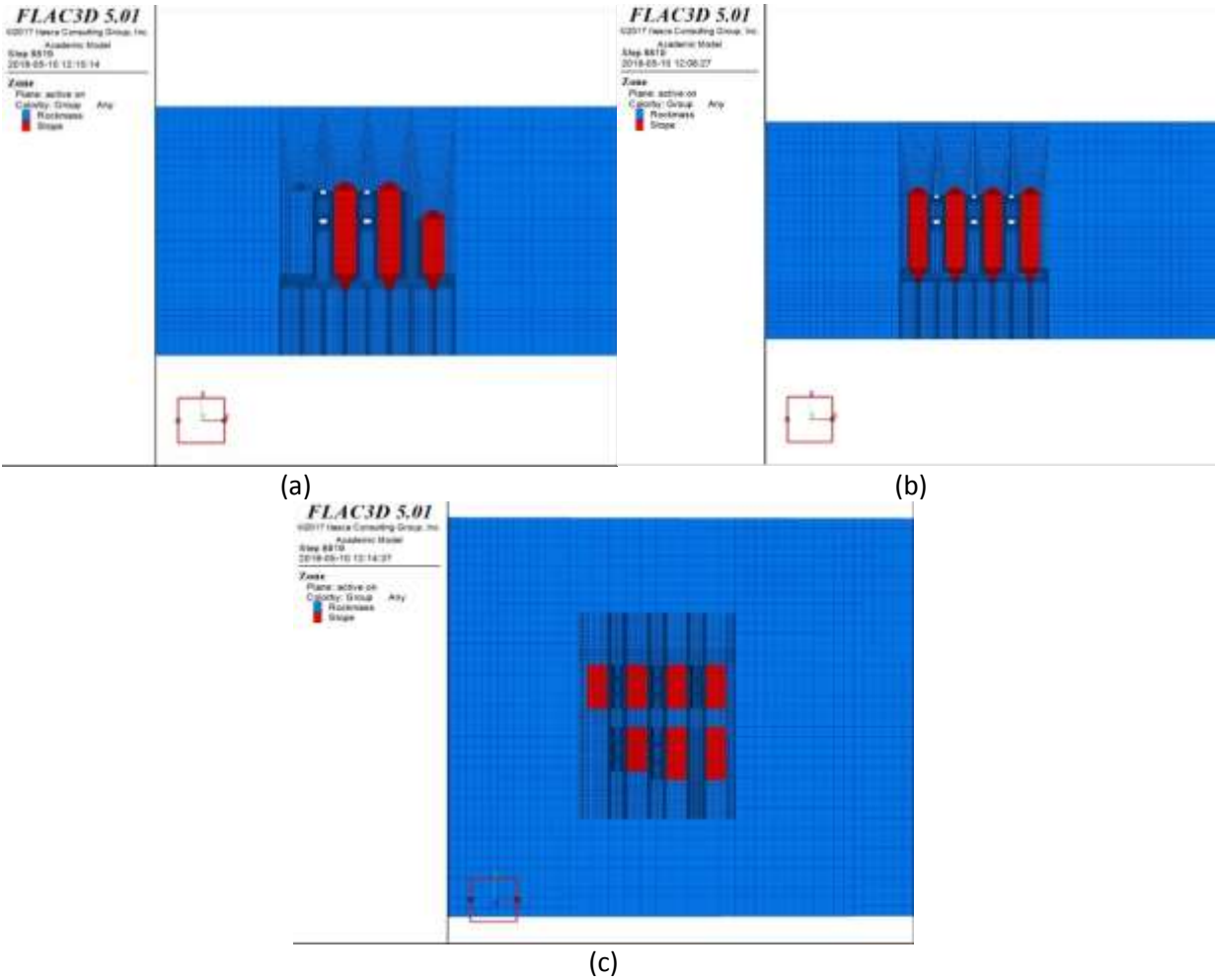


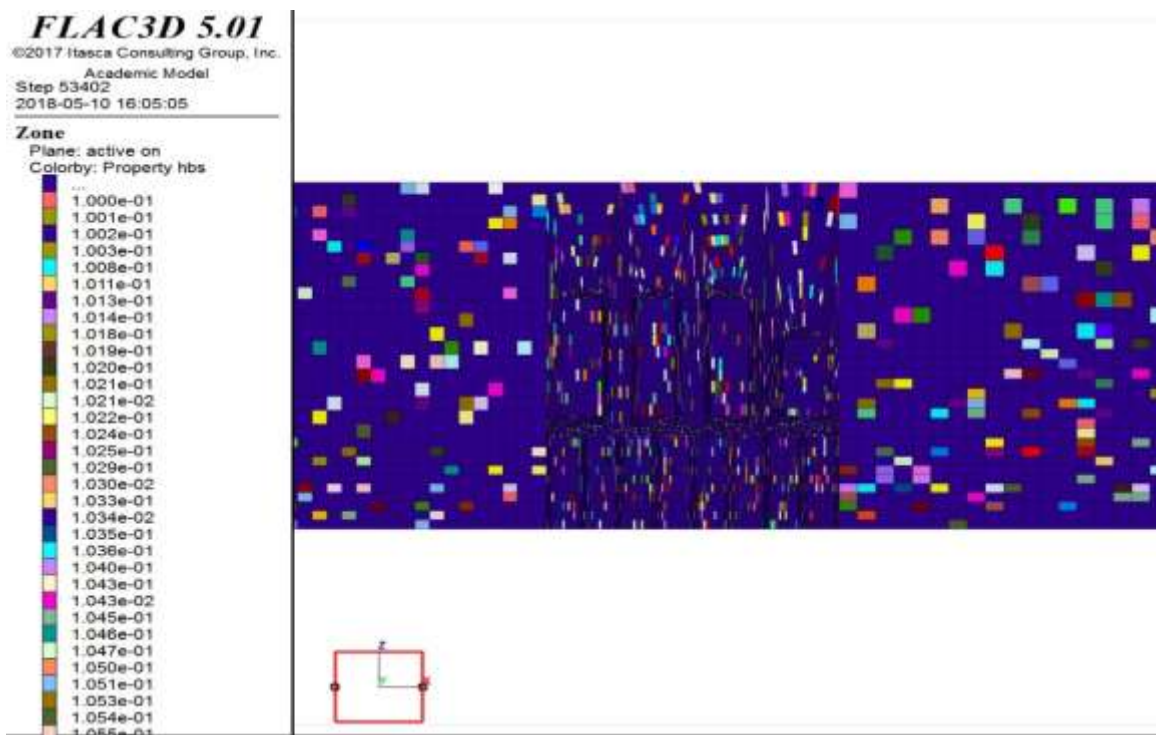
Figure 5-7 - (a) & (b) The sectional views of generated numerical model containing the seven primary open stopes and (c) the plan view of the constructed numerical model containing the seven primary stopes.

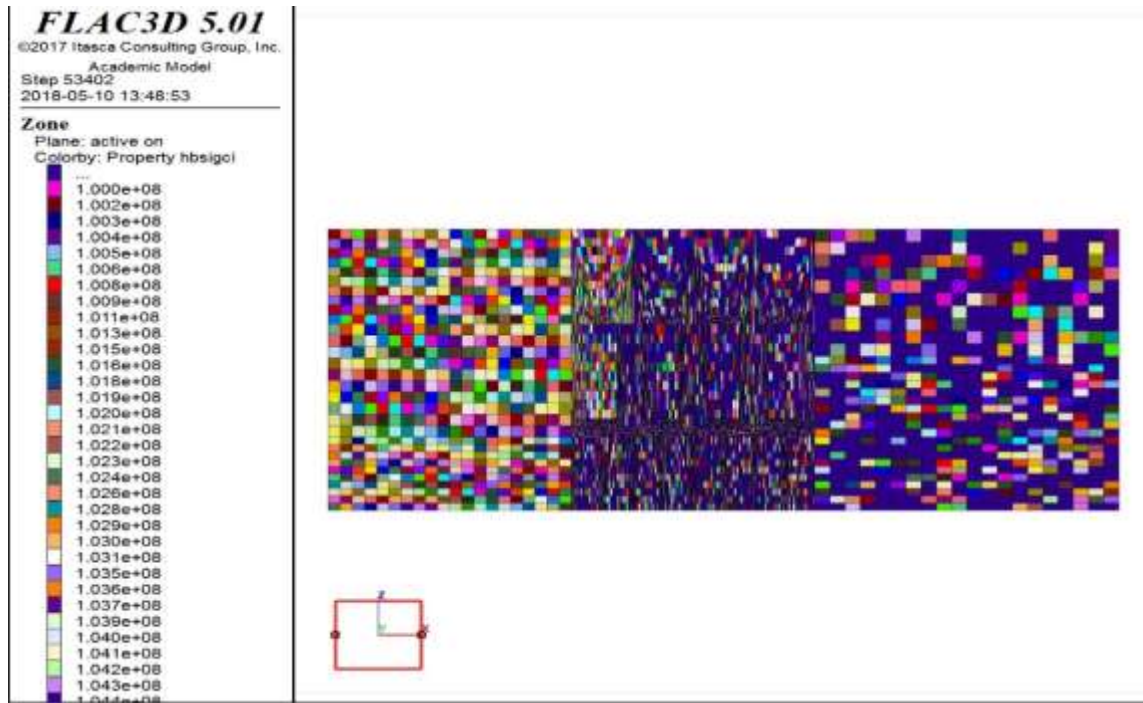
5.5. Results and discussion

Any uncertainties related to the intrinsic variability of the rock mass strength and deformability parameters are accounted for in the numerical analysis; this occurs through running 100 RMCS having random seeds to apply random spatial assignments of the geomechanical parameters to each zone of the rock mass. Examples of the random spatial variation of the rock mass properties are provided in Figs. 5-8a–b. As a result, a range of output parameter values (e.g. BSR, Hoek-Brown compressive safety factor, etc.) are obtained for the different zones of the

model. The 100 produced values for minimum Hoek-Brown compressive and tensile safety factors and maximum BSR around each open stope are plotted to determine their associated POFs and PDI (Figs. 5-8a–b).

A deterministic numerical model was also developed—having identical characteristics as probabilistic models but using the single mean values of UCS, GSI, and m_i for the rock mass—to distinguish the role of variations in the geomechanical parameters of the rock mass on the state of open stope stability.





(b)

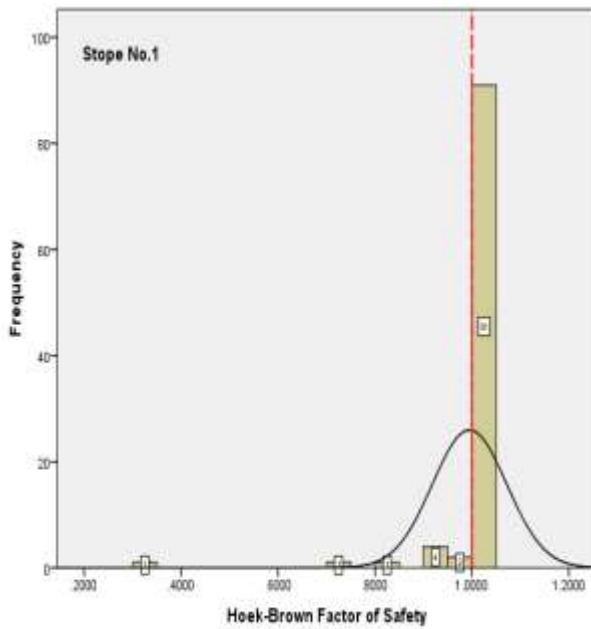
Figure 5-8 - Example of the random spatial distribution of (a) the Hoek-Brown “s” failure constant parameter and (b) the uniaxial compressive strength (UCS) of intact rock for a random seed.

5.5.1. Evaluation of the probability of compressive and tensile failure

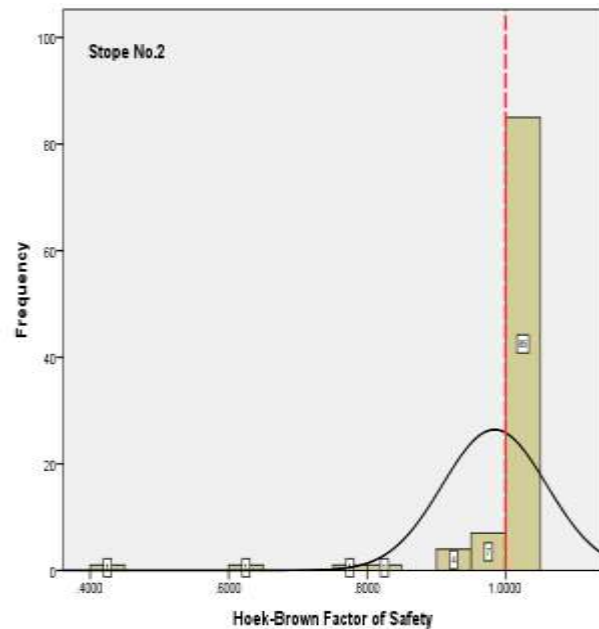
The probability of compressive and tensile damage/failure around each underground stope can be assessed using the minimum values of the Hoek-Brown compressive and tensile safety factors for each model zone. Following equations 5-13 and 5-14, a built-in FISH-language program (Itasca 2015) extracts the minimum principal induced stress for each model zone and determines whether the zone is under a compressive or tensile stress regime. Afterward, the required geomechanical parameters are then restored for the corresponding zone to calculate the relevant safety factor. To facilitate data restoration, as well as optimizing the required computing time, the minimum value of compressive and tensile safety factors are selected in the vicinity of each open stope (over a sufficient width to cover the probable damaged/failed regions). A three-dimensional

virtual frame within the surrounding rock mass is defined for each open stope (the area of interest), which extends up to 10 m in the Y and Z directions (roof, undercut, and side walls), and up to 5 m along the X-axis (hanging and foot walls) from the stope boundaries within the rock mass. For each open stope in all of the model runs, the output parameters are extracted within the area of interest for subsequent calculations.

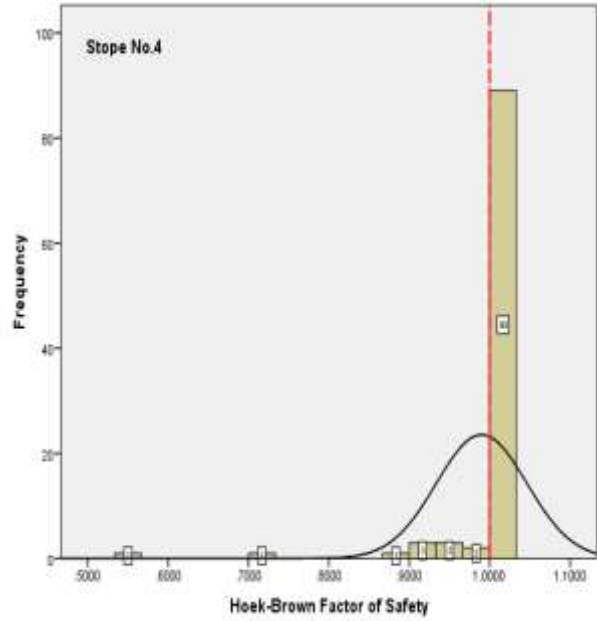
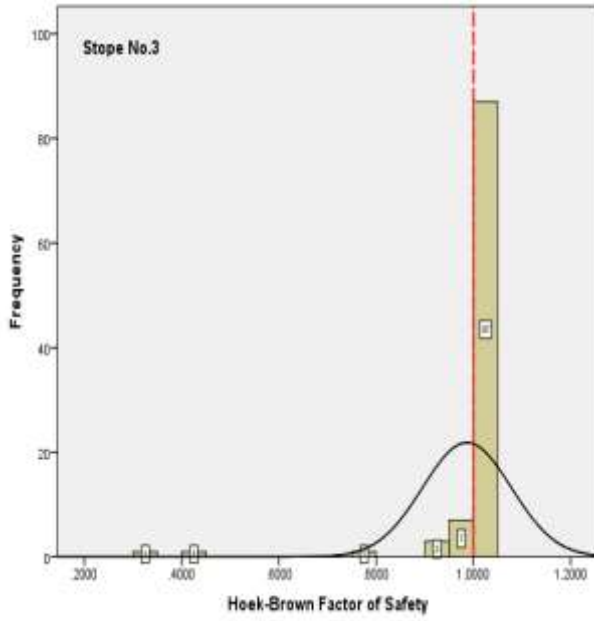
Figs. 5-9a–g illustrate the distributions and associated normal PDFs of the resulting 100 minimum Hoek-Brown compressive safety factor values for all seven open stopes. The mean values of the compressive safety factor and the compressive POFs for all the open stopes are reported in Table 5-4. The minimum and maximum compressive POFs are obtained for stope #1 and stope #7, respectively. Moreover, a general increasing trend is observed for the compressive POF as mining activity progresses.



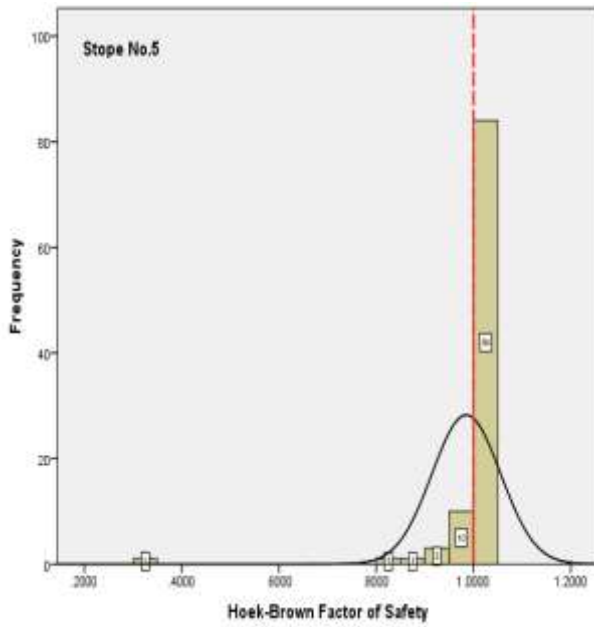
(a)



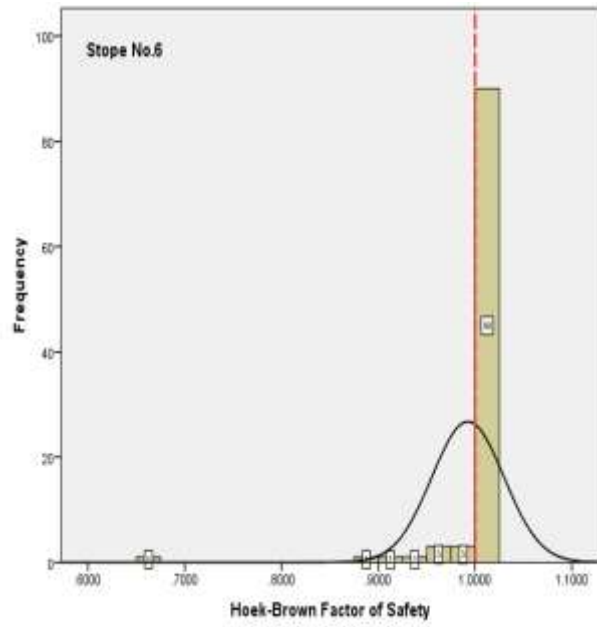
(b)



(c)

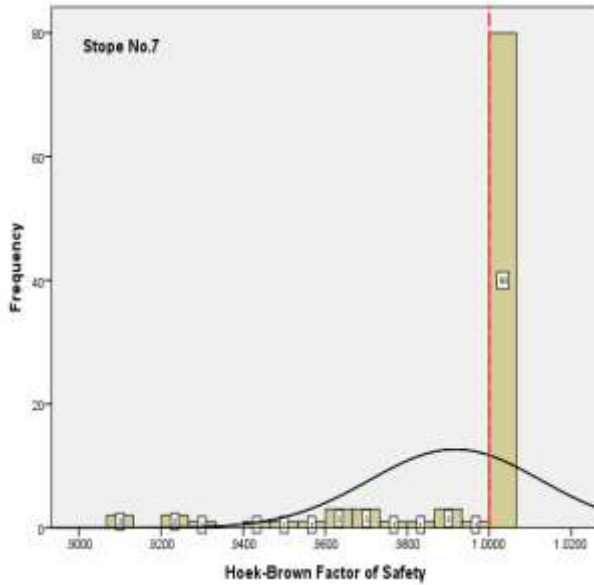


(d)



(e)

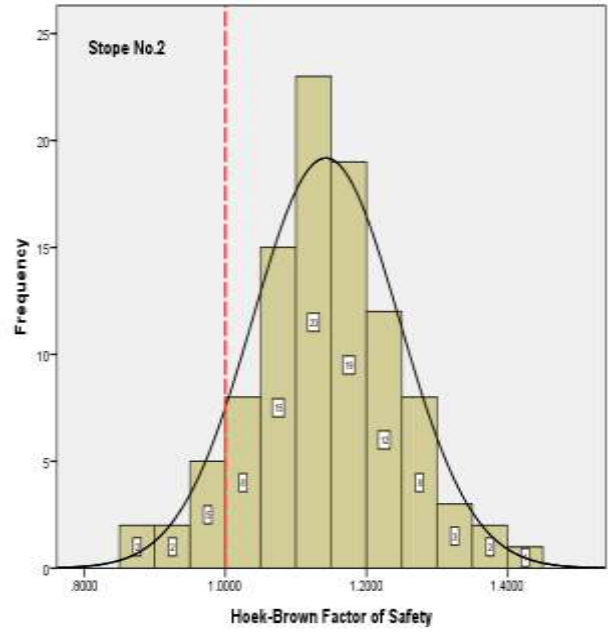
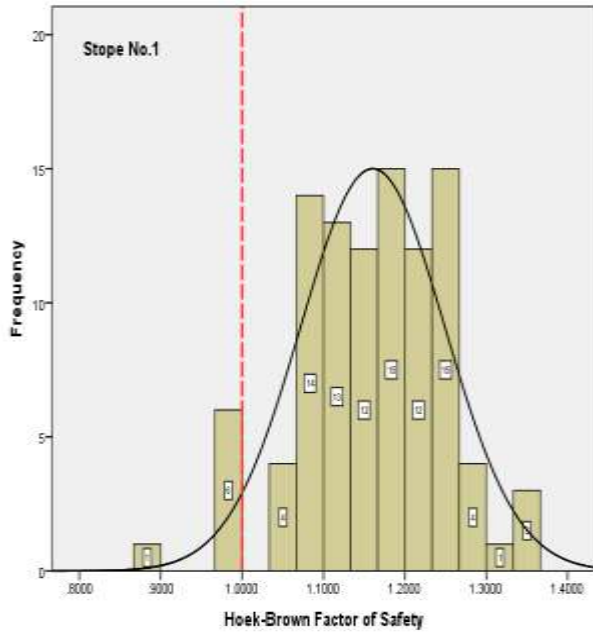
(f)



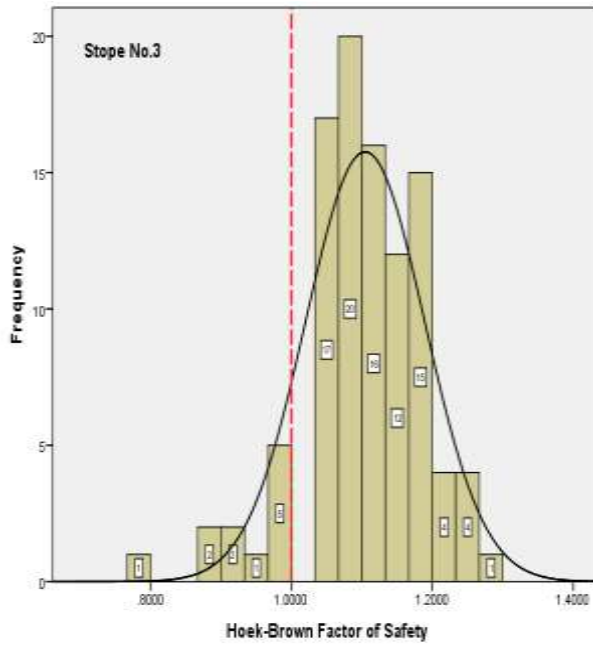
(g)

Figure 5-9 - Normal probability density functions (PDFs) of the minimum Hoek-Brown compressive safety factor around the area of interest for each primary open stope.

Similarly, in the case of tensile failure for all seven open stopes, the distributions and associated normal PDFs of the resulting 100 minimum Hoek-Brown tensile safety factor values are presented in Figs. 5-10a–g. The mean values of the minimum Hoek-Brown tensile safety factor and the tensile POFs for each stope are provided in Table 5-4. The minimum and maximum tensile POFs are observed for stope #1 and stope #4, respectively. The results show an increasing trend in tensile POF for stopes #1 to #4, followed by a dramatic decrease for stopes #5 and #6. Ultimately, excavation of stope #7 leads to a 15% probability of tensile instability.

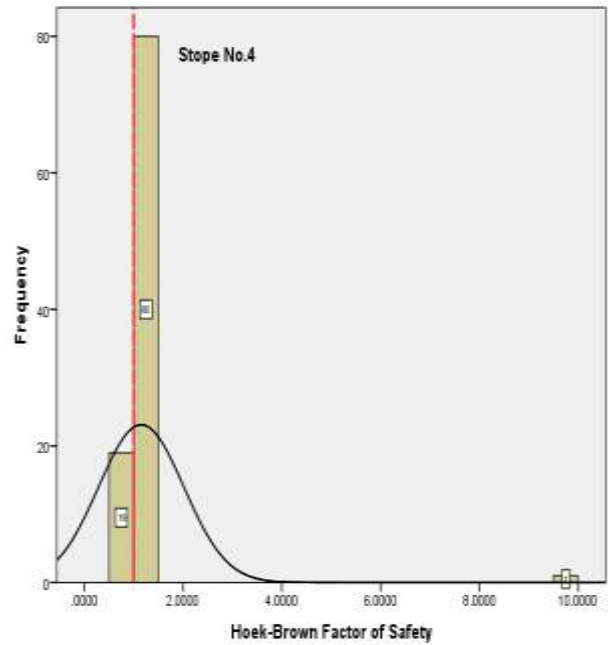


(a)

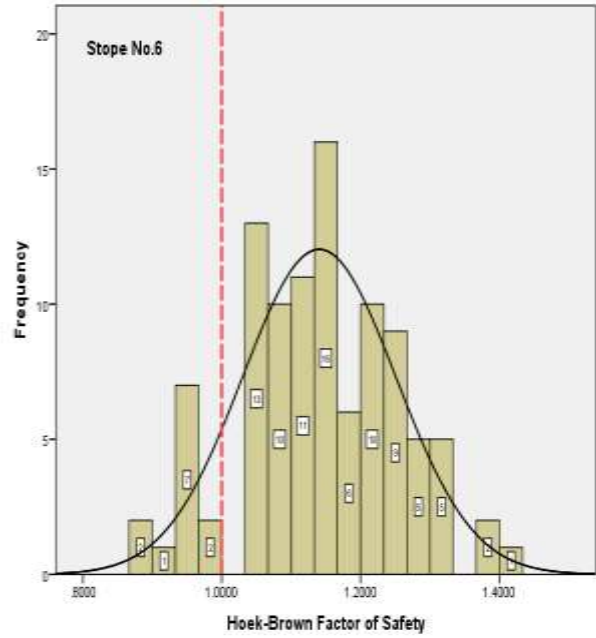
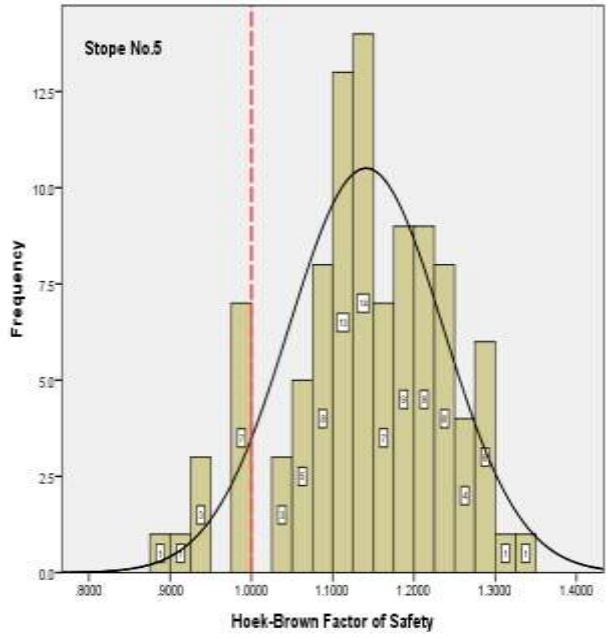


(c)

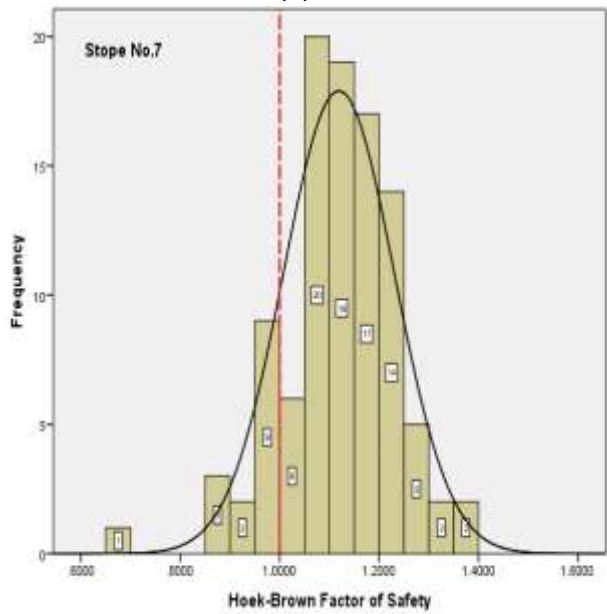
(b)



(d)



(e)



(f)

(g)

Figure 5-10 - Normal probability density functions (PDFs) of the minimum Hoek-Brown tensile safety factor around the area of interest for each primary open stope.

Table 5-4 - The mean values of minimum Hoek-Brown compressive and tensile safety factors (SF) and their associated probabilities of failure for each open stope.

Stope #	Mean compressive SF value	Compressive POF	Mean tensile SF value	Tensile POF	Overall POF
1	99.52e-2	9 %	116.04e-2	7%	16%
2	98.40e-2	15 %	114.23e-2	9%	24%
3	98.65e-2	13 %	110.45e-2	11%	24%
4	99.02e-2	11 %	115.21e-2	19%	30%
5	98.53e-2	16 %	114.09e-2	12%	28%
6	99.25e-2	10 %	114.04e-2	12%	22%
7	99.17e-2	20 %	111.90e-2	15%	35%

The reasons behind these trends for compressive and tensile POFs of each open stope can be explained in relation to the excavation sequence (Fig. 5-4). As a general notion, stope excavation within a same-level mining block perturbs the values of induced stress components around the stope perimeter. As a result, continuing excavation activities reduce stability for neighboring stopes by developing large zones of stress concentration and/or relaxation in the rib and the transverse pillars (Villaescusa 2014; Abdellah 2013). Since the maximum principal stress is oriented normal to the strike length of the open stopes, the excavation of the first stope causes all the remaining stopes to be considerably stress-shadowed. The stress-shadowing phenomenon is generated by excavation of multiple stopes aligned along the maximum principal stress trajectory (Villaescusa 2014). Consequently, stress redistribution may develop in relaxation zones for areas lying within the cast shadow, whereas stress concentration may occur in other areas, such as transverse pillars. Figs. 5-11a–b show, respectively, a plan view of the maximum and minimum principal induced stress contours around excavated stopes. The magnitude of maximum principal induced stress is considerably decreased in rib pillars and stope hanging walls (relaxation zones), while stress concentration zones are visible in transverse pillars and side walls (Fig. 5-11a). The

compressive POF is larger for the stopes having a high maximum principal induced stress and a lower confinement around them. Hence, areas having a concentration of stress are more prone to decreasing the safety factor value below an acceptable threshold and leading to failure (Castro et al., 2012; Martin et al., 2003).

On the other hand, reducing tangential and radial stress on stope walls creates an unconfined (relaxation) area. By excavating a stope, the maximum and intermediate principal induced stresses are aligned parallel to the stope hanging wall, while the minimum principal induced stress is oriented perpendicular to the stope boundary (Henning 2007). Relaxation of stope walls occurs when tangential stresses (the major and/or intermediate principal induced stress) are reduced; thus the confinement is decreased. The creation of low confinement or unconfined areas around a stope reduces the minor principal induced stress to zero or less, creating areas that are prone to tensile failure (Diederichs 1999; Diederichs et al., 2004). Areas around the open stopes that have a minimum principal induced stress below zero are shown in Fig. 5-11b. The obtained tensile POFs for each open stope are directly influenced by the extent of the relaxation zones around them.

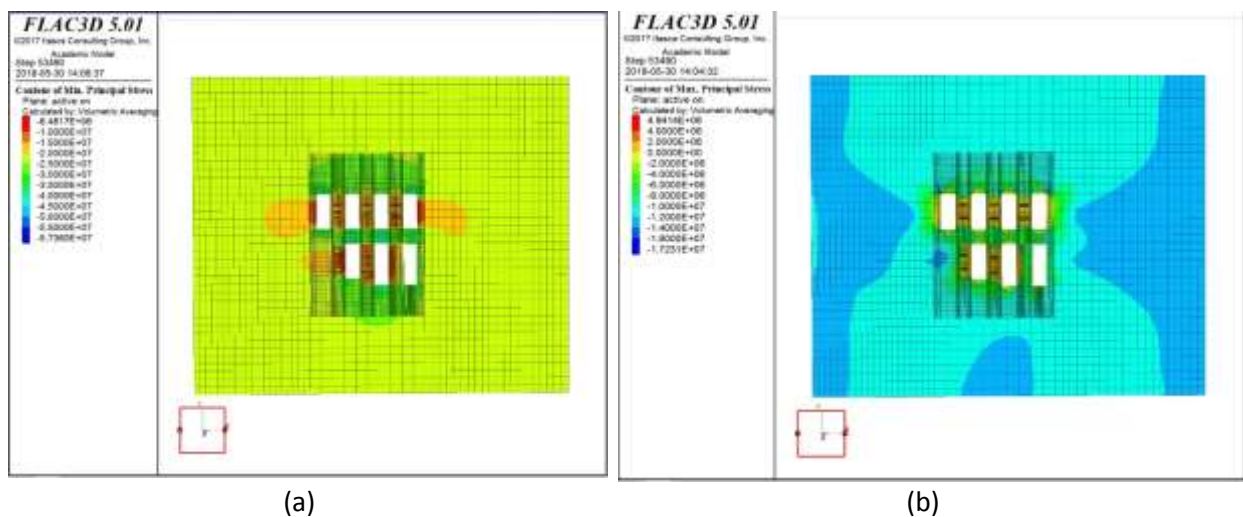


Figure 5-11 - A plan view of maximum principal induced stress contours around open stopes and (b) a plan view of minimum principal induced stress contours around open stopes.

In terms of overall stability, stopes #7 and #4 are most prone to failure (as they have the highest overall POFs), while stopes #1 and #2 are the most stable stopes in mining blocks V and VI of the Niobec Mine (Table 5-4).

5.5.2. Evaluation of the probability of brittle damage initiation

The maximum value of BSR (Eqn. 5-12) is the output parameter used to calculate the PDI for each open stope. Thus, we developed a built-in FISH-language program to calculate the BSR for all zones of the simulated models using the value of maximum shear stress at each zone (Heidarzadeh et al., 2018a). Figs. 5-12a–b illustrate, respectively, an example of a sectional and a planar view of the obtained BSR contours from the numerical model. The maximum BSR value of each open stope is selected from within an area of interest having the same dimensions as the area selected for the compressive and tensile stability analyses.

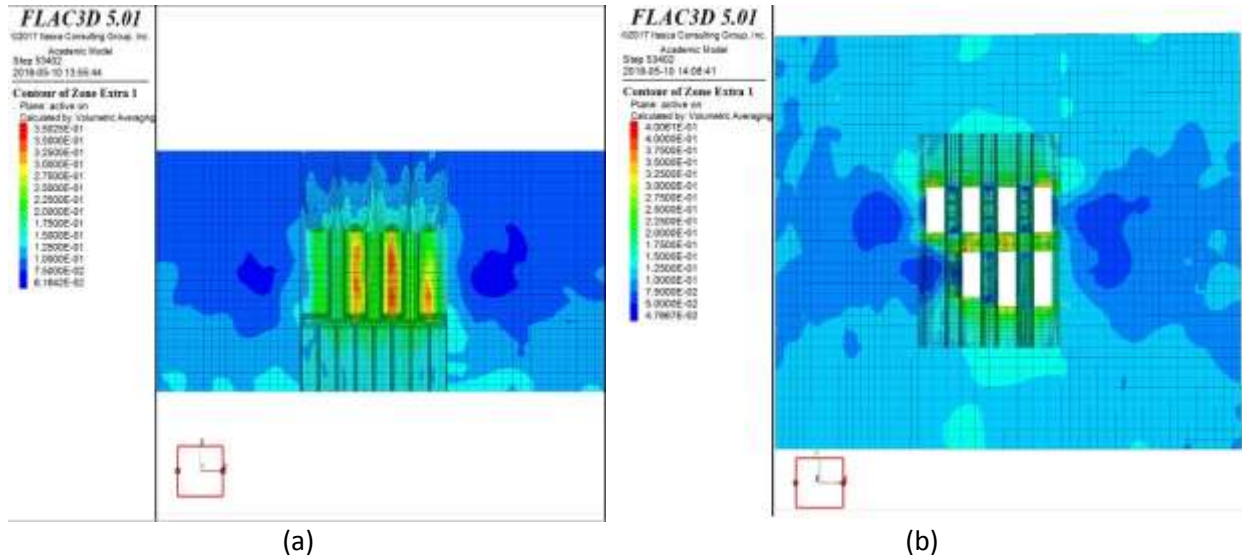
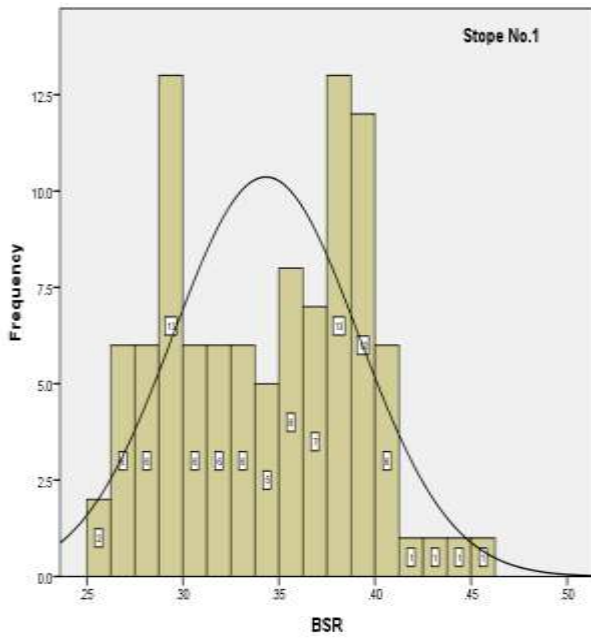
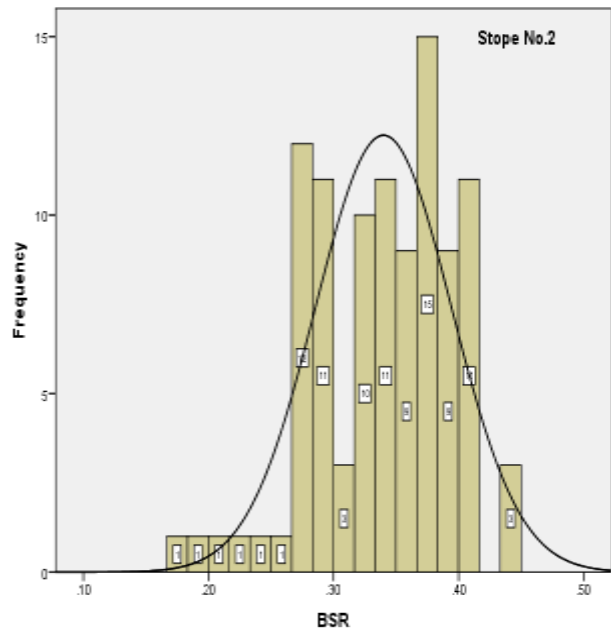


Figure 5-12 - The (a) profile view and (b) plan view of brittle shear ratio (BSR) contours around open stopes.

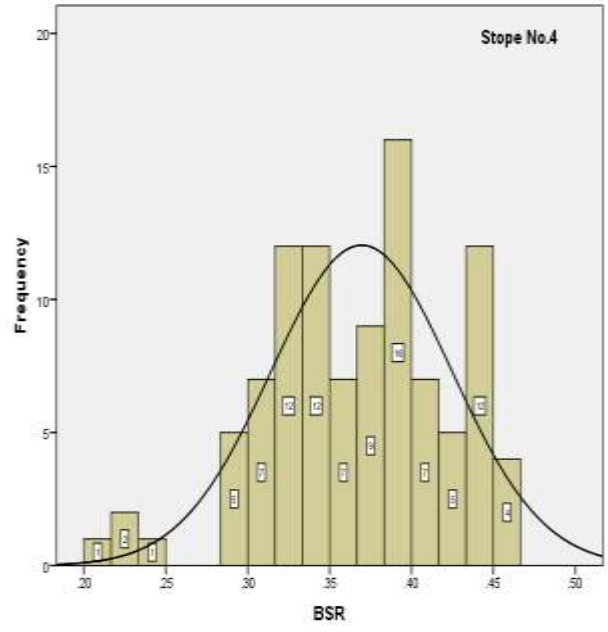
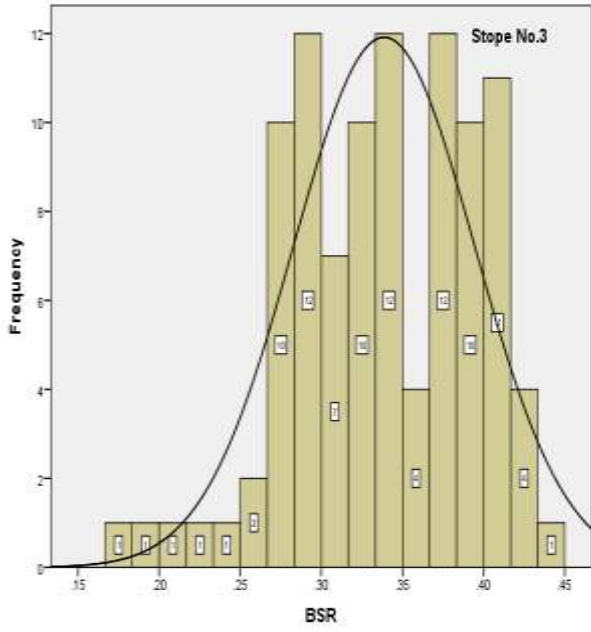
The obtained distributions and normal PDFs of 100 maximum BSR values for all seven stopes are shown in Figs. 13a–g. The PDI and the mean value of maximum BSR for each stope are reported in Table 5-5. The PDI (where BSR exceeds the 0.4 threshold) (Castro et al., 2012) increases with continuing mining activity. In particular, in excavating stope #4, the PDI increases rapidly over 40% and ultimately reaches 83% for stope #7.



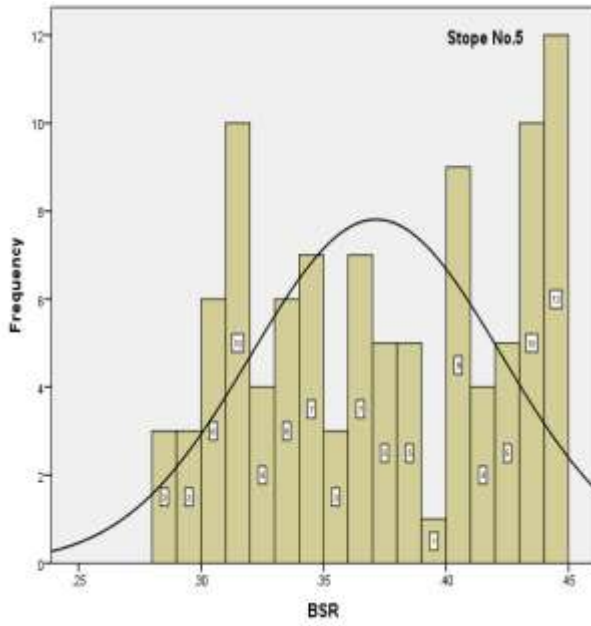
(a)



(b)

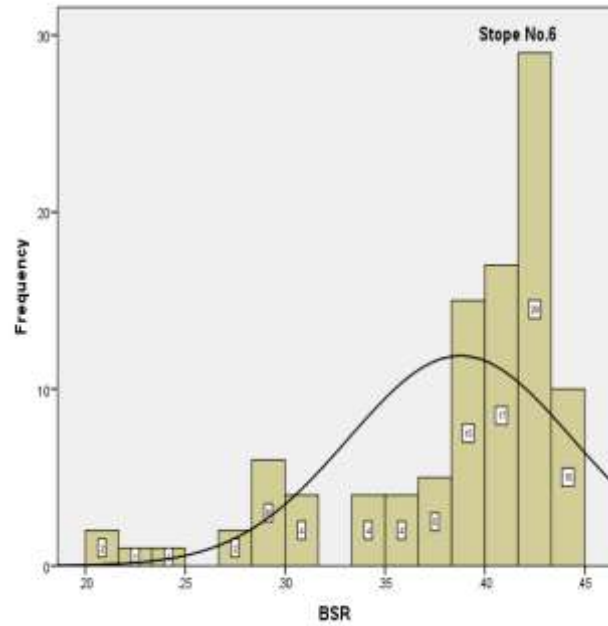


(c)

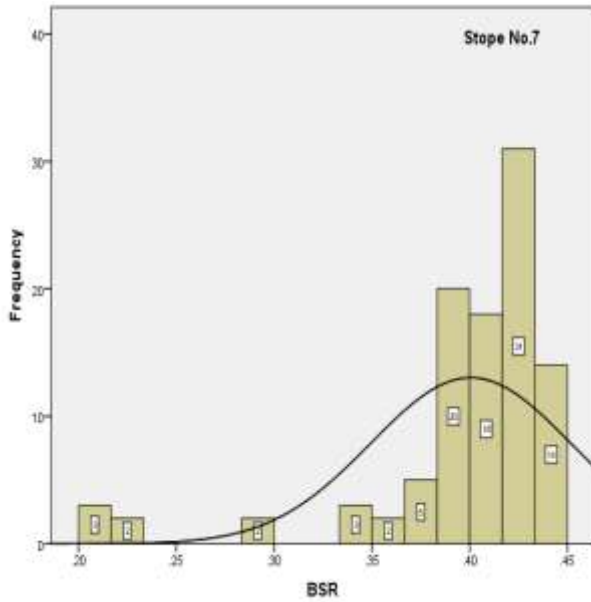


(e)

(d)



(f)



(g)

Figure 5-13 - Normal probability density functions (PDFs) of the maximum brittle shear ratio (BSR) value around the area of interest for each primary open stope.

Increasing the PDI will eventually lead to spalling and slabbing failure of stope walls. This occurs due to a significant reduction in the minimum principal induced stress (σ_3) near the excavation walls accompanied by an increase of the tangential stresses to their maximum (Diederichs 1999; Milne 1996). The deviation of the principal induced stress components is perfectly reflected by the parameter BSR. This can also be expressed in terms of the maximum shear stress around each stope as it is related directly to the BSR formula (Eqn. 5-15).

Table 5-5 - The mean values of maximum brittle shear ratio (BSR) and the associated probability of brittle damage initiation for each open stope.

Stope #	Mean value of maximum BSR (100 runs)	Probability of brittle damage initiation
1	0.34	10 %
2	0.34	14 %
3	0.34	16 %
4	0.37	41 %
5	0.37	40 %
6	0.39	71 %
7	0.40	83 %

Zones of maximum shear stress concentrations are generated mainly in the transverse pillars and side walls around the stopes (Fig. 5-14). This causes the brittle damage potential to increase. The obtained PDI value for each open stope is dependent on the extent of shear stress concentration around the stope. Therefore, stopes #6 and #7 are certainly expected to be damaged, while stopes #1 to #3 are less prone to brittle damage (Table 5-5). However, according to the obtained ranges of maximum BSR value for each stope, the brittle failure condition would not occur under the existing circumstances as the maximum BSR value never exceeds the failure limit of 0.7 (Castro et al., 2012).

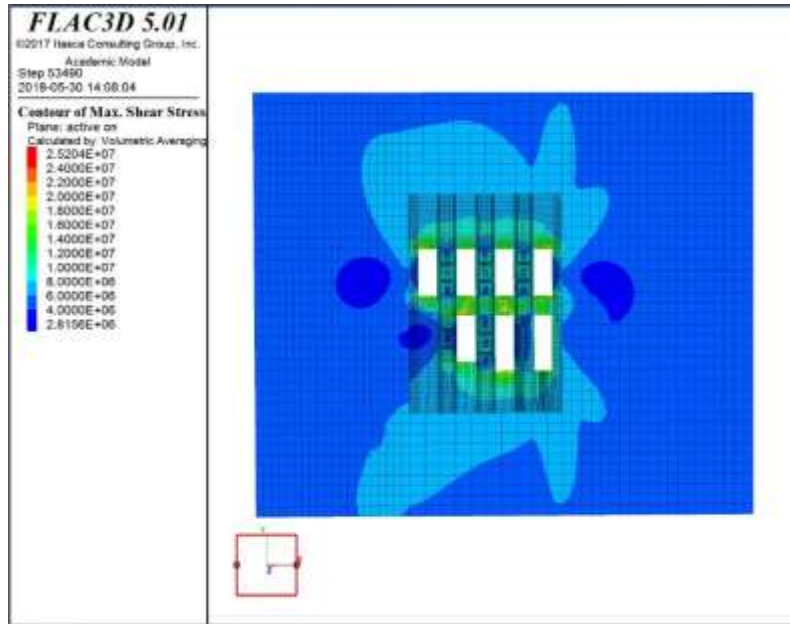
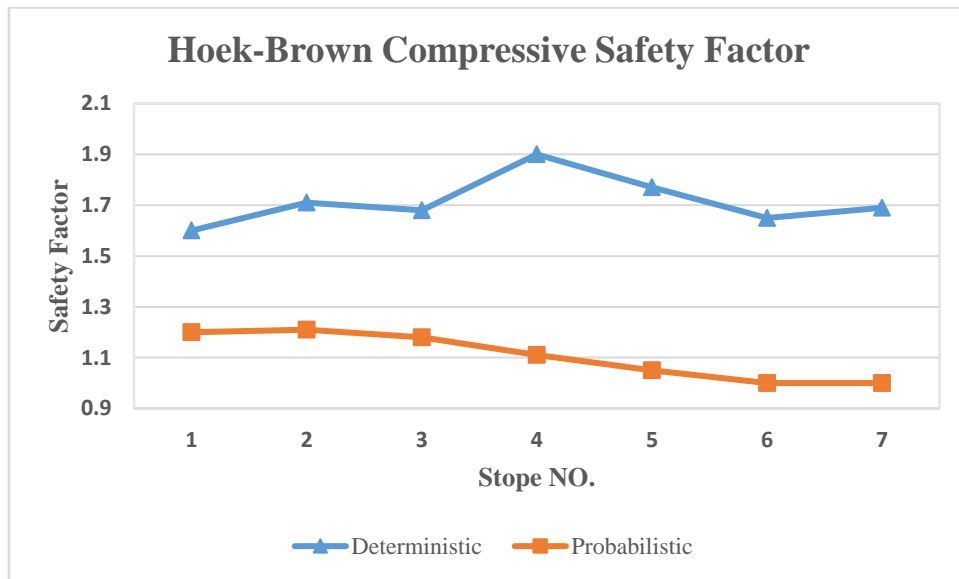


Figure 5-14 - A plan view of maximum shear stress contours around the open stopes.

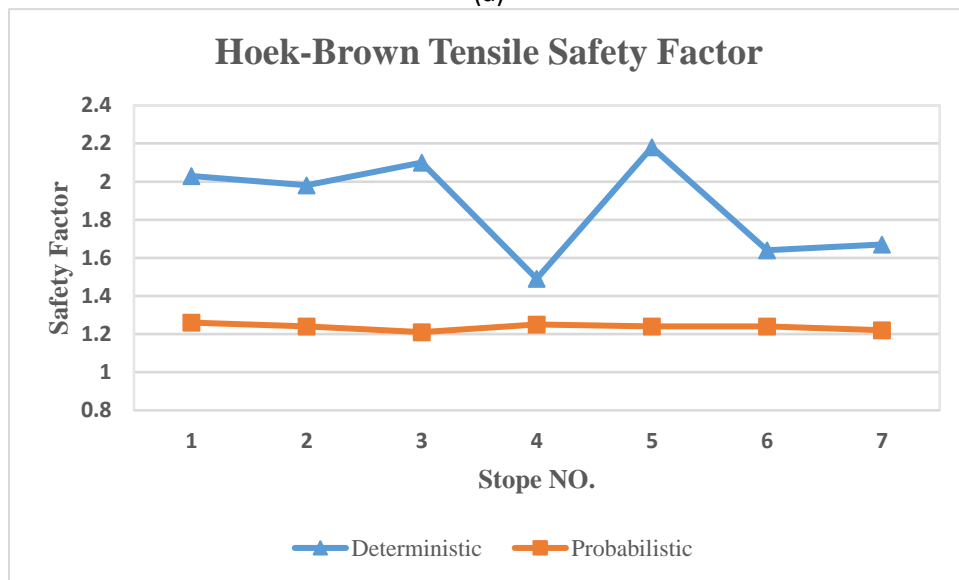
5.5.3. Comparison of probabilistic and deterministic analysis

Comparing the obtained Hoek-Brown compressive and tensile safety factors using a deterministic numerical model with the results obtained via probabilistic numerical modeling provides insight into the effect of the geomechanical variability of a rock mass on the state of stability. We developed a deterministic model using the average values of the geomechanical parameters (Tables 5-1-5-2) and keeping all other model setups (e.g. geometry, state of in-situ stress, and boundary conditions) unchanged. Figs. 5-15a–b present the minimum Hoek-Brown compressive and tensile safety factor as derived from the respective deterministic and probabilistic models. For all the open stopes, the deterministic analysis produced higher average values for the minimum Hoek-Brown compressive safety factor (Fig. 5-15a) than those of the probabilistic models. A similar pattern occurs for the minimum Hoek-Brown tensile safety factor values (Fig. 5-15b). This clearly demonstrates that the deterministic evaluation assumes a better rock mass quality in terms of strength and stiffness. However, given the nature of the rock mass, the presence

of inherent variability in the strength and stiffness properties within the rock mass is inevitable. Therefore, deterministic analysis will produce false results that could be misleading for open-stope design and evaluation purposes. It is therefore recommended to incorporate uncertainties associated with the variability of rock mass parameters into numerical analyses to ensure that the actual behavior of the rock mass is considered.



(a)



(b)

Figure 5-15 - Outcomes from deterministic and probabilistic numerical analyses for (a) the minimum Hoek-Brown compressive safety factor and (b) the minimum Hoek-Brown tensile safety factor.

5.6. Conclusion

Random Monte Carlo simulations, in conjunction with the finite difference code *FLAC3D*, were used to develop numerical models of seven existing primary open stopes in mining levels V and VI at the Niobec Mine and to comprehensively evaluate their stability by including the inherent variability of the geomechanical parameters of the rock mass.

The potential of compressive, tensile, and brittle failure for each open stope was investigated by adopting the Hoek-Brown tensile and compressive safety factor and the brittle shear ratio (BSR) as stability criteria to determine respectively the tensile and compressive POFs and PDI. For the existing rock mass quality and the in-situ stress regime at the Niobec Mine, tensile and compressive failure is probable, and this is influenced directly by the excavation sequence.

Similarly, the probability of brittle damage initiation was determined to be very high and reaching 100% for the most recently excavated stopes even though no brittle failure is expected to occur for all the stopes. The physical phenomenon behind the observed behavior of the rock mass is well explained in terms of changes in major and minor principal induced stresses and the resulting stress relaxation/concentration envelopes in the vicinity of the open stopes.

Furthermore, a better understanding of the role of inherent variability within a rock mass on different modes of instability was obtained by comparing the results of a deterministic and probabilistic numerical model. Deterministic models do not reflect the actual behavior of the rock mass as they overestimate the strength and stiffness of the rock mass. Therefore, for all the open stopes, the average value of minimum Hoek-Brown tensile and compressive safety factors obtained from the deterministic analysis were higher than those for the probabilistic models.

However, we identify some potential stope instabilities within the mining blocks V and VI at Niobec Mine, but no major concern should be raised regarding the state of stability. In fact, since the magnitude of in situ stress components were approximated empirically and the rock mass quality were subjected to simplifications through defining a single rock type (combined syenite-carbonatite) within the numerical models, the obtained results of the POFs and PDI are not supposed to precisely reflect the actual state of stability in mining blocks V and VI at the Niobec mine. Besides, we concluded that the Hoek-Brown tensile and compressive safety factors may not provide a reliable evaluation of stability in semi-deep to deep underground mines, since the resulting values of safety factors for all the open stopes were mostly very close to 1.000. This proximity of the Hoek-Brown compressive and tensile safety factor values to unity would complicate reaching the ultimate conclusion about the state of stability when considering other engineering failure thresholds of the safety factor (e.g. $SF = 1.5$). Albeit, the results of this study contribute in better understanding the influence of rock mass geomechanical parameter variability both in terms of value and spatial randomness, on the rock mass tensile, brittle and compressive damage of multiple underground open stopes excavated within a same-level mining block. Moreover, the reliability of employing probabilistic methods over the conventional deterministic methods for underground stability analysis is highlighted. In fact, to address the real behavior of the rock mass for underground stability analysis, we recommend the use of a probabilistic approaches in conjunction with the numerical analysis to deal with uncertainties associated with the variability of rock mass parameters.

Acknowledgments

The authors would like to acknowledge the funding received by a grant from Natural Sciences and Engineering Research Council of Canada (NSERC) for this study. We also thank the personnel at the Niobec Mine for their assistance.

5.7. References

- Abdellah W. Geotechnical risk assessment of mine haulage drifts during the life of a mine plan. PhD thesis, McGill University, Montreal, Canada, 2013.
- Abdellah W, Mitri HS, Thibodeau D, Moreau-verlaan L. Stability of mine development intersections — a probabilistic analysis approach. 2014a; 195:184–95.
- Abdellah W, Raju GD, Mitri HS, Thibodeau D. Stability of underground mine development intersections during the life of a mine plan. *Int J Rock Mech Min Sci*. 2014b; 72:173–181.
- Aglawe JP. Unstable, violent failure around underground openings in highly stressed ground. PhD thesis, Queen’s University at Kingston, 1999.
- Brown ET. Risk assessment and management in underground rock engineering—an overview. *Journal Rock Mech Geotech Eng.*; 2012(3):193–204.
- Bétournay, M.C., Gorsky, B., & Situm, M. Tetrauville limestone of the Niobec crown pillars comparison of strength and deformation properties from various tests. Division Report M&ET/MRL 86-144 (TR), Mining Research Laboratories, CANMET, Energy, Mines and Resources Ottawa, Canada, 14 p. *Contrôle de terrains*, 1986.
- Cai M, Kaiser PK, Martin CD. A tensile model for the interpretation of micro-seismic events near underground openings. *Pure and Applied Geophysics* 1998; 153(1): 67-92.
- Cai, M. Rock mass characterization and rock property variability considerations for tunnel and cavern design. *Rock Mechanics and Rock Engineering* 2011; 44(4), 379-399.
- Castro LAM, Bewick RP, Carter TG. An overview of numerical modelling applied to deep mining. In: Azevedo R, editor. *Innovative numerical modelling in geomechanics*. London: CRC Press — Taylor & Francis Group; 2012; p. 393–414.

- Chen G, Jia Z, Ke J. Probabilistic analysis of underground excavation stability. *Int. J. Rock Mech. & Min. Sci.* 1997; 34:3–4, paper No. 051.
- Corthésy R. Investigation géomécanique du 3e bloc minier : essais en laboratoire - Mine Niobec. Centre de développement technologique de l'École Polytechnique. Montréal, Canada, 2000a.
- Corthésy R. Mesure des contraintes In-situ : Mine Niobec. Centre de développement technologique de l'École Polytechnique. 2000b; Montréal, Canada.
- Corthésy R., & Leite M.H. Mesures des contraintes In-situ : Mine Niobec. Centre de développement technologique de l'École Polytechnique. 2013a; Montréal, Canada.
- Corthésy R., & Leite M.H. Mesures des contraintes In-situ, Mine Niobec – Niveau 2400. Centre de développement technologique de l'École Polytechnique. 2013b; Montréal, Canada.
- Desbiens S. Étude géomécanique du massif de carbonatite de la Mine Niobec au niveau 1000 et analyse de stabilité. (Projet de fin d'études). Université du Québec à Chicoutimi, Chicoutimi, Canada, 1997.
- Diederichs MS, Kaiser PK. Rock instability and risk analyses in open stope mine design. *Can Geotech J.* 1996; 33(3):431–439.
- Diederichs MS. Instability of hard rock masses: the role of tensile damage and relaxation. PhD Thesis. Waterloo, Ontario: University of Waterloo; 1999.
- Diederichs MS, Kaiser PK, Eberhardt E. Damage initiation and propagation in hard rock during tunneling and the influence of near-face stress rotation. *International Journal of Rock Mechanics and Mining Sciences* 2004; 41(5):785-812.48.
- Dong L, Sun D, Li X, Zhou Z. Interval non-probabilistic reliability of a surrounding jointed rockmass in underground engineering: A case study. *IEEE Access*, 2017, 5, 18804-18817.
- Dorion JF, Hosseini Z. Implementation of a Seismic System at Niobec Mine. 47th U.S. Rock Mechanics/Geomechanics Symposium, San Francisco, California, 2013.
- Einstein HH. Risk and risk analysis in rock engineering. *Tunneling and Underground Space Technology* 1996; 11 (2):141–55.
- Golder. Review of In Situ Stress Measurement at Niobec Mine. Project 002-11-1221-0087 MTA Rev0, February, 2012.
- Grenon, M. Essais de laboratoire – Résistance en compression uniaxiale – Résistance en tension indirecte. Laboratoire de mécanique des roches (LMR). 2013; Université Laval, Québec, Canada 116 p.

- Griffiths, D.V., Fenton, G.A., Lemons, C.B. Probabilistic analysis of underground pillar stability. *Int. J. Numer. Anal. Methods Geomech.* 2002; 26, 775-791.
- Guarascio M., Oreste P. Evaluation of the stability of underground rock pillars through a probabilistic approach. *American Journal of Applied Sciences*, 2012; 9 (8), 1273-1282.
- Heidarzadeh S, Saeidi A, Rouleau A. Assessing the effect of open stope geometry on rock mass brittle damage using a response surface methodology. *Int J Rock Mech Min Sci.* 2018a; 106:60–73.
- Heidarzadeh S, Saeidi A, Rouleau A. Evaluation of the effect of geometrical parameters on stope probability of failure in the open stopping method using numerical modeling. *Int J Min Sci Tech;* 2018b.
- Henning JG. Evaluation of Long-Hole Mine Design Influences on Unplanned Ore Dilution. PhD thesis, McGill University, Montreal, Canada, 2007.
- Henning JG, Mitri HS. Numerical modelling of ore dilution in blasthole stopping. *Int J Rock Mech Min Sci.* 2007; 44:692–703.
- Hoek E. Practical rock engineering. <http://www.rocscience.com/hoek/PracticalRockEngineering.asp>, 2007, World Wide Web edition.
- Hudson JA. *Comprehensive Rock Engineering: Principles, Practice & Projects*. Vol 5. Pergamon Press; 1993.
- Idris MA, Saiang D, Nordlund E. Probabilistic analysis of open stope stability using numerical modelling. *Int. J. Min. Miner. Eng.* 2011; 3(3):194–219.
- Idris MA, Basarir H, Nordlund E, Wettainen T. The Probabilistic Estimation of Rock Masses Properties in Malmberget Mine, Sweden. *Electron J Geotech Eng.* 2013; 18:269–287.
- Idris MA. Probabilistic stability analysis of underground mine excavations. PhD thesis, Lulea University of Technology, Lulea, Sweden, 2014.
- Itasca Consulting Group, Inc. *FLAC3D – Fast Lagrangian Analysis of Continua in 3 Dimensions*, Ver. 5.1 (License number: 242-001-0456-27682), User's Guide. Minneapolis: Itasca 2015.
- Itasca. *Geomechanical Feasibility Analyses of Caving at Niobec Mine*. Ref.13-2768-62, February, 2014.
- Labrie, D. Étude de stabilité à la mine Niobec. Projet STM-526, Centre de Recherches Minérales, Supplément No. 4 : Essais en laboratoire, 1987.

- Labrie, D. Caractérisation et instrumentation du pilier horizontal situé entre les niveaux 600 et 700 de la zone 102 à la mine Niobec. Rapport LMSM 96-083 (RC), Laboratoires de recherche minière, CANMET, Énergie, Mines et Ressources Canada, Ottawa, Canada, 1997.
- Labrie D., & Conlon B. Essais de compression sur le matériau de la mine Niobec, Saint-Honoré (Saguenay), Québec - résultats finaux. Projet 603 017. 9 p, 2005.
- Lajoie P.-L. Caractérisation du massif de carbonatite de la mine Niobec sous le niveau 1000 et analyse de la stabilité du pilier de niveau. (Mémoire de maîtrise). Université du Québec à Chicoutimi, Chicoutimi, Canada. 403 p 2010.
- Lalancette S. Dimensionnement des chantiers remblayés de la mine Niobec en utilisant la modélisation 3D. M.Sc. thesis, University of Quebec at Chicoutimi, Chicoutimi, Canada, 2018.
- Langston RB, Kirsten HAD. Probabilistic assessment of sub-level hanging wall stability at the Stillwater Mine, Nye, Montana. American Rock Mechanics Association. The 38th U.S. Symposium on Rock Mechanics (USRMS), 2001, Washington, D.C. US.
- Lavoie C. Analyse de l'effet du remblayage des chantiers souterrains de la mine Niobec sur leur stabilité. M.Sc. thesis, University of Quebec at Chicoutimi, Chicoutimi, Canada, 2018.
- Lü Q, Low BK. (2011). Probabilistic analysis of underground rock excavations using response surface method and SORM. *Comput Geotech* 2011; 38:1008–21.
- Martin CD, Kaiser PK, Christiansson R. Stress, instability and design of underground excavations. *International Journal of Rock Mechanics and Mining Sciences* 2003; 40 (7-8):1027-47.
- Milne D. Underground design and deformation based on surface geometry. PhD Thesis, Mining Department, University of British Columbia, Vancouver, 1996.
- Pytel W, Świtoń J. Assessment of the Impact of Geomechanical Parameters Variability on Underground Excavations Stability Using Response Surface Method. *Stud Geotech Mech* 2013; 35 doi: 10.2478/sgem-2013-0014
- Shnorhokian S, Mitri HS, Moreau-verlaan L. Stability assessment of stope sequence scenarios in a diminishing ore pillar. *Int J Rock Mech Min Sci*. 2015; 74:103–118.
- Shnorhokian S, MacNeil B, Mitri H. Volumetric analysis of rock mass instability around haulage drifts in underground mines. *Journal of Rock Mechanics and Geotechnical Engineering*, Volume 10, Issue 1, February 2018, Pages 60-71.

- Thivierge S., Roy D.-W., Chown, E.H. et Gauthier, A. Évolution du complexe alcalin de St.-Honoré (Québec) après sa mise en place. *Mineralium Deposita*, 18, 267-283, 1983.
- Vallieres D. et al. NI 43-101 Technical Report, Update on Niobec Expansion, IAMGOLD Corporation, Quebec, Canada, 2013.
- Villaescusa E. Geotechnical design for sublevel open stoping. CRC Press. 2014.
- Wang J. Influence of stress, undercutting, blasting, and time on open stope stability and dilution. PhD thesis, University of Saskatchewan, Saskatoon, Canada, 2004.
- Zhang Y, Mitri HS. Elastoplastic stability analysis of mine haulage drift in the vicinity of mined stopes. *Int J Rock Mech Min Sci*. 2008; 45(4):574–593.
- Zhao, H., Li, Z., Kong, C.S. Probabilistic method to determine the overall rock block failure based on failure mode. *Engng. Trans*. 2016; 64 (1), 105–113.

Chapter 6 - Conclusions

Sublevel stoping creates large underground openings called “Stopes” to extract the mineral deposits. Maintaining the stope stability has become a challenging task for underground engineers since it directly influences the production capacity of the mine as well as the overall safety of the work force. Underground instability and the probable failure conditions, for open stopes located in deep hard rock, occur as a result of the two dominant mechanisms, namely; (1) stress-induced spalling and slabbing (brittle failure); and (2) structurally-controlled gravity-driven failures (i.e. tensile). Independent of failure mechanism, stope stability is influenced by several factors, most notably the rock mass geomechanical parameters, the natural and mining-induced stresses, and the stope geometrical parameters.

The present thesis, employed different probabilistic methods in conjunction with the finite difference code *FLAC3D*, to provide a methodology to assess the individual and interaction effect of stope geometrical parameters on the rock mass brittle damage as well as the stope probability of failure by considering the both aforementioned failure mechanisms. Also, to evaluate the effect of rock mass geomechanical parameter variability on stope stability; a stochastic numerical analysis by *FLAC3D* is performed on seven primary open stopes located in mining blocks V and VI at the Niobec underground mine to evaluate the stability state of multiple neighboring stopes, taking into consideration the inherent variability associated with the geomechanical parameters of the rock mass. The most important findings of the accomplished thesis are presented below:

6.1. Assessing the effect of open stope geometry on the rock mass brittle damage

- The BSR value increases for all three defined geometry clusters with increasing mining depth, due to the increasing *in situ* stress magnitude.
- The highest range of BSR (independent from mining depth) is observed for the stopes having moderate range of hanging wall HR and high range of hanging wall dip.
- The lowest range of BSR (independent from mining depth) is observed for the stopes having low-moderate range of hanging wall HR and low-moderate range of hanging wall dip.
- The individual and interactive effect of stope geometrical parameter variations on the rock mass brittle damage is found to be significant.
- Stope strike length and stope width respectively shows decreasing and increasing effect on BSR value in all geometry clusters.
- Increasing the stope height over 69m showed a significant increasing effect on BSR value.
- For shallow to moderately dipping stopes (up to 54°) increasing hanging wall dip causes BSR value to increase, while for steeply dipping stopes, increasing hanging wall dip decreases the BSR value.
- For geometry cluster I, interaction effect of width and dip shows very significant increasing effect; for geometry cluster II, interaction effect of height and dip shows very significant decreasing effect and for geometry cluster III, interaction effect of length/width showed very significant decreasing effect on BSR.

6.2. Evaluation of the effect of geometrical parameters on the stope probability of failure

- Under the presumed state of *in situ* stress and rock mass quality; structurally-controlled gravity driven failure is the dominant mode of failure.
- The three parameters stope hanging wall HR, stope span width and stope hanging wall dip have a strong influence on the stope stability state.
- The probability of stope failure is significantly controlled by interaction effects between span width / hanging wall HR and hanging wall dip / hanging wall HR.
- The interaction effects between the parameters, does alter the way each parameter affects the probability of stope failure; hence, the effect of each geometrical parameter on POF must be assessed by considering the variation level of other parameters.
- A key finding of this study is that whatever the stope hanging wall dip, increasing the stope span width from 4 m to 12 m, increases the POF in all categories of stope hanging wall HR.
- Aside from stope span width range, when hanging wall HR ranged between 2.5-5 m, the most unstable condition occurs for hanging wall dip range of 45-60°, while the most stable condition occurs for hanging wall dip between 60-75°.
- For stopes having their hanging wall HR ranging between 5 and 7 m, the most stable condition occurs for the hanging wall dip range of 45-60°, while the maximum instability is observed for hanging wall dip between 75 and 90°.
- Independent of stope span width, increasing the stope hanging wall HR range from 2.5-5 m to 7-10 m decreases the POF for the stopes dipping up to 60°. While for stopes dipping

greater than 60° , the most unstable condition occurs for the hanging wall HR range of 5-7 m for all span width groups.

- The mathematical optimization predicts that the maximum stability (in terms of POF) would be achieved for narrow stopes (span width of 4 m) whose hanging wall dip ranges between 20 and 45° and hanging wall HR ranges between 7 and 10 m.
- In contrast, the maximum instability would occur in wider stopes (span width equal to 12 m) whose hanging wall HR ranges between 2.5 and 5 m, and hanging wall dip ranges between 45 and 60° .

6.3. Probabilistic evaluation of the effect of rock mass geomechanical variability on open stope probability of failure

- The obtained results demonstrate that for the existing rock mass quality and *in situ* stress regime at the Niobec mine, a tensile and compressive failure is probable (however not majorly), and is influenced directly by the excavation sequence.
- Accordingly, the stope #7 and #4 are recognized to be more unstable compare to the stope #1 and #2 which are expected to be the most stable ones.
- Similarly, probability of brittle damage initiation is determined to be very high and reaching 100% for the latest excavated stopes, even though no brittle failure would expect to occur for all the stopes.
- The physical phenomenon behind the observed behavior of rock mass was well explained in terms of changes in the magnitude of major and minor principal induced stresses causing the development of stress relaxation / concentration envelopes in the vicinity of the open stopes.

- It is found that deterministic models do not reflect the real behavior of the rock mass by overestimating the strength and stiffness of the rock mass. Therefore, the average values of minimum Hoek-Brown tensile and compressive safety factors obtained from deterministic analysis, were higher than the results of probabilistic models for all the open stopes.
- The results of this study should not arise a concern for Niobec mine authorities since delayed backfilling is predicted to be used in the actual excavation process which may help to maintain the overall stability of each open stope.
- Probabilistic approaches accompanied by numerical analysis should be used to deal with the uncertainties associated with the variability of rock mass parameters, in order to assess the real behavior of the rock mass for stability analysis.

6.4. Perspectives for further research

- The developed probabilistic analysis methodology for assessment of geometrical parameters, can be used in the future studies for different excavation geometries having different *in situ* stress conditions and rock mass properties.
- By using the proposed stochastic methodology, the effect of geometrical parameters can also be assessed on the probability of rockburst or fault slip occurrence.
- The proposed stochastic methodology can be used to analyse the effect of rock mass geomechanical parameter variability on the state of stability for different underground cases.

- Using discontinuum numerical analysis, the effect of uncertainties associated with joint strength and distributions on the state of excavation stability can be assessed by the proposed methodology.

Chapter 7 – Appendices

7.1. Appendix A – Numerical modeling verifications

The generated model below, has been selected and rebuilt according to the dimensions proposed by the run #8 of the table 3-4 (page 55) of the Chapter 3, having the stope strike length = 23.5 m, stope span width = 11.3 m, stope height = 27.6 and HW dip = 39.0°. The mining depth was set as 1125 m below surface; hence, the magnitudes of maximum and minimum horizontal, and the vertical component of in situ stress were calculated respectively as equal to 52.9 MPa, 35.1 MPa and 23.6 MPa.

The planar symmetrical models were built based on a transverse stope configuration, containing multiple neighboring primary stopes having identical dimensions excavated in sequence. A constant value of 0.4 was assigned to the rib pillar W/H ratio. A finer mesh was generated for enhancing accuracy near the stopes and pillars, while the mesh becomes coarser for the rock mass surrounding the area of interest. Considering different stope sizes for each model, the conditions of external boundaries in displacement (roller conditions) have been positioned far enough to avoid any undesirable effect on the results obtained in the region of interest (Fig. 7-1).

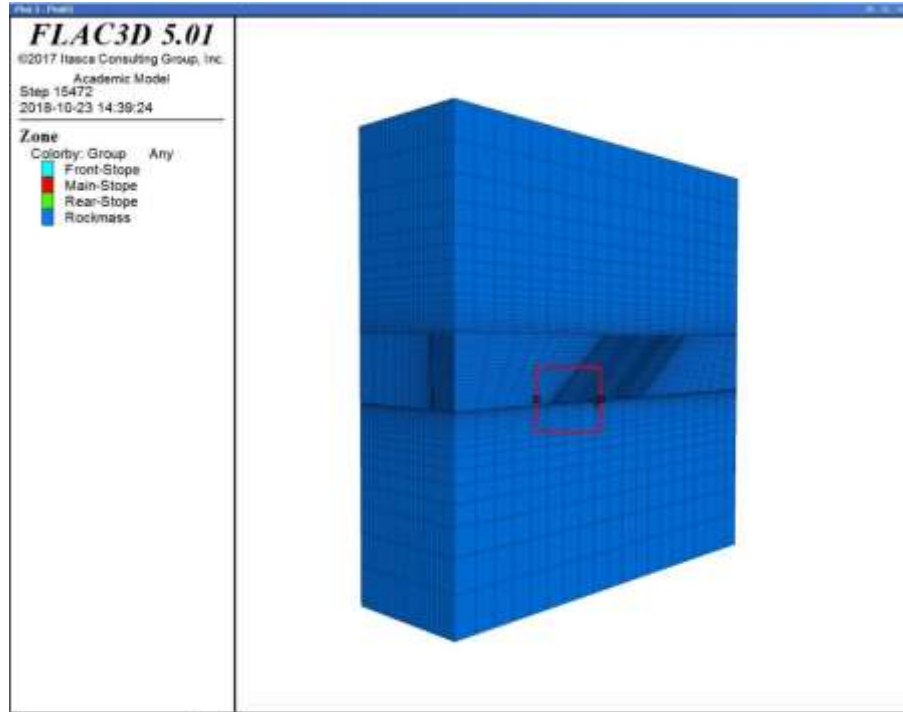
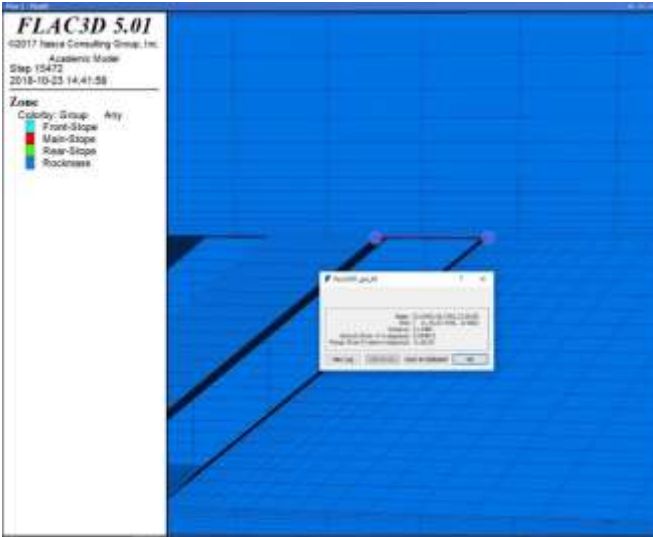
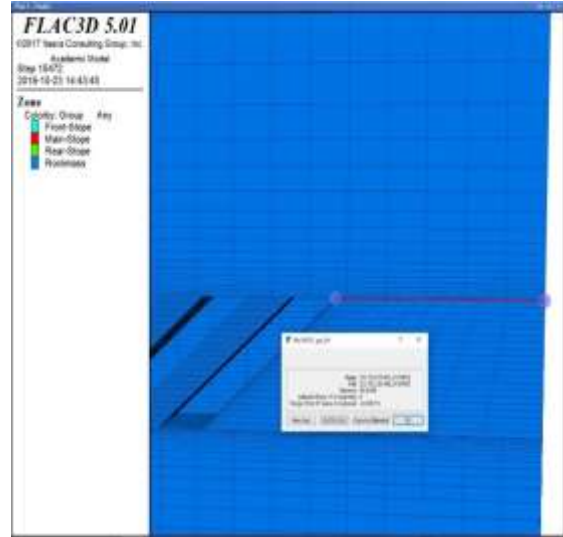


Figure 7-1- The FLAC3D model preview.

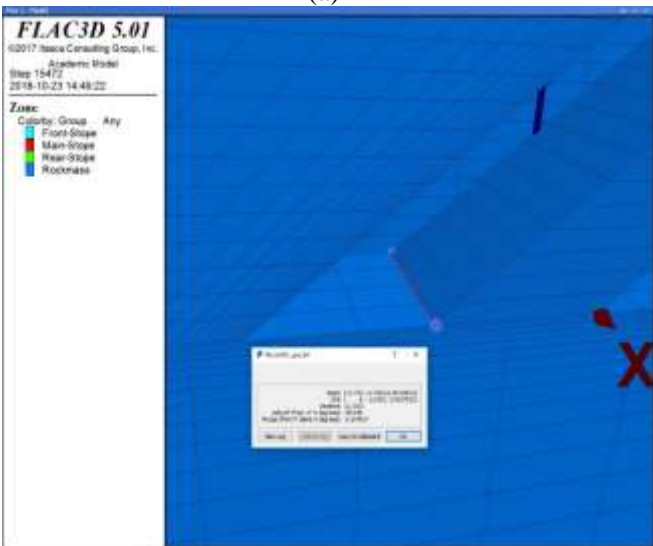
The provided figures below (Figs. 7-2a-f), show the measured dimensions of each stope geometry parameter (i.e. strike length, stope height) comparing to the defined model boundary dimensions. It should be noted that, in order to provide convenience for modeling different designed stope geometries at each simulation, a FISH code has been generated to define the model boundaries equal to almost four times larger than the corresponding geometry parameter at each direction.



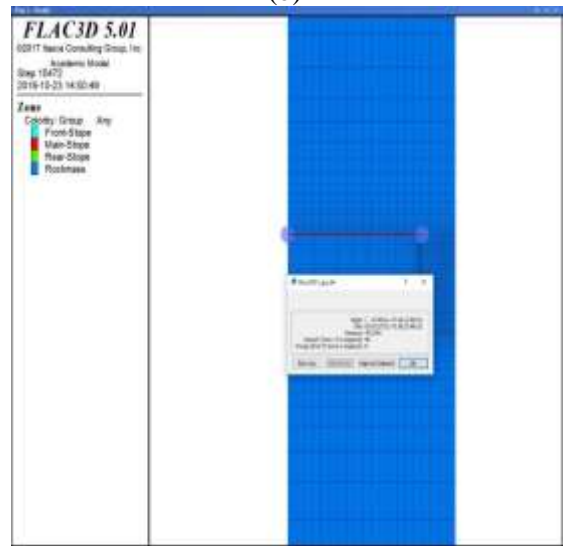
(a)



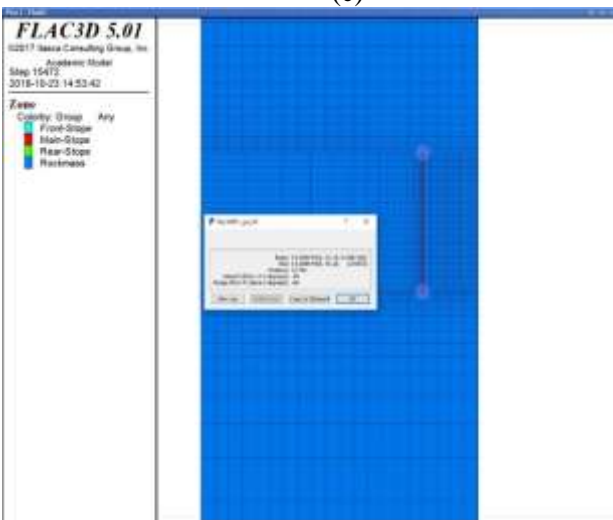
(b)



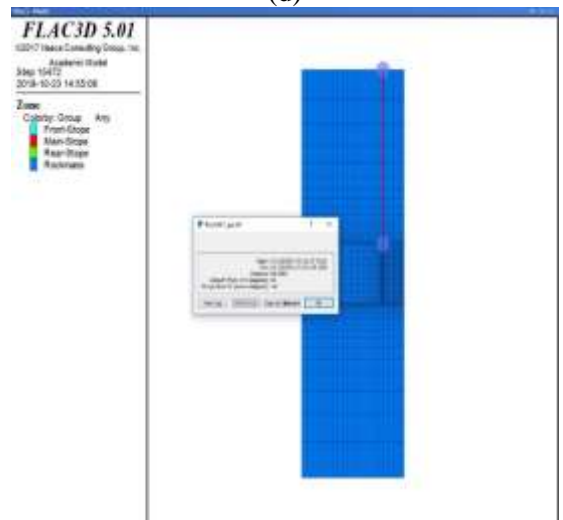
(c)



(d)



(e)



(f)

Figure7- 2- Measured dimension of (a) stope span width (m), (b) from the stope wall to the model boundary in X-direction (m), (c) stope strike length (m), (d) from the stope wall to the model boundary in Y-direction (m), (e) stope height (m), (f) from the stope wall to the model boundary in Z-direction (m).

According to the provided figure below (Fig. 7-3), the area of interest in the generated models (Pillars and stope walls) has not been adversely affected by the boundary dimensions, since the total displacement contours reached to zero around the region of interest.

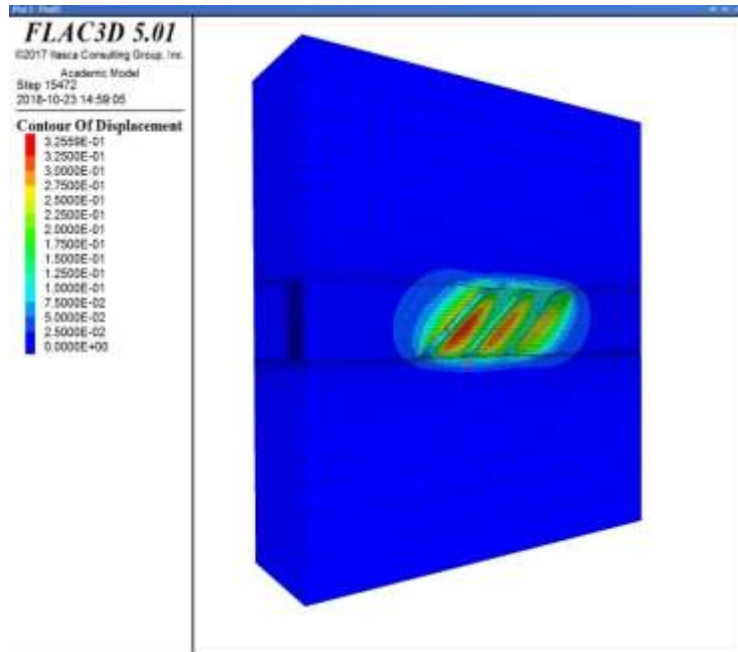
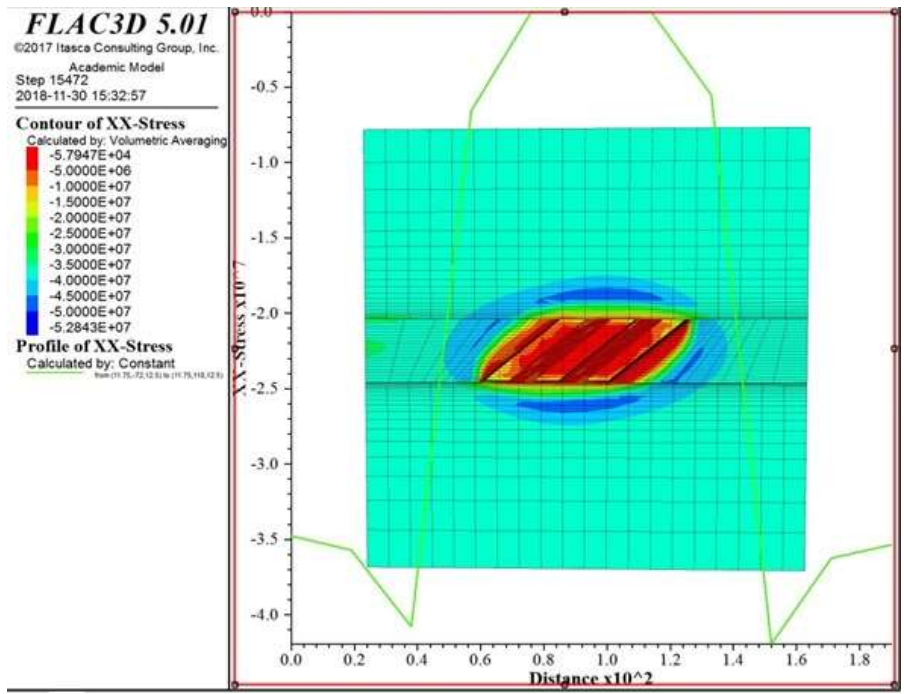
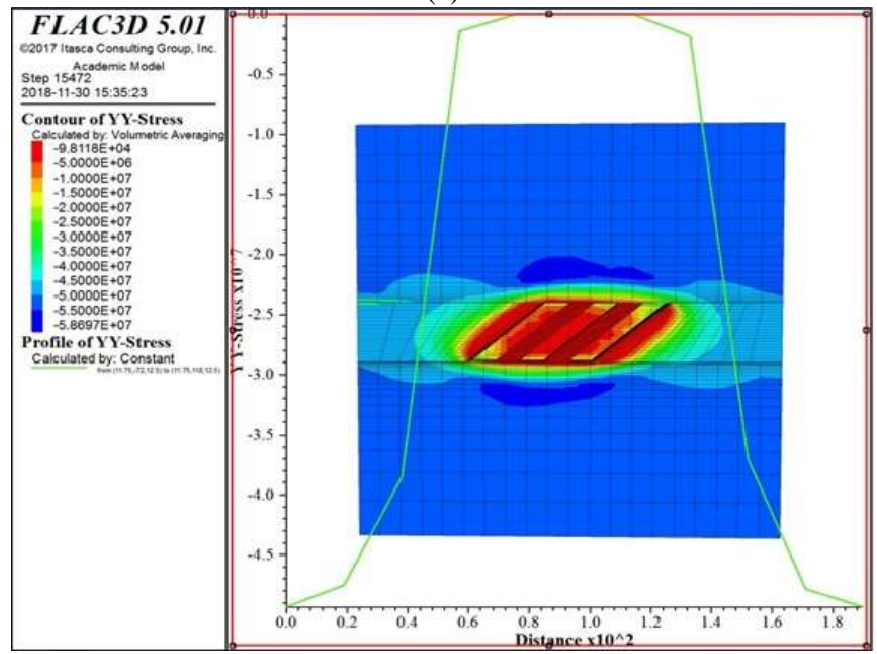


Figure 7-3- Contours of total displacement.

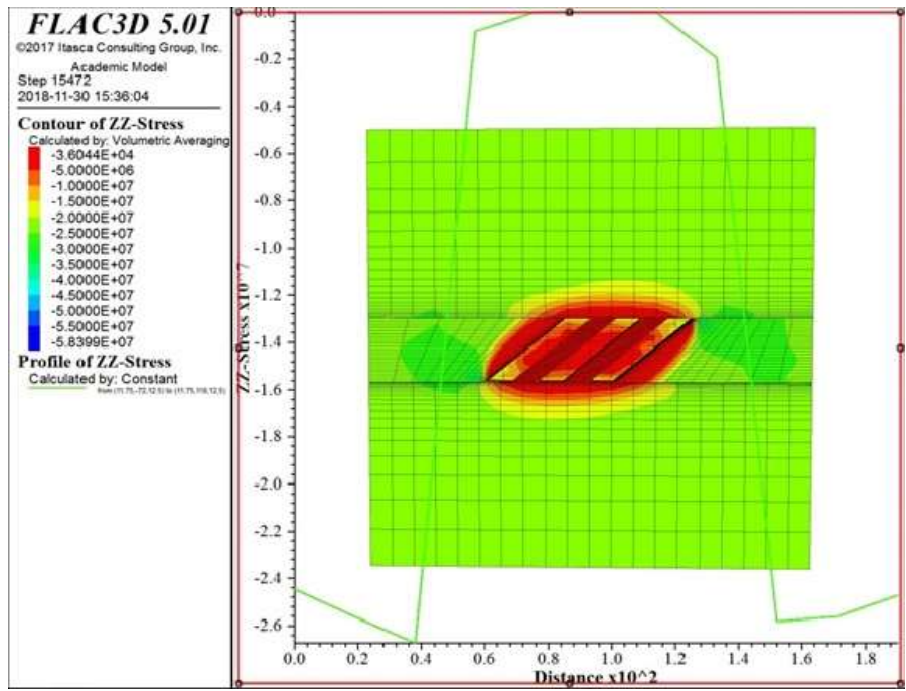
Moreover, Fig. 7-4a-c present the contours and mid-section profile of the magnitudes of horizontal and vertical induced stress components in the model. The magnitude of each induced stress component remained constant and reached to the magnitudes of initial in situ stress state at the boundaries of the model. Hence, the area of interest in the generated models (Pillars and stope walls) has not been adversely affected by the boundary dimensions, since the induced stress state has reached to equilibrium around the region of interest.



(a)



(b)



(c)

Figure 7-4- The contours and mid-section profile of the magnitudes of (a) minimum horizontal induced stress component, (b) maximum horizontal induced stress component and (c) vertical induced stress component in the model.